

Syracuse University

**SURFACE**

---

Dissertations - ALL

SURFACE

---

December 2014

## Coordination polymers of the alkaline earth metals for applications in synthesis and gas storage

Peter Josue Rosado Flores  
*Syracuse University*

Follow this and additional works at: <https://surface.syr.edu/etd>



Part of the [Physical Sciences and Mathematics Commons](#)

---

### Recommended Citation

Rosado Flores, Peter Josue, "Coordination polymers of the alkaline earth metals for applications in synthesis and gas storage" (2014). *Dissertations - ALL*. 200.

<https://surface.syr.edu/etd/200>

This Dissertation is brought to you for free and open access by the SURFACE at SURFACE. It has been accepted for inclusion in Dissertations - ALL by an authorized administrator of SURFACE. For more information, please contact [surface@syr.edu](mailto:surface@syr.edu).

## ABSTRACT

The work presented in this thesis outlines our efforts to synthesize alkaline earth metal coordination complexes that could potentially serve as gas storage and synthetic precursor materials. The properties of these complexes are heavily influenced by factors such as the propensity to aggregate and the absence of energetically available *d*-orbitals which provide directionality. These often pose a challenge in obtaining suitable, stable compounds.

Some challenges in the crystallization of alkaline earth coordination complexes involve the precipitation of insoluble aggregates. Thus, a great part of the work focused on studying suitable reaction conditions towards the formation of X-ray quality crystals for structural elucidation. Slow concentration and hydro/solvothermal techniques, amongst others, were prime crystallization methods in this work.

The bulk of this thesis is divided in two parts. The first part details our attempts to synthesize metal organic frameworks (MOFs) of Mg, Ca, Sr and Ba. Our ligands of choice were the *p*, *m*, *o*-pyridinecarboxylic acids which provide two different binding sites. These consist of an N-donor and an anionic carboxylic acid, the N-donor located at different positions in the pyridyl ring depending on the isomer. These are also of low cost and soluble in different organic solvents.

The use of pyridinecarboxylic acids resulted in the systematic isolation of five magnesium coordination complexes, three of which exhibit open-framework character and remain stable after removal of guests, and two of which are hydrogen bonded networks. Further, systematic work with the heavier metals resulted in three fully 3-dimensional complexes based on Ca, Sr and Ba and one hydrogen-bonded Ca complex. A pattern is observed when using the linear *p* or angular *m*-pyridinecarboxylic acid in the presence of MeOH/DMF mixtures, in which

3-dimensional motifs with open-framework (*p*) and dense (*m*) character (Mg, Ca and Sr) are displayed. The dimensionality decreases in the presence of water or strongly coordinating donors, leading to the formation of hydrogen bound or 2-dimensional complexes.

The second part of this thesis involves the isolation of crown stabilized alkaline earth tosylates. The work resulted in the isolation of four new crown stabilized alkaline earth tosylates. Trends observed include an increase in coordination number as the size of the metal increases. Variation of crown:metal stoichiometry was also studied and resulted in two different calcium species displaying fully separated (1:1) and contact separated (1:2) ion association modes. For Sr and Ba, (1:1) stoichiometries resulted in hydrogen bound contact species.

This thesis provides a selection of alkaline earth metal coordination complexes. The preparation of these complexes has led to the elucidation of their synthetic routes. Full characterization of the complexes is also provided.

Coordination polymers of the alkaline earth metals for applications in synthesis and gas storage

By:

Peter Josué Rosado Flores

Department of Chemistry, Syracuse University

M. Phil. in Chemistry, Syracuse University

DISSERTATION

Submitted in partial fulfillment of the requirements of Doctor of Philosophy in Chemistry in the  
Graduate School of Syracuse University

December, 2014

Copyright © 2014

By

Peter Josué Rosado Flores

All rights reserved.

## ACKNOWLEDGEMENTS

This enormous endeavor and quest for knowledge would not have been possible without the guidance of my advisor, Dr. Karin Ruhlandt. This is why I want her to be the first person I thank in this humble acknowledgement.

Karin, I want to thank you for providing me with the tools to be successful in this chemistry and for being there when I needed you the most academically and sometimes personally. You have been abundantly helpful in every aspect and I hope you continue to be as I walk on from being your student to practicing chemistry in places beyond our lab. I respectfully say, that I will miss working *with* you.

I want to express my deepest gratitude to my committee chair: Dr. Gina Lee-Glauser. Gina thank you for always being there with a watchful eye for me from the start, it was an honor having you as chair and it's an honor having you as a mentor. To all committee members: Dr. Mathew Maye, Dr. Jon Zubieta, Dr. Ivan Korendovych, Dr. Marion Bickford and Dr. Karin Ruhlandt-Senge, thank you for your time and guidance.

I sincerely owe my deepest gratitude to the Syracuse Chemistry Staff: Cathy, Jodi, Deb, Joyce, Linda, Nancy, Sally, Mike, Steve and so forth. Thank you for your time and beautiful contributions to my life.

My best wishes also go out to my current and past lab mates, who are also my friends: Alan, Yuriko, Valerie, Catherine, Ana T., Ana O., Victoria, Matt, Josh and Cody. Thank you very much for all you did for me. I would like to extend a special thank you to Ana Torvisco (my second boss) for training me in the art of air sensitive chemistry and Victoria for sharing life experiences with me. To Valerie, thank you for the home-made meals. It was fun.

I am eternally indebted to my family: my mother Alida Flores Rodriguez, my father Peter Rosado Vega and my brother Peter Anthony Rosado Flores. You have walked alongside me in the path of life and never abandoned me. Your sacrifice for me will never be forgotten.

To my dear uncles and grandparents, I offer many thanks. Grandma, although you will probably never read this thesis, I say now that your humbleness, perseverance and faithfulness is what guided me through this process and has made me what I am today. I especially address my late uncle Carlos: *Rest in Peace Tio Carlitos. I never got to say "bye" but I will say hi to you someday, this thesis is for you.*

To my best friend and now wife (July 5<sup>th</sup> 2014): Aymi Janelle Rosado Flores: Although you came in later in this process, you came at just the right time. It is your wisdom and your insights on life that have made me focus on what is important and never give up. To her parents, Joan Buckley-White and Willie White: thank you for being my second parents and thank you for believing in me.

I am deeply grateful for my friends: Sandeep, Jean Michel Lacour, Kaitlin, Valerie, Maria, Mireille, James, Saleh, Lana, Paula, Brian, Crystal, Pickle, Farha, Faraj, Seema, Rosemary, Sneha and Natasha. Without your fun times, I wouldn't have made it.

I would like to also acknowledge the very important and powerful figure in my life that is Dr. Tulio Chavez-Gil. Professor, you took me under your wing as a youngling and watched me grow as a scientist. Now, years later, I will never forget the help you have offered me in all aspects of life. *In our small lab, we did wonders.*

Finally and most importantly, I am grateful to God for allowing me to pursue my dream in great health, insight and humbleness. I started this journey because I wanted to help others; with your help I will do so. In love, honor and grace for you, I thank you my Lord.

## TABLE OF CONTENTS

Abstract.....	i
Title page.....	iii
Copyright notice.....	iv
Acknowledgements.....	v
Table of Contents.....	vii
List of Illustrative Materials: Tables.....	xii
List of Illustrative Materials: Figures.....	xiii
List of Illustrative Materials: Schemes.....	xvi

### CHAPTER 1: The Chemistry and Applications of Alkaline Earth Metals

1.0 Introduction	
1.1 General Properties of the Alkaline Earth Metals	1
1.1.1 Trends in the Periodic Table	4
1.1.2 Coordinative Saturation	6
1.1.3 Chelate Effect	6
1.2 Non-covalent interactions in alkaline earth coordination polymers	7
1.2.1 Hydrogen bonding	8
1.2.2 Crystallographic location of hydrogen bonds	9
1.2.3 $\Pi$ -stacking interactions in metal organic complexes	10
1.2.4 Ion Association	13
1.3 Some Applications of Alkaline Earth Metals	
1.3.1 Organometallics	14



1.3.2 Hydrogen storage	16
1.4 Alkaline earth coordination polymers	
1.4.1 Porous Coordination Polymers: Metal Organic Frameworks	
–Structure and Composition	18
1.4.2 Alkaline earth metal organic frameworks	21
1.4.3 Effect of Ligand Topology on MOF Dimensionality	22
1.4.4 Multi-topic Ligands: Carboxylate and Nitrogen Binding Sites	24
1.4.5 Isonicotinic acid, nicotinic acid, picolinic acid	25
1.4.6 Hydrothermal and solvothermal Crystallization	26
1.4.7 Reaction variables: effect of solvent in MOFs	28
1.4.8 Hydrogen storage in alkaline earth MOFs	29
1.4.9 Effect of donors on coordination chemistry	31
1.4.10 Sulfonates	35
1.4.11 Alkaline Earth Tosylates	37
1.5 References	38
<b>CHAPTER 2: Scope of Thesis</b>	
2.0 Summary of Content	54
2.1 Study on Metal Organic Frameworks:	
ligand choice, reaction solvent composition and metal size dependency	56
2.2 Crown ether stabilized alkaline earth tosylates: donor studies	58
2.3 References	62

**CHAPTER 3: Novel magnesium coordination networks based on the *p*-pyridinecarboxylic acid ligands**

3.0 Introduction	65
3.1 Experimentals	
3.1.1 General and Physical Measurements	68
3.1.2 Synthesis	70
{[Mg(in) <sub>2</sub> ] <sub>2</sub> ·DMF} <sub>∞</sub> ( <b>1a</b> )	70
{[Mg(in) <sub>2</sub> ] <sub>2</sub> ·ACN} <sub>∞</sub> ( <b>1b</b> )	70
{[Mg(in)]·0.5THF} <sub>∞</sub> ( <b>1c</b> )	71
{[Mg(in) <sub>2</sub> (H <sub>2</sub> O)]·EtOH} <sub>∞</sub> ( <b>2</b> )	71
{[Mg(Hin)(OH) <sub>2</sub> ][NO <sub>3</sub> ]} <sub>∞</sub> ( <b>3</b> )	71
3.2 Results and Discussion	
3.2.1 Synthesis	72
3.2.2 Structural Characterization of <b>1a-c</b> , <b>2</b> and <b>3</b>	76
3.3 Thermal Analysis and Structural Integrity of <b>1a-c</b> , <b>2</b> and <b>3</b>	96
3.4 Conclusions	100
3.5 References	101

**CHAPTER 4: Synthesis, characterization and crystal structure of the 3-dimensional hydrogen bonded coordination complex {[Ba(in)(H<sub>2</sub>O)<sub>6</sub>][in]}<sub>∞</sub>**

4.0 Introduction	104
4.1 Experimentals	
4.1.1 General and Physical Measurements	105
4.1.2 Synthesis of <b>4</b>	107

4.2 Structural Characterization of <b>4</b>	108
4.3 Thermogravimetric Analysis of <b>4</b>	112
4.4 Conclusions	114
4.5 References	115

**CHAPTER 5: Novel calcium, strontium and barium coordination networks based on the *p*-pyridinecarboxylic acid and *m*-pyridinecarboxylic acid**

5.0 Introduction	117
5.1 Experimentals	
5.1.2 General and Physical Measurements	119
5.1.3 Synthesis of <b>5-8</b>	120
$\{[\text{Ca}(\text{nic})_2]\}_\infty$ ( <b>5</b> )	120
$\{[\text{Ca}(\text{in})(\text{CH}_3\text{CN})(\text{OH}_2)]\}_\infty$ ( <b>6</b> )	121
$[\text{Sr}(\text{in})_2]_\infty$ ( <b>7</b> )	121
$[\text{Ba}(\text{in})(\text{Cl})]_\infty$ ( <b>8</b> )	121
5.2 Results and Discussion	
5.2.1 Synthesis Discussion	122
5.2.2 Structural Characterization of <b>5-8</b>	124
5.2.3 Analysis of the Carboxylate Binding Modes	146
5.2.4 Effect of ligand structural isomerism	148
5.5 Thermal analysis of <b>5-8</b>	151
5.6 Conclusions	153
5.7 References	154

<b>CHAPTER 6: Crown Ether Stabilized Heavy Alkaline Earth Metal Tosylates</b>	
6.0 Introduction	158
6.1 Experimentals	
6.1.1 General and Physical Measurements	161
6.1.2 General Syntheses	163
$\{[\text{Ca}(\text{OTs})(18\text{-crown-6})(\text{OH}_2)_2]_3[\text{OTs}]_3 \cdot 3\text{H}_2\text{O}\}_\infty$ , <b>9</b>	163
$\{[\text{Ca}(\text{OH}_2)_2(18\text{-crown-6})][\text{OTs}]_2\}_\infty$ , <b>10</b>	163
$[\text{Sr}(\text{OTs})_2(18\text{-crown-6})(\text{OH}_2)]_\infty$ , <b>11</b>	163
$[\text{Ba}(\text{OTs})_2(18\text{-crown-6})(\text{OH}_2)_2]_\infty$ , <b>12</b>	164
6.2 Results and Discussion	
6.2.1 Synthesis Discussion	164
6.2.2 Structural characterization of <b>9-12</b>	166
6.2.3 Hydrogen bonding in <b>9 – 12</b>	180
6.3 Thermogravimetric Analysis of <b>9 – 12</b>	181
6.4 Conclusions	183
6.5 References	184
<b>CHAPTER 7: Conclusions</b>	186

## List of Illustrative Materials: Tables

Table 1.1 Redox potential for alkaline earth metals	2
Table 1.2 Ionic radii of the alkaline earth metals	5
Table 1.3 Pauling electronegativities of the alkaline earths as compared to common atoms in organic ligands	5
Table 1.4 Examples of organic ligands used in the synthesis of MOFs	20
Table 1.5 Ionic diameter and size comparison of alkali-, alkaline earth metals vs. different polyethers' cavity sizes	34
Table 3.1 Solvent systems in the synthesis of <b>1a - c</b> and <b>2</b>	74
Table 3.2 Structural characterization for compounds <b>1a - c</b> , <b>2</b> and <b>3</b>	76
Table 3.3 Summary of selected bond lengths (Å) and angles (°) in <b>1a - c</b>	82
Table 3.4 Window sizes for <b>1a-c</b> , and {[Mg(in) <sub>2</sub> ] <sub>2</sub> ·H <sub>2</sub> O}	87
Table 3.5 Selected bond lengths (Å) and angles (°) for <b>2</b>	89
Table 3.6 Selected bond lengths (Å) and angles (°) for <b>3</b>	93
Table 3.7 TGA data for compounds <b>1a-c</b> , <b>2</b> and <b>3</b>	96
Table 4.1 Crystallographic data and structural refinement for <b>4</b>	108
Table 4.2 Selected bond lengths (Å) and angles (°) for <b>4</b>	109
Table 4.3 Selected hydrogen bonding distances (Å) for <b>4</b>	110
Table 5.1 Structural characterization for <b>5-8</b>	124
Table 5.2 Selected bond lengths (Å) and angles (°) for <b>5</b>	125
Table 5.3 Selected bond lengths (Å) and angles (°) for <b>6</b>	130
Table 5.4 Selected bond lengths (Å) and angles (°) for <b>7</b>	136

Table 5.5 Selected bond lengths (Å) and angles (°) for <b>8</b>	141
Table 5.6 Carboxylate binding motifs in <b>5-8</b>	147
Table 6.1 Metal:crown (M:C) ratio and its resulting compounds	165
Table 6.2 Crystallographic data and structural refinement for compounds <b>9-12</b>	166
Table 6.3 Selected bond lengths (Å) and angles (°) for <b>9</b>	170
Table 6.4 Selected bond lengths (Å) and angles (°) for <b>10</b>	173
Table 6.5 Selected bond lengths (Å) and angles (°) for <b>11</b>	175
Table 6.6 Selected bond lengths (Å) and angles (°) for <b>12</b>	179
Table 6.7 TGA data for compounds <b>9-12</b> and crown-ether-free tosylates	181

#### List of Illustrative Materials: Figures

Figure 1.1 Benzene molecule and $\pi$ -interactions	12
Figure 1.2 Ion association modes in alkaline earth metals	13
Figure 1.3 An example of a Cd based MOF ( $[\text{Cd}_4(\text{OH})_2(4\text{-pt})_6(\text{DMF})_4]$ )	19
Figure 1.4 From left to right: benzoic acid and 1,4-benzenedicarboxylic acid	23
Figure 1.5 (a) 5-(pyridine-4-yl)isophthalic acid and (b) 5-(pyridine-4-yl)isophthalic acid	24
Figure 1.6 From left to right: isonicotinic acid (Hin), nicotinic acid (Hnic) and picolinic acid (Hpic)	25
Figure 1.7 Stainless steel autoclave set-up	27
Figure 1.8 Type I adsorption isotherm	30
Figure 1.9 (a) 4,4'-bipyridine (b) 4,5-imidazolecarboxylic acid	32
Figure 1.10 18-crown-6	33

Figure 1.11 Coordination modes for $\text{RSO}_2\text{O}^-$ .	
From left to right $\eta^1$ ; $\eta^2$ ; $\eta^1:\mu^1$ ; $\eta^2:\mu^2$ ; $\eta^2:\mu^2$ .	36
Figure 2.1 para, meta and ortho-pyridinecarboxylic acid	57
Figure 2.2 Triflic acid	59
Figure 2.3 <i>p</i> -toluenesulfonic acid (HOTs, $\text{p}K_a = -6.56$ )	60
Figure 3.1 Pyridinecarboxylic acids and binding modes	67
Figure 3.3 Six coordinate magnesium center in <b>1a-c</b>	79
Figure 3.4 Representation of the formation of the 3-dimensional network in compounds <b>1a – c</b>	81
Figure 3.5 Rhombohedral shaped cavities in <b>1a</b> showing disordered DMF	83
Figure 3.6 Channel view of <b>1b</b> with acetonitrile guest molecules	84
Figure 3.7 Space filling plot for <b>1a</b> and calculated solvent plot for <b>1a</b>	85
Figure 3.8 The 6-coordinate metal environment in compound <b>2</b>	88
Figure 3.9 Compound <b>2</b> as seen through b-axis	90
Figure 3.10 Side by side comparison of <b>2</b> and <b>1a</b>	91
Figure 3.11 Square shaped spaces in <b>2</b>	92
Figure 3.12 Magnesium coordination environment in compound <b>3</b>	94
Figure 3.13 A chain formed by hydrogen bonding from water to nitrates and carboxylates	95
Figure 3.14 Overlay of TGA of <b>1a-c</b> , <b>2</b> and <b>3</b>	97
Figure 3.15 Thermodiffractogram of (a) <b>1a</b> and (b) <b>1b</b> and (c) <b>1c</b> from 25-300 °C	99
Figure 4.1 Zig-zag 1D chains	110

Figure 4.2 3D network showing hydrogen bonds	111
Figure 4.3 2D layers associated <i>via</i> $\pi$ --- $\pi$ interactions and hydrogen bonding	112
Figure 4.4 TGA plot for <b>4</b>	113
Figure 5.1 The 6-coordinate calcium center in <b>5</b>	126
Figure 5.2 Structural propagation in <b>5</b>	128
Figure 5.3 Coordination environment around the calcium center in <b>6</b>	129
Figure 5.4 The one-dimensional chain structure of <b>6</b>	131
Figure 5.5 The hydrogen bonded network in <b>6</b>	132
Figure 5.6 Seven coordinate strontium centers in compound <b>7</b>	134
Figure 5.7 The one-dimensional bridging motif in <b>7</b>	135
Figure 5.8 Chains formed through pyridyl metal coordination in <b>7</b>	137
Figure 5.9 A side view of <b>7</b>	138
Figure 5.10 Space filling model in <b>7</b> and oval shaped channels	140
Figure 5.11 The 7-coordinate barium center in <b>8</b>	141
Figure 5.12 2D sheets in <b>8</b>	142
Figure 5.13 Part of the 3-dimensional network in <b>8</b>	143
Figure 5.14 Comparison of structural propagation	151
Figure 5.15 TGA analysis of <b>5-8</b>	153
Figure 6.1: Ion association modes for alkaline earth metal compounds	159
Figure 6.2 Coordination environments at calcium in <b>9</b>	168
Figure 6.3 Hydrogen bonded network in <b>9</b>	170
Figure 6.4 Coordination environment at the calcium centers in compound <b>10</b>	172
Figure 6.5 Extended hydrogen bonded network of <b>10</b>	173



Figure 6.6 Graphic representation of the nine-coordinate strontium center	175
Figure 6.7 Hydrogen bonded network in <b>11</b>	176
Figure 6.8 The coordination environment on the 10-coordinate barium in compound <b>12</b>	178
Figure 6.9 The hydrogen bonded network in <b>12</b>	179
Figure 6.10 TGA overlay of the crown ether based compounds <b>9-12</b> showing water loss	182
Figure 6.11 TGA overlay of the tosylate hydrate compounds showing water loss	183

#### List of Illustrative Materials: Schemes

Scheme 1.1 Displacement of NH <sub>3</sub> by ethylenediamine	7
Scheme 2.1 Salt metathesis reaction	58
Scheme 2.2 Synthesis of M(OTs) <sub>2</sub>	61
Scheme 3.1 Synthesis of <b>1a-c</b> , <b>2</b> and <b>3</b>	72
Scheme 5.1 Synthesis of <b>5-8</b>	123
Scheme 6.1 Preparation of alkaline earth metal tosylates	165
Scheme 6.2 Synthesis of <b>9-12</b>	165

## CHAPTER 1

### The Coordination Chemistry of Alkaline Earth Metals

#### 1.0 Introduction

#### 1.1 General Properties and Applications of the Alkaline Earth Metals

The alkaline earth metals, or Group II metals, beryllium (Be), magnesium (Mg), calcium (Ca), strontium (Sr), barium (Ba) and radium (Ra) belong to a very important family in the periodic table. Unlike transition metals, in which metal-ligand bonding is achieved through *d*-orbitals, metal ligand bonding in Group II metals is dominated by interaction of the ligand with *s*-orbitals. A significant shift in properties exists for the lighter and the heavier metals, rendering the chemistry of the lighter metals beryllium and magnesium significantly different from that of calcium, strontium and barium.<sup>[1, 2]</sup> For the heavier metals, the *s*-valence electrons are easily removed under formation of the dications, as also indicated by the highly negative redox potentials of the metals (Table 1.1).<sup>[1]</sup>

**Table 1.1** Redox potential for alkaline earth metals

Element	Redox potential $E^0$ [ $M^{2+} + 2e = M(s)$ ] (V)
Be	-1.70
Mg	-2.37
Ca	-2.87
Sr	-2.89
Ba	-2.90
Ra	-2.92

As a result, the metals are highly reactive, and readily react with water or oxygen. If stored and handled under air, the surface of the metals is therefore covered with a protective oxide layer. In the absence of this layer, the metals might spontaneously ignite when exposed to water or oxygen. This property is much reduced for the lightest alkaline earth metal element, beryllium, which only reacts with hot water vapor,<sup>[3]</sup> whereas magnesium adopts an intermediate position, in which the reaction with water and oxygen is less exothermic. The heaviest alkaline earth element, radium, is radioactive, and only exists as a trace element.<sup>[4-6]</sup> It follows the trend described above: the loss of the s-valence electrons is facile, making the element highly reactive. However, only limited studies are available, due to the metals' scarcity and radioactive nature.<sup>[7, 8]</sup>

Some alkaline earth metals are very abundant in nature and have found applications in a large variety of commercial and medical fields. Beryllium and its compounds are toxic. Nevertheless, beryllium compounds are used in a range of technical applications, the most important being an

alloy with copper, yielding a significant enhancement in strength, along with improvement of heat capacity.<sup>[9]</sup>

Magnesium and calcium are non-toxic and are important minerals in the human body, with functions as diverse as enzyme co-factors<sup>[10]</sup> to being the main components of the bone structure.<sup>[11]</sup> The metals also have a wide variety of technical uses as corrosion deterrents, such as calcium phosphate coatings on magnesium alloys which express lower corrosion rates.<sup>[12]</sup> Strontium and barium are significantly less abundant. Barium and its compounds are highly toxic. There are few applications for the metals themselves, but some of their compounds have been used widely. Strontium and barium nitrates are used in pyrotechnics,<sup>[13]</sup> and barium oxide is widely used as an additive in glass ceramics.<sup>[14]</sup> Perhaps best known is the use of  $\text{BaSO}_4$  as a contrast agent in medical applications, as the compound is X-ray opaque. This is possible because of its extremely limited solubility, which limits exposure to the toxic barium ions to a minimum. However, care must be taken to remove any soluble barium salts from the  $\text{BaSO}_4$  suspension to avoid exposure. Radium has few applications, due to its scarcity and radioactivity. Its isotope, Radium-223, has found applications as a powerful cancer targeting agent.<sup>[15]</sup>

### 1.1.1 Trends in the Periodic Table

The group of alkaline earth metals serves well to analyze and rationalize chemical trends with specific properties of the metals pertaining to physical and chemical characteristics. Perhaps most obvious is the increase of size as atomic number increases. Indeed, barium (and radium) are amongst the largest elements in the periodic table, only surpassed by the heaviest alkali metals. Table 1.2 summarizes the size of the metals and their respective dications. Along with the significant size, come multiple properties. The lightest elements have the highest charge/size ratios, resulting in a significant polarization of metal ligand bonds. It is this property that dictates the organometallic chemistry of beryllium and magnesium, as the covalence of the compounds is significantly greater than that of the heavier analogues. This effect is further exacerbated by the decrease in electronegativity for the heavier elements (Table 1.3), introducing increased polarity (or ionicity) in a given metal-ligand bond. This goes hand-in-hand with an unfavorable overlap of the large metal centers and the smaller ligand orbitals. These combined factors result in weak-metal-ligand bonds, making the compounds rather labile. For the heavier metals, the small covalent bond contribution results in mainly electrostatic metal-ligand bonding, that is governed by the need for steric saturation. As mentioned above, except for the heaviest elements, d-orbitals are energetically not available for bonding in the alkaline earth metals. This results in the absence of orbital controlled coordination chemistry. As such, compound geometry is difficult to control, as many factors may contribute towards the steric saturation of the complexes.

The large metal size also results in a significant tendency towards aggregation and the formation of sparingly soluble compounds. Aggregation may be suppressed by the use of sterically demanding or multidentate ligands, often in combination with Lewis donors, which again may be mono or multidentate. Non-covalent, secondary interactions also serve an important

role in suppressing aggregation, although much less is known about how these can be used in a rationale fashion.

**Table 1.2** Ionic radii of the alkaline earth metals

Ae <sup>2+</sup>	CN	IR (ionic radii) <sup>[16]</sup>
Be	6	0.45
Mg	6	0.72
Ca	6	1.00
Sr	6	1.18
Ba	6	1.35

**Table 1.3** Pauling electronegativities of the alkaline earths as compared to common atoms in organic ligands

Element	EN <sup>[17,18]</sup>
Be	1.47
Mg	1.23
Ca	1.04
Sr	0.99
Ba	0.89
H	2.20
C	2.50
N	3.07
O	3.50
S	2.44

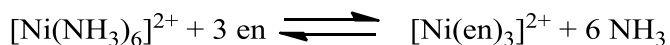
### 1.1.2 Coordinative Saturation

As outlined above, the coordination chemistry of the alkaline earth metals is driven by the sum and characteristics of the metal-ligand bonds (covalent and electrostatic contributions). As the size of the metals increases, the number of contacts increases; however, the overall bond strength weakens.

The smaller metals (Be and Mg) usually have lower coordination numbers (4-6) than the larger, heavier metals (Ca-Ba) (6-10),<sup>[1]</sup> depending on the size and nature of the ligands and donors. For the heavier metal compounds, aggregation is a common observation, with the formation of complex coordination polymers of low solubility. Aggregation may be suppressed by the judicious introduction of co-ligands satisfy the metal's coordination sphere. This will be discussed further in **Section 1.3.6**.

### 1.1.3 Chelate Effect

As mentioned above, co-ligand coordination is a key strategy in controlling metal coordination. Co-ligands may be monodentate (e.g., tetrahydrofuran) or multidentate, as for example in the crown ether 18-crown-6, in which typically six metal-crown interactions are observed.<sup>[19]</sup> The chelate effect is largely an entropic process governed by the Gibbs free energy formula ( $\Delta G = \Delta H - T\Delta S$ ).<sup>[20]</sup> A textbook example of the chelate effect can be the substitution of 6 NH<sub>3</sub> molecules by 3 ethylenediamine (en) co-ligands in [Ni(NH<sub>3</sub>)<sub>6</sub>]<sup>2+</sup> (Scheme 1.1).<sup>[18]</sup>



**Scheme 1.1** Displacement of  $\text{NH}_3$  by ethylenediamine

As coordination of ethylenediamine and ammonia is largely similar in enthalpy, the change in entropy drives the reaction, as expressed by the number of co-ligands present at the beginning and end of the reaction. Thus, in the reaction above, there are four species on the left and seven species on the right resulting in a significant increase in the entropy of reaction. The resulting “chelate complex” will be the more thermodynamically stable species.

The tendency of a complex to adopt a certain coordination chemistry or aggregation state further depends on the ability of the ligand to bridge neighboring metal centers and the ability of ligands and co-ligands to engage in non-covalent interactions. Other factors to consider in the chelating process include the steric properties of the ligand, which in the case of multidentate ligands is dictated by the bite angle which will determine the chelating power of the co-ligand.<sup>[20-22]</sup>

## 1.2 Non-covalent interactions in alkaline earth coordination polymers

A range of non-covalent interactions have been reported. Often these interactions have important structure-determining effects. Non-covalent interactions include hydrogen bonding interactions, agostic interactions,  $\text{M}\cdots\text{F}$  interactions,  $\pi$ - $\pi$  stacking interactions, and  $\pi\cdots\text{H-C}$  bonding<sup>[23]</sup> amongst others. This section deals with hydrogen bonding and  $\pi$ - $\pi$  stacking interactions, as they both have relevance to the structures described in this thesis.



### 1.2.1 Hydrogen bonding

Hydrogen bonding is a well-studied, important structure-determining force.<sup>[24-26]</sup> Commonly, the synthesis of coordination complexes under aqueous conditions leads to the formation of networks exclusively or partially held together *via* hydrogen bonding interactions.<sup>[27]</sup> A hydrogen bond involves a D-H...A moiety, with D being a donor (e.g. the oxygen atom in H<sub>2</sub>O; other typical donors are nitrogen or fluoride) whilst A is the proton acceptor, typically fluorine, oxygen, nitrogen or less common sulfur. Theoretical studies reported in a review by Steiner<sup>[28]</sup> place the overall energy of hydrogen bonds in the wide range from the weakest, -0.2 kcal mol<sup>-1</sup> (hydrogen bond in CH<sub>4</sub>...F-CH<sub>3</sub>) to the strongest, -40 kcal mol<sup>-1</sup> (hydrogen bond in [F-H-F]<sup>-</sup>) (for more information see Table 1 of reference [40]).

The strength of the hydrogen bond is determined by several factors including the bond angles and length of H...A. The strength of a hydrogen bond is inversely proportional to its length: a weak hydrogen interaction is typically longer than 2.2 Å for H...A (electrostatic and dispersion forces) whereas a strong interaction is found in the range of 1.2 to 1.5 Å for H...A. This interaction is considered strongly covalent.<sup>[29]</sup> Frequently, the strength of hydrogen interactions depend on the type of donor-acceptor atoms involved. However, locating hydrogen bonds from an X-ray diffraction experiment is difficult.

Since hydrogen bonding is of critical importance to the structural propagation of some of the compounds reported in this thesis, the following section will offer details about the crystallographic location and refinement of hydrogen atoms and hydrogen bonds.

### 1.2.2 Crystallographic location of hydrogen bonds

Locating hydrogen atoms in a Fourier difference map can be a difficult task.<sup>[30]</sup> This is related to the X-ray diffraction experiment, in which hydrogen's scattering power is very low. Specifically, in a D-H bond, the electronegativity of the donor atom causes a withdrawal of electron density from the hydrogen atom towards the bond formed, which contributes to large experimental uncertainties.<sup>[28, 30, 31]</sup> The result is an electron deficiency in hydrogen, which causes an averaging of the hydrogen atom's position relative to the donor atom, thus increasing the challenge of locating the hydrogen atom in the Fourier map. As hydrogen bonding, as also shown extensively in this thesis is a major structure determining force, the location of these interactions is important.

Though locating hydrogen atoms can be a difficult task, it is necessary to locate them since they are integral to the structural characteristics. Crystallographically, there are two ways to identify hydrogen atoms in a molecular structure: (a) chemical sense (for example, locating the oxygen of a water molecule and assigning a position on the basis of O-H bond lengths and H-O-H angles) and (b) placement of hydrogen atoms on calculated positions. It is necessary to mention that the mobility of the hydrogen atom makes the D-H bond appear shorter than it really is; thus, D-H distances found in the Fourier map are typically less than 1 Å.

An effective way to obtain good hydrogen binding data is to perform neutron diffraction experiments. Considered by many complementary to X-ray diffraction, neutron diffraction has been a successful technique in the elucidation of structures in areas such as biology<sup>[32]</sup> and

material sciences.<sup>[33]</sup> Hydrogen and its isotope, deuterium, are strong neutron scatterers, as opposed to X-ray scatterers.<sup>[34]</sup>

When the hydrogen atoms are located and assigned to positions, these positions must be refined to improve accuracy of data. The hydrogens can be stabilized by applying positional restraints (through the refinement software, some examples include DFIX and DANG) which improve the accuracy of the distances.

Frequently, it is not possible to locate hydrogen atoms in the Fourier difference map. Water of crystallization, for example, often exists as disordered species, preventing the location of hydrogen atoms.

In this work, wherever possible, hydrogen atoms in water molecules, on oxygen or nitrogen atoms were located in the Fourier difference map and included in the refinement using positional restraints. Non-water bound hydrogens (hydrogens on carbon atoms etc.) were fixed to calculated positions. Hydrogens on some waters of crystallization could not be located.

### 1.2.3 $\pi$ -stacking interactions in metal organic complexes 00000

Extended structures of coordination polymers containing aromatic ligands (or ligands with aromatic moieties) often display  $\pi$ -stacking interactions. These interactions arise from the intermolecular attraction of aromatic molecules or moieties. They are typically weak result in distances longer than the sum of van der Waals radii (carbon); thus, the atoms do not touch. These are not to be confused with the  $\pi$ -ion interactions that occur with some cations<sup>[35-37]</sup> or anions<sup>[38-40]</sup> (e.g. cation: metal- $\pi$  or anion: halogen- $\pi$ ). They are also non-covalent.

$\pi$ -stacking interactions have been known to play important structural roles, such as in the stabilization of the vertical base-base interaction in the double helix structure of DNA,<sup>[41]</sup> or the packing structure of aromatic molecules in crystals.<sup>[42]</sup> They thus offer stability in inclusion complexes and novel optical materials.<sup>[43]</sup> An extensive literature is available regarding the interactions between aromatic molecules in solution and in the solid state.<sup>[44]</sup>

What arises during  $\pi$ - $\pi$  stacking interactions depends on the type of  $\pi$ -interaction involved, as shown in Figure 1.1b-d with the benzene dimer. The benzene molecule has a delocalized molecular orbital with a  $\delta^-$  charge above and below the plane of the molecule, whilst the hydrogens on the ring possess partial positive charges,  $\delta^+$  (Figure 1.1a). At least three types of interactions are commonly reported:

(1) For eclipsed interactions (face-to-face) (Figure 1.1b), the hydrogen atoms and the delocalized  $\pi$ -orbitals come into direct contact with their counterparts on the other ring. This brings like charges in proximity, causing repulsion. (2) In the edge-to-face mode (Figure 1.1c), the hydrogen atoms on the ring actively interact with the delocalized  $\pi$ -orbitals in a weak C-H--- $\pi$  type interaction (weak hydrogen bond). (3) The offset motif finds hydrogens from both rings displaced over the aromatic  $\pi$ -cloud (Figure 1.1d).

The stability of these conformations can be related to the stabilizing arrangements arising from the quadrupole moments between the aromatic rings.<sup>[45]</sup> *Ab initio* calculations have demonstrated that edge-to-face and offset interactions are the most stable, since they minimize repulsion and maximize the partial charge interactions between the aromatic systems and hydrogens.<sup>[46, 47]</sup>

Finally, the distances between aromatic rings are obtained by measuring centroid-to-centroid distances. Typically, distances for the edge-to-face mode can reach values of up to 5 Å or greater,<sup>[48]</sup> whilst the face-to-face configurations are within 3.3-3.6 Å in a crystal structure.<sup>[49]</sup>

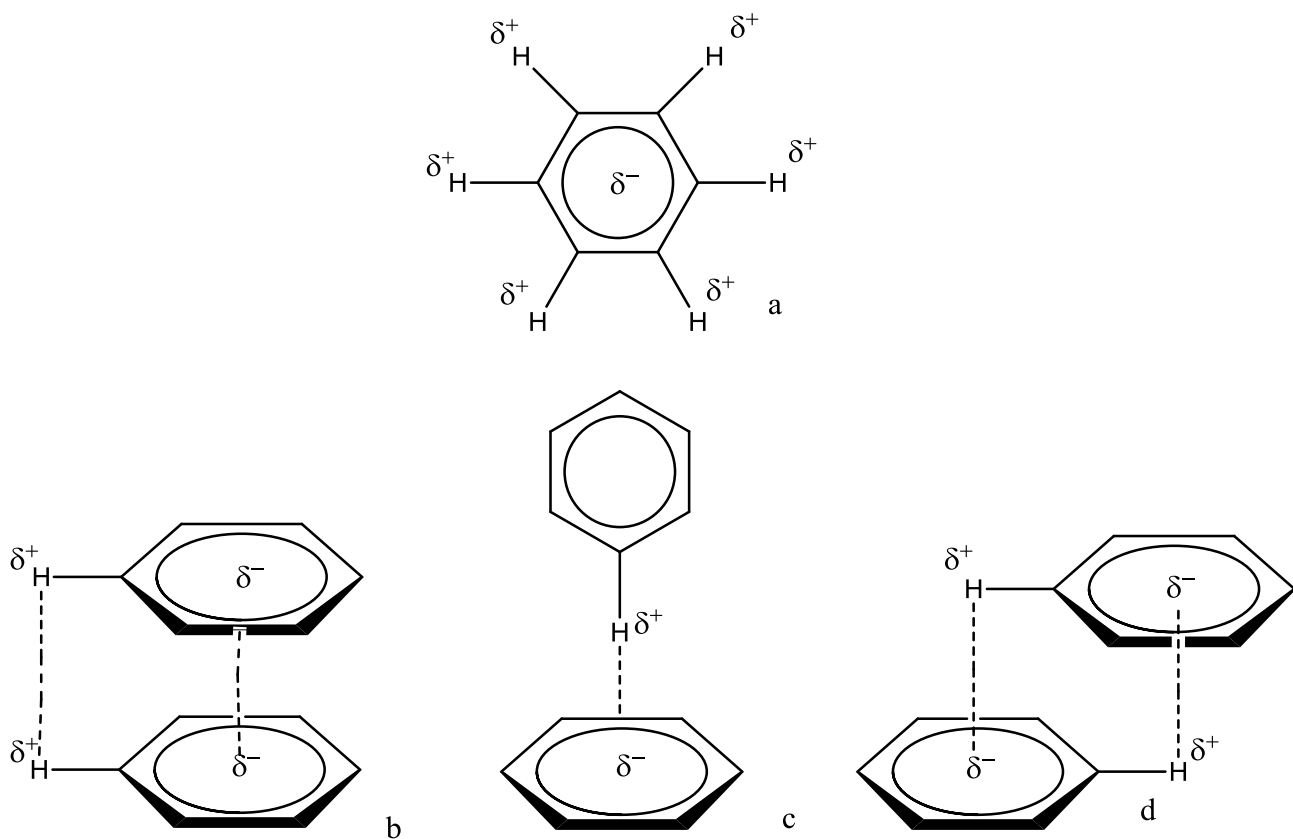


**Figure 1.1** (a) The relative charges of the benzene molecule,  $\pi$ -interactions from left to right: (b) face-to-face (eclipsed), (c) edge-to-face and (d) offset

### 1.2.4 Ion association

For the alkaline earth metals, the metal ions may be coordinated to ligands in three ways: (i) contact molecules, with two ligands bound to the metal center, (ii) contact separated, with one ligand metal bound, whereas the other is unassociated, and (iii) dissociated ions with both ligands being unassociated. The three different association modes are illustrated in Figure 1.2. The type of ion association depends on metal-ligand bond strengths and metal-co-ligand bond strengths, in which the chelate effect (see **Chapter 6**) plays a major role. This is nicely demonstrated by complexes involving crown ethers, where separated ions are commonly observed.

Additional factors affecting ion association include the ability of the ligand to distribute negative charge. As charge density on the ligand decreases, the propensity for separated ions increases. More commonly, a complex equilibrium exists, with a range of factors governing the ion association. The resulting structures include a summation over all the different factors, making the prediction of structural features very challenging.

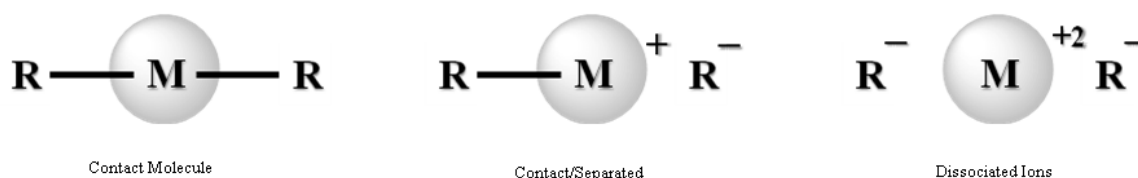


**Figure 1.2** Ion association modes in alkaline earth metals

### 1.3 Some Applications of Alkaline Earth Metal Materials

#### 1.3.1 Organometallics

The exploration of novel organoalkaline earth metal species is essential for the progress of a variety of fields. For example, metal organic chemical vapor deposition (MOCVD) is widely used for the manufacture of electronic or photonic materials, such as thin films of barium-strontium-titanate films for photonic applications ( $\text{Ba}_x\text{Sr}_{1-x}\text{TiO}_3$ ).<sup>[50]</sup> Other examples include various semiconducting materials, where doping with alkaline earth metals is a key technique.<sup>[51]</sup>

MOCVD involves the volatilization of an organometallic or metalorganic precursor followed by decomposition and deposition on a substrate. Key properties for suitable MOCVD materials include high volatility and sufficient thermal stability to allow the transport of the metal through the gas phase onto the substrate.<sup>[52]</sup> This is followed by the requirement of efficient decomposition to yield the desired compounds (typically oxides) in high purity without impurities imposed by the precursors (such as carbon or fluorine).<sup>[53, 54]</sup> Further, to allow for an efficient industrial process, the substrate must volatilize completely with no or little residue.<sup>[55, 56]</sup>

Frequently used alkaline earth MOCVD precursors include the bidentate  $\beta$ -diketonates<sup>[57]</sup> in which the bidentate nature of the ligand provides sufficient bulk to suppress extensive aggregation and thus offers sufficient volatility and low sublimation temperatures.<sup>[56]</sup> Other MOCVD precursors are based on fluoroalkoxides, a family of compounds recently examined in the Ruhlandt group at Syracuse University.<sup>[58]</sup> The perfluorinated  $\text{OC}(\text{CF}_3)_3$  alkoxide has shown exceptional promise, with low sublimation temperatures, minimal left-over residues, and air stability, to allow for easy handling.

Other uses for metal organic and organometallic alkaline earth species include their use as starting materials for other alkaline earth complexes. Examples are the alkaline earth amides  $M(\text{HMDS})_2(\text{thf})_2$ , ( $\text{HMDS} = \text{N}(\text{SiMe}_3)_3$ ;  $M = \text{Mg}, \text{Ca}, \text{Sr}$  and  $\text{Ba}$ ), which have been extensively employed in the synthesis of heavy alkaline earth metal organometallics *via* transamination. The amides can be obtained through a variety of routes,<sup>[59]</sup> and their versatile application in synthesis allowed our group to synthesize some of the first strontium and barium sigma bonded alkaline earth organometallics.<sup>[22, 60]</sup>

More recent uses for organometallic and metalorganic alkaline earth species are in catalysis for processes including hydroamination, hydrophosphination, and hydrosilylation.<sup>[2]</sup> These methods rely on earth-abundant metals, specifically calcium, which poses no waste problem. Specifically, hydroamination can be used for the efficient preparation of organonitrogen compounds, which are key ingredients in a variety of chemicals, such as dyes and the synthesis of substances found in nature. An impressive example is the DIPP-nacnac based heteroleptic calcium amide, which proved to be highly active catalyst for the intramolecular hydroamination/cyclization reaction.<sup>[61, 62]</sup>



### 1.3.2 Hydrogen Storage

Decreasing fossil fuel supplies, along with environmental concerns, are prompting the development of alternative energy sources. Among these, hydrogen storage technology and the production of “clean” fuels are key components of a complex plan that is geared to decrease the dependence from fossil fuels, while decreasing the carbon footprint.<sup>[63]</sup>

With three times higher energy content than gasoline on a weight basis ( $H_2 = 123 \text{ MJ/kg}^{-1}$ , gas =  $47.2 \text{ MJ/kg}^{-1}$ ),<sup>[64]</sup> hydrogen poses attractiveness as an energy carrier due to its clean combustion into water, *via* controlled combustion in a PEM (proton exchange membrane) fuel cell.<sup>[65]</sup> Hydrogen in its compounds is widely abundant, and multiple techniques for its production are known. Common sources for hydrogen gas are biomass,<sup>[66]</sup> coal gasification<sup>[67]</sup> or water-splitting through electrolysis.<sup>[68]</sup> However, all these techniques require significant amounts of energy; thus hydrogen technology is not without drawbacks. One of the current challenges includes the safe and efficient storage of the flammable hydrogen gas in onboard compressed gas tanks.

The use of hydrogen as fuel in fuel-cell powered vehicles requires the availability of cost effective and safe systems that offer rapid and reversible adsorption/desorption of hydrogen with minimal energetic input and thermodynamic effects. Ideally, a hydrogen storage device would operate at or at near ambient temperatures (between room temperature and  $80^\circ\text{C}$ ) and moderate pressures ( $<100 \text{ bar}$ ). Storage values for such systems have been set by the Department of Energy, which has requested capacities of 5.5% by weight by 2017. Yet, despite numerous efforts, no proposed system has come close to these values, as the current state of the art systems

suffer from insufficient storage capacity, unsafe operational conditions, unacceptable reversibility, unacceptable thermodynamics, and expensive, bulky storage tanks.<sup>[69]</sup>

In a vehicle, these tanks require high pressures and negative temperatures (-256 °C) posing a safety hazard to the driver. Furthermore, frequently, leakage has been detected, which not only pose a safety hazard, but also results in the loss of efficiency.<sup>[70]</sup> As such, alternative, solid state based hydrogen storage systems involving the light weight lithium and magnesium metals have been envisioned as a storage alternative to gaseous or liquid hydrogen.

The most common form of solid-state hydrogen storage material is the metal hydride. MgH<sub>2</sub> has been extensively studied as a potential storage material due to its high content of hydrogen (8% by wt.).<sup>[71]</sup> However, high temperatures are required to release hydrogen from the hydride, making the material less attractive. Other metal hydrides, such as LiH or NaH, offer an even larger hydrogen weight percentage, but their activation temperatures are even higher.<sup>[72, 73]</sup>

Attempts to lower the activation temperatures by the reduction of particle sizes through ball-milling have not been met with success, because frequent oxidation of the hydrides was observed.<sup>[74-76]</sup> Further, attempts at synthesizing mixed alkali- alkaline earth metal hydrides in solution (specifically Li/Mg)<sup>[77]</sup> in order to increase the amount of hydrogen stored have been successful, yet the low solubility of the materials leads to the formation of mixed phases and hard to separate solids.<sup>[78]</sup>

Other hydride sources, including the complex hydrides LiAlH<sub>4</sub>,<sup>[79, 80]</sup> NaAlH<sub>4</sub><sup>[81]</sup> and LiNH<sub>2</sub> (metal amides) have also been examined as storage materials. Yet, these frequently involve difficult to monitor reaction mechanisms upon activation and are often irreversible.<sup>[82, 83]</sup>

Other work is focusing on aminoboranes, NH<sub>3</sub>BH<sub>3</sub> and amidoboranes (e.g. M(NH<sub>2</sub>BH<sub>3</sub>)<sub>x</sub>, M = Mg,<sup>[84]</sup> Ca,<sup>[85]</sup> x = 2; M = Na,<sup>[86]</sup> Li,<sup>[87, 88]</sup> x = 1). These compounds provide a very high

hydrogen content (up to 18% for  $\text{NH}_3\text{BH}_3$ ), yet the thermal decomposition of aminoborane involves the irreversible formation of borazine and BN, making the materials unsuitable for reversible storage.<sup>[89]</sup>

## 1.4 Alkaline earth metal coordination polymers

### 1.4.1 Porous coordination polymers: Metal Organic Frameworks – Structure and Composition

Chapters 3-5 of this thesis describe our research on the synthesis and characterization of s-block (Mg, Ca, Sr and Ba) based metal organic frameworks (MOFs). MOFs are coordination compounds involving a metal center and organic ligands, with the metal centers binding to organic ligands to form infinite three-dimensional motifs, often exhibiting channels which can be occupied by guest molecules. Early work on MOFs was mainly focused on transition metals such Zn,<sup>[90-92]</sup> Cd<sup>[93, 94]</sup>, and main group elements such as Al,<sup>[95]</sup> and involved aromatic carboxylate ligands with specific substitution patterns, including 1,4-benzenedicarboxylic acid<sup>[96, 97]</sup> or trimesic acid, 1,3,5-benzenetricarboxylic acid.<sup>[98, 99]</sup> Perhaps the most prominent of such examples include MOF-5, a coordination polymer involving zinc and 1,4-benzenedicarboxylic acid.<sup>[100]</sup> The combination of copper with 1,3,5-benzenetricarboxylic acid results in the well-studied HKUST-1 MOFs, that are commercially available for gas separation purposes.<sup>[101]</sup> Figure 1.3 shows an example of a MOF.

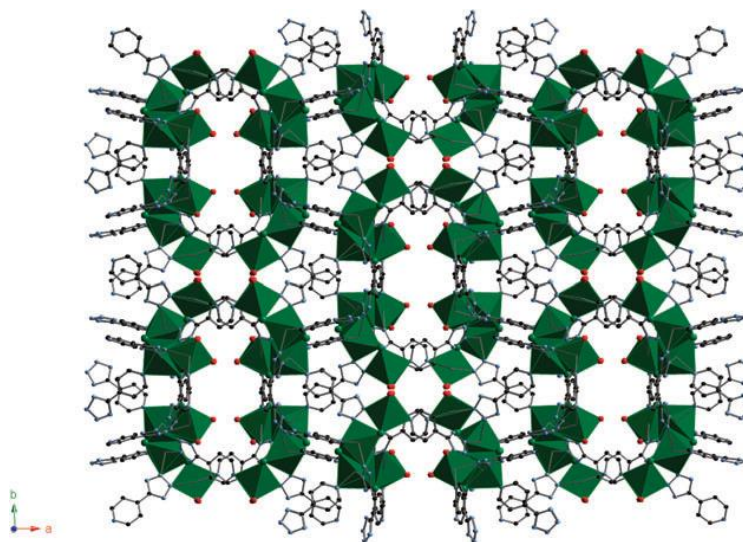


**Figure 1.3** An example of a Cd based MOF ( $[\text{Cd}_4(\text{OH})_2(4\text{-pt})_6(\text{DMF})_4]^{102}$  (pt = 4-pyridyltetrazolate)

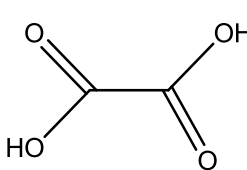
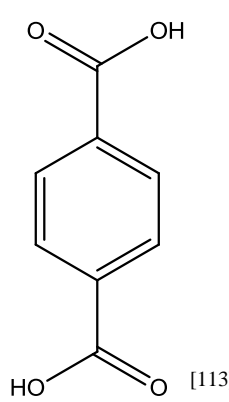
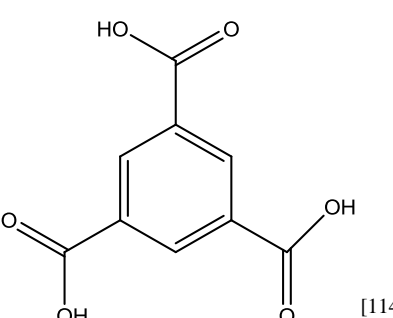
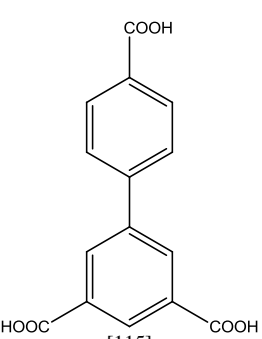
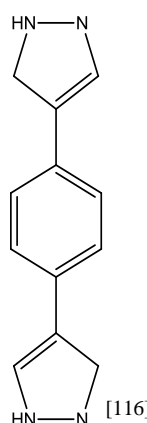
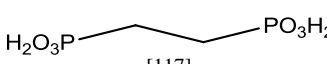
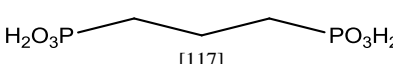
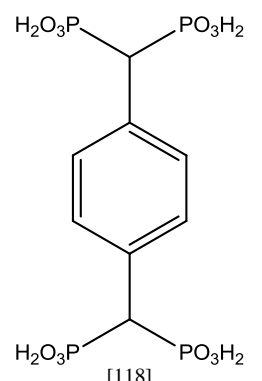
As mentioned above, a MOF structure is determined by the metal center and the ligands. The nature of the metal center will determine factors such as bond strength, coordination number and propensity towards aggregation. The smallest metal,  $\text{Be}^{2+}$ , has been reported to afford microporous MOFs,<sup>[103, 104]</sup> yet Be is toxic and not desirable for day-to-day applications. The larger metals, such as lanthanides, have afforded dense non-porous systems that sparked an interest as luminescent devices.<sup>[105]</sup>

The second building blocks of MOFs are the organic ligands. The organic ligands are important structure-determining factors. Structural dimensionality (0D  $\rightarrow$  3D) can be obtained by using ligands that possess unique substitution points (e.g. O-, N-,  $\text{NH}_2$ , -OH, -COOH) and substitution patterns, imparting specific symmetries.<sup>[106-108]</sup>

The combination of the ligand-metal subunits are called SBUs (secondary building units). SBUs typically consist of small metal-ligand clusters, associated by the organic ligands. They are

crucial to the formation of extended networks.<sup>[109-111]</sup> Table 1.4 shows examples of organic ligands frequently used in MOF synthesis.

**Table 1.4** Examples of organic ligands used in the synthesis of MOFs

Examples of Organic Ligands			
 [112]	 [113]	 [114]	 [115]
 [116]	 [117]	 [117]	 [118]

Frequently, MOFs are prepared *via* simple acid base chemistry, involving a metal salt (e.g. nitrate, acetate, iodide, chloride) and an acidic ligand.<sup>[119]</sup> Depending on the metal, mineralizers such as HF, HCl, NaOH aid in dissolving the reagents and provide crystalline products.<sup>[120, 121]</sup>

One of the major challenge in MOF synthesis is the unpredictability of the resulting structures.<sup>[122]</sup> The combination of a given ligand and metal center may afford a myriad of products, depending on factors such as solvents, which may be applied as mixtures of polar and non-polar solvents,<sup>[95, 123]</sup> reaction temperatures,<sup>[124, 125]</sup> reaction duration; and pressure;<sup>[126]</sup> reaction pH;<sup>[127]</sup> the presence of co-ligands or mineralizers; and others.<sup>[128]</sup> Frequently, modern MOF synthesis makes use of combinatorial, automated high-throughput methods screening thousands of reaction conditions, to pinpoint the required synthetic conditions for the production of the desired materials.<sup>[129-131]</sup>

Lastly, many MOFs exhibit special structural features such as channels,<sup>[132]</sup> the inclusion of guest molecules in cavities and channels,<sup>[133, 134]</sup> and hydrophobic or hydrophilic moieties in the channels<sup>[135]</sup> that allow the interaction with guest molecules through electrostatic or hydrogen bonding interactions. These will be discussed in detail in the following sections.

### 1.4.2 Alkaline earth metal organic frameworks

The spherical nature of the *s* orbital makes the metal-ligand bond strength non-directional. Further, due to the large metal size, especially in the heavy alkaline earth metals, the poor metal-ligand orbital overlap renders the bond weak and labile. Metal-ligand bonds are predominately ionic in nature; thus the coordination environment of the metals is driven by the tendency towards coordinative saturation, and the completion of the metals' coordination environment is influenced by many competing factors. As a result, few alkaline earth-metal based MOFs are

known.<sup>[136-140]</sup> The absence of MOFs for group II metals is more evident for the heavier metals for which there is a larger tendency towards aggregation and insoluble, unidentifiable solids may form. Moreover, the highly oxophilic and hydrophilic nature of the metals often causes the formation of dense hydrogen bonded networks as opposed to 3D open frameworks.<sup>[141-143]</sup>

### 1.4.3 Effect of Ligand Topology on MOF Dimensionality

As illustrated in a recent review article by Paz *et al.*,<sup>[144]</sup> the ligand nature and type have a profound influence on the overall MOF structure. Functional frameworks arise from the combination of several factors, including the nature of the ligands<sup>[145, 146]</sup> and the properties of the metal centers they connect to (e.g. coordination numbers, metal sizes, metal coordination environments).<sup>[140, 147]</sup> Ligands might be obtained commercially, or prepared by organic synthesis.<sup>[148, 149]</sup> The modification of pre-determined ligands<sup>[150-153]</sup> *in situ* during reaction process has also been reported.

An exciting method for custom modification involves post-synthetic modification techniques utilizing metalloligands<sup>[154]</sup> through the “building-block upon building block” approach. This technique involves the modification of pre-existing frameworks and attachment of SBUs (such as metal oxalates<sup>[155]</sup>, donor solvents<sup>[156]</sup> or other small molecular building blocks<sup>[157, 158]</sup>) in efforts to further tailor the framework properties or produce larger supramolecular networks.

Formation of open-frameworks requires ligands which prevent the formation of dense coordination polymers and that also allow the propagation of the network. Multi-topic ligands provide additional anchor points for the formation of extended networks.<sup>[159-161]</sup>

A nice demonstration on how ligand modification, and thus the introduction of the multi-topic ligands principle permits the formation of extended higher dimensional networks is provided by benzoic acid. Unsubstituted benzoic acid in conjunction with zinc<sup>[162]</sup> and other metals (e.g. Cd<sup>[163]</sup>, Al<sup>[164]</sup>) has been reported to afford linear polymeric chains as non-porous solids. The modification of benzoic acid with other substituents (such as azolates,<sup>[165, 166]</sup> phenyls<sup>[167, 168]</sup> and carboxylates<sup>[169]</sup>) affords a variety of three-dimensional open frameworks with interesting characteristics.

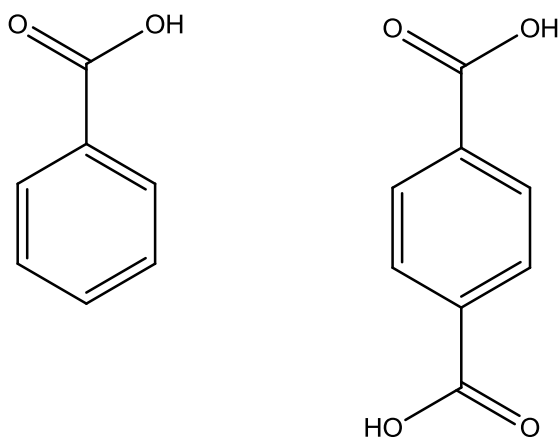


**Figure 1.4** From left to right: benzoic acid and 1,4-benzenedicarboxylic acid

Thus, the functionalization of simple, rigid ligands can provide further avenues for metal coordination and the formation of stable three-dimensional networks. The ligands utilized in this work have two different binding points, carboxylate and pyridyl nitrogen, as discussed in detail in the next section.



### 1.4.4 Multi-topic Ligands: Carboxylate and Nitrogen Binding Sites

The implementation of ligands containing carboxylate-oxygen and pyridyl-nitrogen functions has been shown to produce stable three-dimensional frameworks.<sup>[170]</sup> Ligands which possessing these anchor points will bind to the metal center on the basis of the “softness” or “hardness” of the metal.<sup>[171, 172]</sup>

As an example, Du *et al.*<sup>[173]</sup> reported on the specific fine-tuning of the pore sizes of two Cu MOFs by the use of ligands with different substitution patterns, including the N-donor sites in 5-(pyridine-4-yl)isophthalic acid and 5-(pyridine-4-yl)isophthalic acid (Figure 1.5a-b). While the overall characteristics of both frameworks were similar, the different nitrogen atom positions caused a change in cavity size.

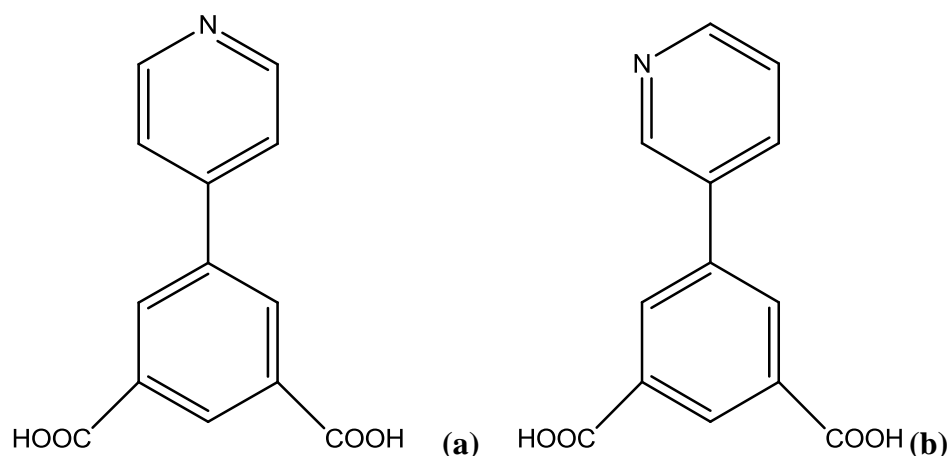


**Figure 1.5** (a) 5-(pyridine-4-yl)isophthalic acid and (b) 5-(pyridine-4-yl)isophthalic acid

### 1.4.5 Isonicotinic acid, nicotinic acid, picolinic acid

The ligands used in this work are the family of pyridinecarboxylic acids: isonicotinic acid, nicotinic acid and picolinic acid (Figure 1.6). These are commercially available and cost effective (\$17-20 per 100 g). Their metal complexes have recently found interest as luminescence sensors<sup>[174, 175]</sup> and non-linear optic materials.<sup>[176]</sup> The ligands' ability to function as linkers in MOF chemistry has also been met with success.<sup>[177]</sup>

The pyridinecarboxylic acid ligands possess two unique binding points. The ligands are monoanionic, with the carboxylic acid moiety being deprotonated, whilst the N-pyridyl donor site is capable of donating electrons to a metal center. Further, the shift of the N-pyridyl atom into *para*, *meta* or *ortho* positions, allows for the systematic investigation of ligand geometry on the overall structural features of the resulting solid. The use of pyridinecarboxylic acid ligands allowed for the isolation of several novel alkaline earth coordination polymers; their synthesis and characterization is described in **Chapters 3 - 5** of this thesis.

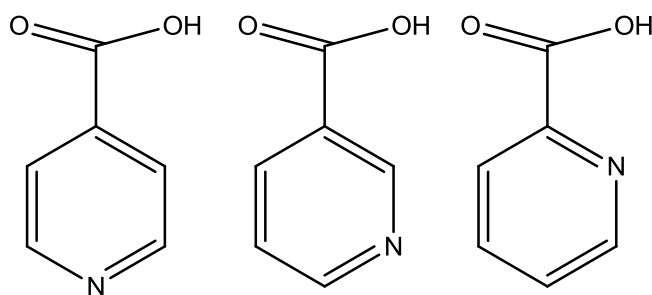


**Figure 1.6** from left to right: isonicotinic acid (Hin), nicotinic acid (Hnic) and picolinic acid (Hpic)

### 1.4.6. Hydrothermal and Solvothermal Crystallization

The preferred crystallization routes for metal organic frameworks are through hydrothermal and solvothermal methods. Hydrothermal methods involve the use of low temperatures (typically 100-300 °C), with pressures ranging from 20-25 mmTorr in the presence of water, whilst solvothermal methods rely on the use of polar organic solvents, with conditions similar to those used in the hydrothermal regimen.

An important factor is that the reactions are carried out in closed containers above the boiling point of the solvent. The resulting high pressure affords increased solubility to provide the conditions for crystal growth.<sup>[178]</sup>

The use of autoclaves, also called digestion bombs, is very common in MOF synthesis (Figure 1.7). The autoclaves are chemically resistant stainless steel vessels outfitted with Teflon (polytetrafluoroethylene) lined cups in which the reaction takes place. The autoclaves are available in several different sizes; the most common one has a fill volume of about 10 mL. The cups are filled with the desired solvent mixtures and the bombs closed tightly. The readied bombs are then placed in ovens at constant temperatures (85-200 °C).

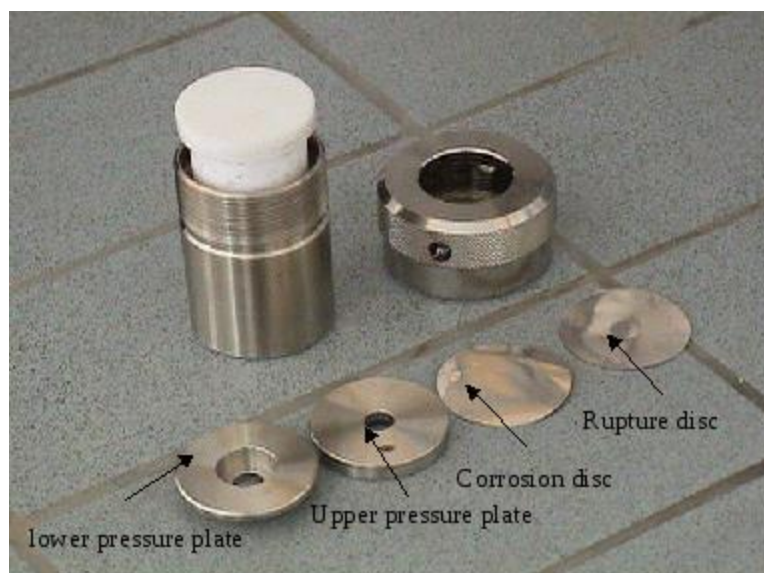


**Figure 1.7** Stainless steel autoclave set-up<sup>[179]</sup>

The stainless steel bombs allow pressures of up to 200 bar. The different sizes allow the easy scale-ups of the reactions. However, as the reaction takes place in closed containers, direct monitoring of the reaction and potential crystal formation is not possible.

An alternative technology is based on the use of Carius tubes. These are thick-walled glass tubes that are, after filling, cooled in a liquid nitrogen bath and sealed under vacuum to provide a closed reaction container. The fill volume of Carius tubes is typically smaller (max. 4 mL or less) and the maximum pressure is limited to 10 bars. It is essential to carefully seal the Carius tubes to avoid tension in the glass that may lead to potential explosion in the oven. Carius tubes are always used with an additional safety measure: they are placed inside the oven in a metal liner that is crimped on one end. The crimped end is pointed towards the oven door, while the open end points towards the back of the oven. Temperatures above 150 °C are not recommended for safety reasons.

### 1.4.7 Reaction variables: effect of solvent in MOFs

As the synthesis of MOFs is highly dependent on reaction conditions, many variables need to be carefully monitored and examined. Perhaps the most important factor is provided by the solvent and, if applicable, the presence of co-ligands. Solvents may (a) coordinate to metal centers, (b) be guest molecules, (c) serve as both guest and ligand, (d) serve as indirect structure directing agents (SDAs).<sup>[180]</sup>

The ability of solvents to coordinate to the metal centers is directly correlated to their base strength. In analogy to coordination compounds, solvents or co-ligands containing N, O or S donor atoms will have coordination preferences that depend on the “softness” or “hardness” of the metal center.<sup>[171]</sup> The removal of these metal-coordinated solvents can result in either an unsaturated metal center<sup>[181-183]</sup> or the collapse of the structure.<sup>[184]</sup>

The influence of solvents and co-ligands, and their role as donor and guest, was demonstrated with a Cd(II) based *S*-spaced-4,4'-bipyridine. Different solvent mixtures (ACN/CH<sub>2</sub>Cl<sub>2</sub>, MeOH/CH<sub>2</sub>Cl<sub>2</sub> and DMF/CH<sub>2</sub>Cl<sub>2</sub>) afforded structures of one, two and three-dimensions depending on the solvent system used.<sup>[185]</sup>

Solvents which do not incorporate into the resulting structures, but play an important role in the crystallization of the material, are denominated SDAs (structure directing agents).<sup>[186]</sup> Furthermore, quite a few examples of MOFs demonstrate single-crystal to single-crystal transformations<sup>[187]</sup> by the exchange of the guest through soaking experiments. This often results in structural changes.

### 1.4.8 Hydrogen storage in alkaline earth MOFs

The microporous MOFs have been studied as potential hydrogen storage materials.<sup>[188, 189]</sup> As hydrogen would be incorporated in pores and channels, hydrogen could be rapidly absorbed and desorbed, providing a solution to the high activation energy, insoluble side products, and irreversible hydrogenation cycles observed with many of the hydride or ammonia borane based materials, as described in **Section 1.3.2**.

A MOF is characterized as a potential hydrogen storage material if it exhibits permanent porosity, determined by N<sub>2</sub> adsorption isotherm analysis. These experiments are typically conducted at liquid N<sub>2</sub> temperatures; low dosages of hydrogen are pumped into the sample holder and the adsorption measured.

There are five types of adsorption isotherms and these are determined by their shapes. The microporous MOFs show Type I isotherms (Figure 1.8) in an N<sub>2</sub> adsorption analysis curve. Often, higher BET (Brunauer Emmett Teller) surface areas (in some cases up to 6240 m<sup>2</sup>g<sup>-1</sup> for MOF-210)<sup>[190]</sup> and pore volumes (the highest being 2060 m<sup>2</sup>g<sup>-1</sup>, MOF-210)<sup>[190]</sup> offer higher hydrogen adsorption (in the case of MOF-210, 176 mg/g at 80 bar and 77 K).

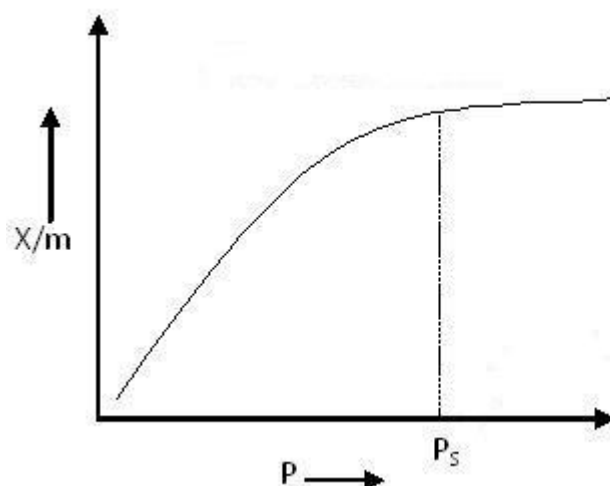


**Figure 1.8** Type I adsorption isotherm (Y axis: amount adsorbed, X axis: relative pressure,  $P_s$ : saturation pressure)<sup>[191]</sup>

A number of microporous MOFs that exhibit hydrogen storage potential have been documented, mainly based on transition metals.<sup>[192-194]</sup> Whilst the hydrogen uptake in these MOFs is promising (up to 8% by wt. in some cases), the values are obtained at very low temperatures (77 K) and high pressures (80 bar),<sup>[195]</sup> thus not providing the storage conditions requested by the Department of Energy (see above **Section 1.3.2**).

Recently, interest has been focused towards alkali- and alkaline earth metals. Much discussion about hydrogen storage in alkaline earth MOFs is available. This includes doping existing transition metal MOFs with alkali- alkaline earth cations to enhance the hydrogen adsorption, yet few examples of MOFs that can store hydrogen exist.<sup>[196-198]</sup>

An advantage of lightweight metals such as lithium and magnesium in a MOF system is lower gravimetric densities, thus potentially delivering more hydrogen.<sup>[199, 200]</sup> In addition to the low molecular weight for the lighter metals, and the potential of high storage percentages (relative to the weight), lithium and magnesium have an appreciable affinity towards hydrogen.

Hydrogen storage in MOFs occurs through weak van der Waals interactions at strongly adsorbing sites. These interactions are stronger at lower temperatures and higher pressures. For efficient hydrogen storage, high specific surface areas are desirable; and lowering of the overall density of the framework could achieve this.<sup>[201]</sup> Furthermore, adsorption temperatures and pressures are factors that depend greatly on heats of adsorption (reported in KJ/mol).<sup>[202-204]</sup> Ideally, a larger heat of adsorption would result in higher temperatures and lower pressures at which the MOF could adsorb hydrogen.<sup>[200, 205]</sup>

Though the alkaline earth MOFs, the theme of this thesis, are rare and difficult to obtain, the promise of having low density materials for the storage and delivery of hydrogen is predicted to be an advantage over current systems.

### 1.5 Effect of donors on coordination chemistry

The structural chemistry of alkaline earth coordination polymers can be altered by the use of donors or co-ligands which will likely affect the dimensionality of the corresponding networks. Ideally, the resulting MOFs are structurally stable, three-dimensional, and have well defined channel geometries. The dimensionality of the networks can be modified by introducing co-ligands that coordinate to the metal and link individual SBUs.

As an example, Jayaramulu *et al.*<sup>[170]</sup> reported on a coordination polymer comprised of Cd<sup>2+</sup> ions with a mixture of ligands, consisting of the 4,4'-bipyridine ligand (Figure 1.9a) and 4,5-imidazolecarboxylic acid (Figure 1.9b) in acetonitrile, affording a 3-dimensional heteroleptic MOF with great structural stability.



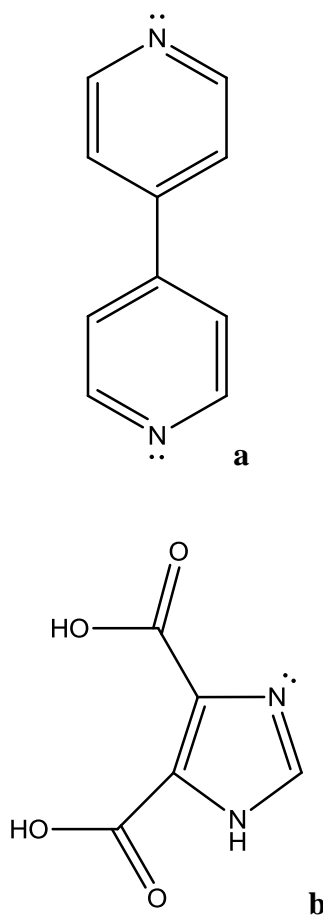


**Figure 1.9** (a) 4,4'-bipyridine (b) 4,5-imidazolecarboxylic acid

For MOFs three-dimensionality is critical to obtain highly stable, insoluble and functional materials. Reduction of dimensionality, achieved by the use of co-ligands, often goes hand-in-hand with increased solubility.

The coordination chemistry of metal- macrocycles which can effectively encapsulate metal centers has been a topic of recent active research.<sup>[206, 207]</sup> Macrocycles are cyclical molecules, often containing multiple metal-binding sites including O-, N-, and S- moieties. In the case of cyclic ethers, also called crown ethers, the most important feature is their ability to stabilize cations on the basis of size.<sup>[208]</sup> This selectivity has prompted their use as separators<sup>[209, 210]</sup> (e.g. hazardous waste ions) and purifiers<sup>[211]</sup> (e.g. water purification).

One of the most commonly used, commercially available cyclic ethers is 1,4,7,10,13,16-hexaoxacyclooctadecane – known under the simpler name 18-crown-6 (Figure 1.10).<sup>[212]</sup> The macrocycle consists of an 18 membered ring with 6 oxygen binding sites (diameter of cavity: 2.6-3.2 Å) and is obtainable through a template Williamson ether synthesis route.<sup>[213]</sup> Other frequently employed but smaller crown ethers, include 12-crown-4 (diameter of cavity: 1.2-1.4 Å) and 15-crown-5 (diameter of cavity: 1.7-2.2 Å).<sup>[214]</sup>

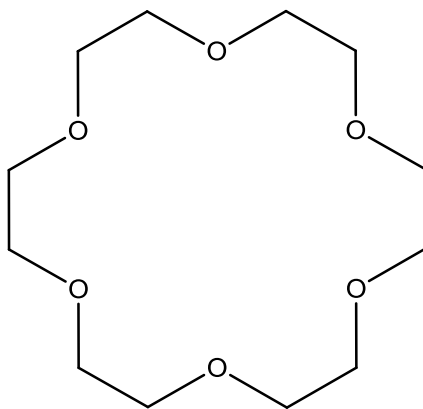


**Figure 1.10** 18-crown-6

Factors that contribute to the stabilization of cations were detailed by Christensen *et al.*<sup>[215]</sup> and include the nature of the binding sites in the ring, the quantity of binding sites in the ring, and the relative size of the stabilized cations, among others.

The different crown sizes and their effect on the stabilization of the respective cations have given rise to a huge array of crown ether stabilized species. It is important to note that small variations in reagent stoichiometry may lead to significant changes in the resulting target compounds.<sup>[216]</sup> A crown:metal stoichiometry of 1:1 might afford a crown stabilized metal ligand compound, whereas a 1:2 stoichiometry might afford separated ions with the cation stabilized by two crown ethers in a sandwich fashion, and a non-coordinated anion.<sup>[215, 217]</sup> From

this example, it becomes clear that for the formation of a coordination compound many competing factors play critical roles. Table 1.5 shows alkali- and alkaline earth metals as compared in size to crown ether cavity diameters.

Practical applications of crown ethers include solubility enhancing effects upon crown coordination,<sup>[218, 219]</sup> a widely known example being “purple benzene”.<sup>[220]</sup> “Purple benzene” contains benzene soluble  $\text{KMnO}_4$ ,<sup>[221]</sup> as achieved by addition of 18-crown-6, to coordinate the  $\text{K}^+$  cation. Crown ethers have been used extensively to provide steric saturation to the large alkali and alkaline earth metal ions.

**Table 1.5** Ionic diameter and size comparison of alkali-, alkaline earth metals vs. different polyethers’ cavity sizes

Cation	Ionic Diameter <sup>[16]</sup> (Å)	Polyether	“Cavity” Diameter (Å) <sup>[215]</sup>
Lithium	1.20	12-crown-4	1.2-1.7
Sodium	1.90	15-crown-5	1.7-2.2
Potassium	2.66	18-crown-6	2.6-3.2
Magnesium	1.45	21-crown-7	3.4-4.3
Calcium	1.94		
Strontium	2.36		
Barium	2.70		

The discovery of crown ethers and their many applications was rewarded with a Nobel Prize in Chemistry in 1987 for Charles Pedersen, Donald Cram and Jean-Marie Lehn.<sup>[222]</sup> Since, an extensive amount of literature has appeared, ranging from effects on transition metals<sup>[223-226]</sup> to lanthanides.<sup>[227-229]</sup> Examples of effects with the alkaline earth metals also exist, although the number of examples strongly depends on the metal center. For example, beryllium in

conjunction with 12-crown-4 is limited to a single example reported by Neumüller *et al.*<sup>[230]</sup>. The cationic Be(12-crown-4) (1:1 and 2:1 stoichiometry) species includes charge balancing [SbCl<sub>4</sub>]<sup>-</sup> ions. For magnesium, examples are more varied, with solvent-separated species involving 12-crown-4,<sup>[231]</sup> 15-crown-5<sup>[232, 233]</sup> and 18-crown-6.<sup>[234, 235]</sup>

For the heavier alkaline earth metals calcium, strontium and barium, 18-crown-6 has been widely used to stabilize contact molecules as well as separated ions. The Ruhlandt group at Syracuse University has shown the versatility of 18-crown-6 in stabilizing heavy alkaline earth phenolates, thiolates and selenolates,<sup>[236]</sup> acetylides<sup>[237]</sup> and amides.<sup>[237]</sup> The structural chemistry of 18-crown-6 complexes will be further explained in **Chapter 6**, in which the isolation of four new alkaline earth metal crown stabilized alkaline earth tosylates is reported.

#### 1.4.10 Sulfonates

A ligand group explored in this thesis is based on the sulfonic acid family; it possesses the formula RSO<sub>2</sub>OH, where R can vary widely. Sulfonic acids may be prepared by sulfonation,<sup>[238]</sup> the oxidation of thiols,<sup>[239]</sup> or free radical additions.<sup>[240]</sup> Sulfonic acids are relatively weak metal coordinators, which may be advantageous, or disadvantageous, due to the limited capacity of displacing coordinated co-ligands from metal centers.<sup>[241]</sup> Metal sulfonates have been evaluated as adsorptive materials<sup>[242]</sup> (e.g. microporous supramolecular frameworks) and are also used as surfactants.<sup>[243, 244]</sup>

The high polarity of the sulfonic group makes sulfonic acids highly acidic (e.g. *pK*<sub>a</sub> of *p*-toluenesulfonic acid = -6.57).<sup>[245]</sup> The sulfonic acid moiety's tetrahedral, triply oxygenated nature allows for a variety of coordination modes, as illustrated in Figure 1.11.

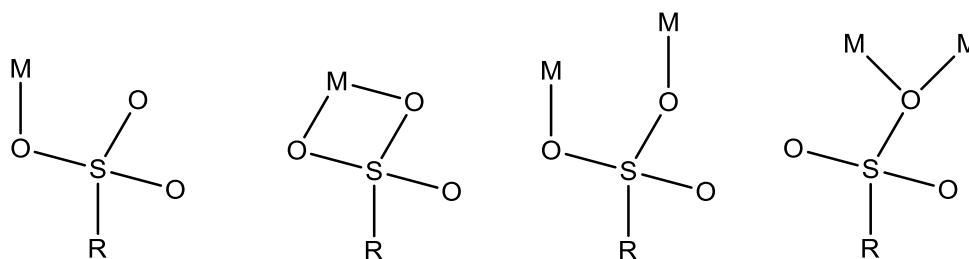


**Figure 1.11** Coordination modes for  $\text{RSO}_2\text{O}^-$ . From left to right  $\eta^1$ ;  $\eta^2$ ;  $\eta^1:\mu^1$ ;  $\eta^2:\mu^2$ ;  $\eta^2:\mu^2$ .

Several examples of alkaline earth metal sulfonates have been reported. These range from separated ions, as reported for magnesium with a fully solvated dication, as seen in  $\{[\text{Mg}(\text{OH}_2)_6](1,5\text{-nds})\}^{2+}$  (1,5-nds = 1,5-naphthalenedisulfonic acid), where magnesium is coordinated with six water molecules to heavier alkaline earth examples. The magnesium-bound water molecules form a complex hydrogen bonded network with the sulfonate oxygens, resulting in an extended chain with the  $[\text{Mg}(\text{OH}_2)_6]^+$  units arranged between the ligand's  $-\text{SO}_3^-$  groups.

For the heavier metals, the same ligand (1,5-nds) affords the contact molecules  $[\text{Ca}(1,5\text{-nds})(\text{OH}_2)_2]$ ,  $[\text{Sr}(1,5\text{-nds})(\text{OH}_2)]$ ,  $[\text{Ba}(1,5\text{-nds})(\text{OH}_2)]$ , where, unlike the magnesium species, the sulfonate ligands coordinate to the metal centers. For each, dense three-dimensional frameworks are achieved through bridging interactions between metal centers.

### 1.4.11 Alkaline earth tosylates

A variant of sulfonic acid is p-toluenesulfonic acid, a versatile reagent in organic chemistry. p-toluenesulfonic acid is obtained by the sulfonation of toluene, though it is commercially available at low cost. p-toluenesulfonic acid is used in several organic reactions, including the preparation of tosylate esters, acetylations<sup>[246]</sup>, and substitution reactions, because the high acidity of tosylic acid ( $\text{p}K_{\text{a}} = -6.57$ )<sup>[245]</sup> makes the tosyl moiety a good leaving group.

A few examples of group II metal tosylates have been described,<sup>[247]</sup> including the DAIP (donor assisted ion pair) ( $\{[\text{Mg}(\text{H}_2\text{O})_6](\text{OTs})_2\}_\infty$ ), with water solvated magnesium centers, and ( $[\text{Ca}(\text{OTs})_2(\text{H}_2\text{O})_4]_\infty$ ), in which four water molecules are coordinated to the metal in addition to two tosylates.<sup>[247]</sup> In both cases, extensive hydrogen bonding links individual units.

## 1.5 References

- [1] F.A. Cotton, G. Wilkinson, *Advanced Inorganic Chemistry*, John Wiley and Sons, 1988.
- [2] A.G. Goos, P.J. Rosado Flores, Y. Takahashi, K. Ruhlandt-Senge, *Alkaline Earth Metals: Organometallic Chemistry* 2012.
- [3] L.I. Grossweiner, R.L. Seifert, *J. Am. Chem. Soc.*, 74 (1952) 2701.
- [4] H.A. Abel-Ghany, *J. Radioanal Nucl Chem*, 295 (2013) 1365-1370.
- [5] P.B. Henderson, P.J. Morris, W.S. Moore, M.A. Charette, *J Radioanal Nucl Chem*, 296 (2013) 357-362.
- [6] B.G. Muhammad, M.S. Jaafar, A. Abdul Rahman, F.A. Ingawa, *Environmental monitoring and assessment*, 184 (2012) 5043-5049.
- [7] S. Geras'kin, T. Evseeva, A. Oudalova, *Journal of environmental radioactivity*, 121 (2013) 22-32.
- [8] T. Wardaszko, D. Grzybowska, J. Nidecka, *Nuclear Instruments and Methods in Physics Research*, B17 (1986) 530.
- [9] D.J. Chakrabarti, D.E. Laughlin, L.E. Tanner, *Bulletin of Alloy Phase Diagrams*, (1987) 269.
- [10] J.A. Cowan, *Chem. Rev.*, 98 (1998) 1067.
- [11] K.D. Cashman, *British Journal of Nutrition*, 87 (2007) S169.
- [12] S. Shadanbaz, G.J. Dias, *Acta Biomater.*, 1 (2012) 20.
- [13] K. Breitenecker, *Environ. Res. Lett.*, 4 (2009) 031002.
- [14] B. Zhai, X. Zhou, S. Zhai, Z. Wang, *Advanced Materials Research*, 299-300 (2011) 503.
- [15] O.S. Bruland, T.J. Jonasdottir, D.R. Fisher, R.H. Larsen, *Current Radiopharmaceuticals*, 1 (2008) 203.
- [16] R.D. Shannon, *Acta Cryst.*, A32 (1976) 751.
- [17] A.L. Allred, E.G. Rochow, *J. Inorg. Nucl. Chem.*, 5 (1958) 264.

- [18] J.E. Huheey, E.A. Keiter, R.L. Keiter, *Inorganic Chemistry: Principles of Structure and Reactivity* 1993.
- [19] J.S. Bradshaw, *Journal of Inclusion Phenomena and Molecular Recognition in Chemistry* 29 (1997) 221.
- [20] E.G. Moschetta, K.M. Gans, R.M. Rioux, *J. Catal.*, 309 (2014) 11-20.
- [21] M.H. Sakhawat, S.U. Rehman, *Inorg. Chim. Acta*, 60 (1982) 231.
- [22] A. Verma, M. Guino-o, M. Gillett-Kunnath, W. Teng, K. Ruhlandt-Senge, *Zeitschrift für anorganische und allgemeine Chemie*, 635 (2009) 903-913.
- [23] D.C. Green, U. Englich, K. Ruhlandt-Senge, *Angew. Chem. Int. Ed.*, 38 (1999) 354.
- [24] B.D. James, *J. Chem. Educ.*, 48 (1971) 176.
- [25] C.N. Sundaresan, S. Dixit, P. Venugopalan, *J. Mol. Struct.*, 693 (2004) 205-209.
- [26] G. Muller, M. Lutz, S. Harder, *Acta Cryst.*, B52 (1996) 1054.
- [27] F. Zhang, K. Li, H. Ratajczak, D. Xue, *Journal of Molecular Structure*, 976 (2010) 69-72.
- [28] T. Steiner, *Angewandte Chemie International Edition*, 41 (2002) 48-76.
- [29] G.A. Jeffrey, *An Introduction to Hydrogen Bonding*, Oxford University Press, Oxford, 1997.
- [30] J. Almlöf, T. Ottersen, *Acta Cryst. Sec. A.*, A35 (1979) 137.
- [31] R. Taylor, O. Kennard, *Acta Cryst.*, B39 (1983) 133.
- [32] A. Taylor, M. Dunne, S. Bennington, S. Ansell, I. Gardner, P. Norreys, T. Broome, D. Findlay, R. Nelmes, *Science*, 315 (2007) 1092.
- [33] A. Sendil Kumar, P.D. Babu, S. Srinath, *J. Appl. Phys.*, 115 (2014) 103904.
- [34] F.H. Allen, I.J. Bruno, *Acta Crystallogr B*, 66 (2010) 380-386.
- [35] C. Rapp, E. Goldberger, N. Tishbi, R. Kirshenbaum, *Proteins*, (2014).



- [36] X. Fang, Y.Z. Zhu, J.Y. Zheng, *The Journal of organic chemistry*, (2014).
- [37] P. Sun, F. Zheng, M. Zhu, Z. Song, K. Wang, M. Zhong, D. Wu, R.B. Little, Z. Xu, H. Zhu, *8* (2014) 850.
- [38] M. Giese, M. Albrecht, C. Bohnen, T. Repenko, A. Valkonen, K. Rissanen, *Dalton Trans*, *43* (2014) 1873-1880.
- [39] N. Li, W.-B. Chen, Y.-F. Guan, Z.-J. OuYang, W. Dong, *Inorg. Chim. Acta*, *409* (2014) 349-352.
- [40] S.T. Schneebeli, M. Frasconi, Z. Liu, Y. Wu, D.M. Gardner, N.L. Strutt, C. Cheng, R. Carmieli, M.R. Wasielewski, J.F. Stoddart, *Angew Chem Int Ed Engl*, *52* (2013) 13100-13104.
- [41] W. Saenger, *Principles of Nucleic Acid Structure*, Springer-Verlag, New York, 1984.
- [42] G.R. Desiraju, A. Gavezzotti, *Chem. Commun.*, (1989) 621.
- [43] B. Dong, H. Maeda, *Chem Commun (Camb)*, *49* (2013) 4085-4099.
- [44] S.E. Wheeler, *Acc. Chem. Res.*, *46* (2013) 1029.
- [45] R.P. Matthews, T. Welton, P.A. Hunt, *Phys Chem Chem Phys*, *16* (2014) 3238-3253.
- [46] C.A. Hunter, K.R. Lawson, J. Perkins, C.J. Urch, *J. Chem. Soc.*, (2001) 651-669.
- [47] O.M. Sinnokrot, E.F. Valeev, D.C. Sherrill, *J. Am. Chem. Soc.*, *124* (2002) 10887.
- [48] E. Arunan, H.S. Gutowsky, *J. Chem. Phys.*, *98* (1993) 4294.
- [49] T. Dahl, *Acta Chem. Scand.*, *48* (1994) 95.
- [50] N. Kuzmina, I. Malkerova, A. Alikhanyan, D. Tsymbarenko, K. Lyssenko, O. Kreinin, G. Shuster, E. Lakin, E. Zolotoyabko, *Chemical Vapor Deposition*, *15* (2009) 342-349.
- [51] H. Niimi, K. Mihara, Y. Sakabe, M. Kuwabara, *J. Am. Ceram. Soc.*, *90* (2007) 1817-1821.
- [52] E. Veuhoff, *Handbook of Compound Semiconductors*, William Andrew Inc., 1996.
- [53] C.-Y. Hwang, M.J. Schurman, W.E. Mayo, *J. Electron Mater.*, *26* (1997) 243.

- [54] R.P. Tompkins, T.A. Walsh, M.A. Derenge, K.W. Kirchner, S. Zhou, C.B. Nguyen, K.A. Jones, P. Suvarna, M. Tungare, N. Tripathi, F. Shahedipour-Sandvik, *J. Mater. Res.*, 26 (2011) 2895-2900.
- [55] B.D. Fahlman, *Current Organic Chemistry*, 10 (2006) 1021.
- [56] T.T. Kostas, M.J. Hampden-Smith, *The Chemistry of Metal CVD*, Wiley-VCH, 1994.
- [57] I.M. Watson, M.P. Atwoods, S. Haq, *Supercond. Sci. Technol.*, 7 (1994) 672.
- [58] W.D. Buchanan, M.A. Guino-o, K. Ruhlandt-Senge, *Inorg. Chem.*, 49 (2010) 7144.
- [59] A. Torvisco, A. O'Brien, K. Ruhlandt-Senge, *Coord. Chem. Rev.*, 255 (2011) 1268.
- [60] A. Torvisco, D. Katharina, F. Uhlig, K. Ruhlandt-Senge, *Inorg. Chem.*, 48 (2009) 11459.
- [61] M.H. Chisholm, J. Gallucci, K. Phomphrai, *Chem. Commun.*, (2003) 48-49.
- [62] M.H. Chisholm, J.C. Gallucci, K. Phomphrai, *Inorg. Chem.*, 43 (2004) 6717.
- [63] U.S. Department of Energy, <http://www.hydrogen.energy.gov/>
- [64] M. Paik Suh, J.H. Park, P.T. Prasad Kootteri, D.-W. Lim, *Chem. Rev.*, (2012) 782.
- [65] L. Wu, Z. Zhang, J. Ran, D. Zhou, C. Li, T. Xu, *Phys Chem Chem Phys*, 15 (2013) 4870-4887.
- [66] J. Han, A. Elgowainy, J.B. Dunn, M.Q. Wang, *Bioresour. Technol.*, 133 (2013) 421-428.
- [67] Y.K. Salkuyeh, T.A. Adams, *Energy Conversion and Management*, 74 (2013) 492-504.
- [68] Y. Wang, L.T. Zhou, H. Yuan, W.H. Shen, R. Tang, M. Qiang Fan, Y.K. Shu, *Int. J. Electrochem. Sci.*, 8 (2013).
- [69] U.S. Department of Energy, <http://www.hydrogen.energy.gov/storage.html>, 2013.
- [70] A. Nakano, H. Ito, T. Maeda, T. Munakata, T. Motyka, C. Corgnale, S. Greenway, J.M. Perez-Berrios, *J. Alloys Compd.*, 580 (2013) S418-S422.

- [71] J. Wang, S. Han, W. Zhang, D. Liang, Y. Li, X. Zhao, R. Wang, *Int. J. Hydrogen Energy*, 38 (2013) 14631-14637.
- [72] M.V.C. Sastri, B. Viswanathan, S.S. Murthy, *Metal Hydrides*, 1 ed., Narosa Publishing House, Madras, India, 1998.
- [73] B. Sakintuna, F. Darkrim-Lamari, M. Hirscher, *Int. J. Hydrogen Energy*, 32 (2007) 1121-1140.
- [74] R.A. Dunlap, Z.H. Cheng, G.R. MacKay, J.W. O'Brien, D.A. Small, *Hyperfine Interact.*, 130 (2001) 109-126.
- [75] L. Zaluski, A. Zaluska, J.O. Strom-Olsen, *J. Alloys Compd.*, 253-254 (1997) 70-79.
- [76] J. Lu, Y. Choi Joon, Z. Fang Zak, Y. Sohn Hong, *J. Power Sources*, 195 (2010) 1992-1997.
- [77] E.C. Ashby, R.D. Schwartz, *Inorg. Chem.*, 10 (1971) 355-357.
- [78] A. Zaluska, L. Zaluski, J.O. Strom-Olsen, *J. Alloys Compd.*, 307 (2000) 157-166.
- [79] C.P. Hsu, D.H. Jiang, S.L. Lee, J.L. Horng, M.D. Ger, J.K. Chang, *Chem. Commun.*, 49 (2013) 8845-8847.
- [80] Z. Xueping, L. Shenglin, *J. Alloys Compd.*, 481 (2009) 761-763.
- [81] M.C. Jensen, R. Zidan, N. Mariels, A. Hee, C. Hagen, *Int. J. Hydrogen Energy*, 24 (1999) 461-465.
- [82] E. Ronnebro, *J. Phys. Chem. Solids*, 71 (2010) 1154-1158.
- [83] Y. Nakamori, A. Ninomiya, G. Kitahara, M. Aoki, T. Noritake, K. Miwa, Y. Kojima, S. Orimo, *J. Power Sources*, 155 (2006) 447-455.
- [84] J. Luo, X. Kang, P. Wang, *Energy & Environmental Science*, 6 (2013) 1018.
- [85] P.-F. Yuan, F. Wang, Q. Sun, Y. Jia, Z.X. Guo, *Int. J. Hydrogen Energy*, 38 (2013) 11313-11320.

- [86] Z. Xiong, G. Wu, S.Y. Chua, J. Hu, T. He, W. Xu, P. Chen, *Energy Environ. Sci.*, 1 (2008).
- [87] K. Wang, J.-G. Zhang, W. Yang, M. Wu, T.-T. Man, T.-L. Zhang, S.-W. Zhang, *Struct. Chem.*, 24 (2012) 1527-1536.
- [88] J. Chen, T. He, G. Wu, Z. Xiong, P. Chen, *Int. J. Hydrogen Energy*, 38 (2013) 10944-10949.
- [89] H. Li, Q. Yang, X. Chen, S.G. Shore, *J. Organomet. Chem.*, (2013).
- [90] Z. SHi, G. Li, L. Wang, L. Gao, C. Xiaobo, J. Hua, S. Feng, *Cryst. Growth Des.*, 4 (2004).
- [91] L. Xie, S. Liu, B. Gao, C. Zhang, C. Sun, D. Li, Z. Su, *Chem. Commun.*, (2005) 2402-2404.
- [92] Q. Fang, G. Zhu, M. Xue, Z. Wang, J. Sun, S. Qiu, *Cryst. Growth Des.*, 8 (2008).
- [93] Q. Fang, G. Zhu, X. Shi, G. Wu, G. Tian, R. Wang, S. Qiu, *J. Solid State Chem.*, 177 (2004) 1060-1066.
- [94] J.-X. Chen, S.-X. Liu, E.-Q. Gao, *Polyhedron*, 23 (2004) 1877-1888.
- [95] M. Sindoro, A.Y. Jee, S. Granick, *Chem. Commun.*, 49 (2013) 9576-9578.
- [96] L. Alaerts, M. Maes, L. Giebeler, P.A. Jacobs, J.A. Martens, J.F.M. Denayer, C.E.A. Kirschhock, D.E. De Vos, *J. Am. Chem. Soc.*, 130 (2008) 14170.
- [97] C.K. Brozek, M. Dincă, *Chemical Science*, 3 (2012) 2110.
- [98] M. Oh, L. Rajput, D. Kim, D. Moon, M.S. Lah, *Inorg. Chem.*, 52 (2013) 3891-3899.
- [99] C. Volkringer, D. Popov, T. Loiseau, G. Férey, M. Burghammer, C. Riekel, M. Haouas, F. Taulelle, *Chem. Mater.*, 21 (2009) 5695-5697.
- [100] D.J. Tranchemontagne, J.R. Hunt, O.M. Yaghi, *Tetrahedron*, 64 (2008) 8553-8557.
- [101] Sigma-Aldrich,  
<http://www.sigmaaldrich.com/catalog/product/aldrich/688614?lang=en&region=US>
- [102] W. Ouellette, J. Zubieta, *Chem. Commun.*, (2009) 4533-4535.

- [103] W.-X. Lim, A.W. Thornton, A.J. Hill, B.J. Cox, J.M. Hill, M.R. Hill, *Langmuir*, 29 (2013) 8524-8533.
- [104] M. Kang, D. Luo, Z. Lin, G. Thiele, S. Dehnen, *Cryst. Eng. Comm.*, 15 (2013) 1845.
- [105] Zheng, Wang, S. Gao, Liao, Yan, Jin, *Eur. J. Inorg. Chem.*, 2004 (2004) 2968-2973.
- [106] R.F. D'Vries, V.a. de la Peña-O'Shea, N. Snejko, M. Iglesias, E. Gutiérrez-Puebla, M.A. Monge, *J. Am. Chem. Soc.*, 135 (2013) 5782-5792.
- [107] A. Tian, X. Lin, X. Liu, J. Ying, X. Wang, *RSC Advances*, 3 (2013) 17188.
- [108] M.C. Das, S.K. Ghosh, E.C. Sannudo, P.K. Bharadwaj, *Dalton Transactions*, (2009) 1644-1658.
- [109] L. Xue, D. Luo, X. Luo, H. Zeng, Z. Lin, *Solid State Sci.*, 19 (2013) 80-84.
- [110] A.D. Burrows, M. Jurcic, L.L. Keenan, R.A. Lane, M.F. Mahon, M.R. Warren, H. Nowell, M. Paradowski, J. Spencer, *Chem. Commun.*, 49 (2013) 11260-11262.
- [111] M.-D. Zhang, H.-G. Zheng, Z.-Z. Lu, X.-Q. Yao, *Cryst. Eng. Comm.*, 15 (2013) 9265.
- [112] B. Zhang, Y. Zhang, D. Zhu, *Dalton Trans*, 41 (2012) 8509-8511.
- [113] X. Zhang, Y.-Y. Huang, J.-K. Cheng, Y.-G. Yao, J. Zhang, F. Wang, *Cryst. Eng. Comm.*, 14 (2012).
- [114] W. Chen, J.-Y. Wang, C. Chen, Q. Yue, H.-M. Yuan, J.-S. Chen, S.-N. Wang, *Inorg. Chem.*, 42 (2003).
- [115] W.W. He, S.L. Li, G.S. Yang, Y.Q. Lan, Z.M. Su, Q. Fu, *Chem Commun (Camb)*, 48 (2012) 10001-10003.
- [116] V. Lozan, P.Y. Solntsev, G. Leibelng, K.V. Domasevitch, B. Kersting, *Eur. J. Inorg. Chem.*, (2007).
- [117] V. Bampoh, *Doctoral Thesis*, in, Syracuse University, 2012.

- [118] M. Plabst, T. Bein, *Inorg. Chem.*, (2009).
- [119] L.S. James, *Chem. Soc. Rev.*, 32 (2003) 276.
- [120] N.G. Armatas, W. Ouellette, K. Whitenack, J. Pelcher, H. Liu, E. Romaine, C.J. O'Connor, J. Zubieta, *Inorg. Chem.*, 48 (2009) 8897-8910.
- [121] J. Xu, Z.-S. Bai, M.-S. Chen, Z. Su, S.-S. Chen, W.-Y. Sun, *Cryst. Eng. Comm.*, 11 (2009) 2728.
- [122] J.L.C. Rowsell, O.M. Yaghi, *Microporous and Mesoporous Materials*, 73 (2004) 3-14.
- [123] D. Banerjee, J. Finkelstein, A. Smirnov, P.M. Forster, L.A. Borkowski, S.J. Teat, J.B. Parise, *Cryst. Growth Des.*, 11 (2011) 2572-2579.
- [124] M. Hu, Z. Wu, J. Yao, X. Gu, H. Su, *Inorg. Chem. Commun.*, 36 (2013) 31-34.
- [125] D. Saha, T. Maity, S. Das, S. Koner, *Dalton. Trans.*, 42 (2013) 13912-13922.
- [126] N. Campagnol, T. Van Assche, T. Boudewijns, J. Denayer, K. Binnemans, D. De Vos, J. Fransaer, *J. Mater. Chem.*, 1 (2013) 5827.
- [127] F. Yuan, J. Xie, H.-M. Hu, C.-M. Yuan, B. Xu, M.-L. Yang, F.-X. Dong, G.-L. Xue, *CrystEngComm*, 15 (2013) 1460.
- [128] P. Mishra, S. Edubilli, B. Mandal, S. Gumma, *Microporous and Mesoporous Materials*, 169 (2013) 75-80.
- [129] P. Canepa, C.a. Arter, E.M. Conwill, D.H. Johnson, B.a. Shoemaker, K.Z. Soliman, T. Thonhauser, *J. Mater. Chem. A*, 1 (2013) 13597.
- [130] H. Reinsch, N. Stock, *Microporous Mesoporous Mater.*, 171 (2013) 156-165.
- [131] M. Lammert, S. Bernt, F. Vermoortele, D.E. De Vos, N. Stock, *Inorg. Chem.*, 52 (2013) 8521-8528.

- [132] X.Y. Dong, R. Wang, J.B. Li, S.Q. Zang, H.W. Hou, T.C. Mak, *Chem. Commun.*, 49 (2013) 10590-10592.
- [133] Q. Zheng, F. Yang, M. Deng, Y. Ling, X. Liu, Z. Chen, Y. Wang, L. Weng, Y. Zhou, *Inorg. Chem.*, 52 (2013) 10368-10374.
- [134] J. Wack, R. Siegel, T. Ahnfeldt, N. Stock, L. Mafra, J. Senker, *J. Phys. Chem. C*, 117 (2013) 19991-20001.
- [135] A.K. Chaudhari, S. Mukherjee, S.S. Nagarkar, B. Joarder, S.K. Ghosh, *Cryst. Eng. Comm.*, 15 (2013) 9465.
- [136] I. Senkovska, S. Kaskel, *Eur. J. Inorg. Chem.*, 2006 (2006) 4564-4569.
- [137] Z. Guo, G. Li, L. Zhou, S. Su, Y. Lei, S. Dang, H. Zhang, *Inorg. Chem.*, 48 (2009) 8069-8071.
- [138] A. Mallick, S. Saha, P. Pachfule, S. Roy, R. Banerjee, *Inorg. Chem.*, 50 (2011) 1392-1401.
- [139] Z.-F. Wu, B. Hu, M.-L. Feng, X.-Y. Huang, Y.-B. Zhao, *Inorg. Chem. Commun.*, 14 (2011) 1132-1135.
- [140] K.M. Fromm, *Coord. Chem. Rev.*, 252 (2008) 856.
- [141] R. Murugavel, R. Korah, *Inorg. Chem.*, 46 (2007) 11048-11062.
- [142] J. Soleimannejad, H. Aghabozorg, S. Hooshmand, H. Adams, *Acta Crystallogr., Sect. E: Struct. Rep. Online*, 63 (2007) m3089-m3090.
- [143] L.-L. Wen, F.-M. Wang, X.-K. Leng, M.-M. Wang, Q.-J. Meng, H.-Z. Zhu, *J. Inorg. Organomet. Polym.*, 20 (2010) 313-319.
- [144] F.A. Almeida Paz, J. Klinowski, M.F.S. Vilela, J.P.C. Tomé, J.A.S. Cavaleiro, J. Rocha, *Chem. Soc. Rev.*, 41 (2012) 1088.

- [145] L. Bellarosa, J.J. Gutierrez-Sevillano, S. Calero, N. Lopez, *Phys Chem Chem Phys*, 15 (2013) 17696-17704.
- [146] H. Jasuja, K.S. Walton, *Dalton Trans*, 42 (2013) 15421-15426.
- [147] F. Gschwind, O. Sereda, K.M. Fromm, *Inorg. Chem.*, 48 (2009) 10535-10547.
- [148] A. Beziau, S.A. Baudron, A. Fluck, M.W. Hosseini, *Inorg Chem*, 52 (2013) 14439-14448.
- [149] A.K. Crane, E.Y.L. Wong, M.J. MacLachlan, *Cryst. Eng. Comm.*, (2013).
- [150] F. Sun, G. Zhu, *Inorg. Chem. Commun.*, 38 (2013) 115-118.
- [151] H.-G. Jin, M.-F. Wang, X.-J. Hong, J. Yang, T. Li, Y.-J. Ou, L.-Z. Zhao, Y.-P. Cai, *Inorg. Chem. Commun.*, 36 (2013) 236-240.
- [152] A.J. Calahorra, D. Fairen-Jiménez, A. Salinas-Castillo, M.E. López-Viseras, A. Rodríguez-Diéguez, *Polyhedron*, 52 (2013) 315-320.
- [153] A. Rodríguez-Diéguez, J. Cano, R. Kivekas, A. Debdoubi, E. Colacio, *Inorg. Chem.*, 46 (2007).
- [154] G. Kumar, R. Gupta, *Chem Soc Rev*, 42 (2013) 9403-9453.
- [155] C. Li, L. Huang, M. Zhou, J. Xia, H. Ma, S. Zang, L. Wang, *J. Solid State Chem.*, 208 (2013) 86-92.
- [156] X.-G. Guo, W.-B. Yang, X.-Y. Wu, Q.-K. Zhang, L. Lin, R. Yu, C.-Z. Lu, *Cryst. Eng. Comm.*, (2013) 3654.
- [157] Y. Ren, X. Cheng, S. Yang, C. Qi, H. Jiang, Q. Mao, *Dalton Trans*, 42 (2013) 9930-9937.
- [158] S. Zhang, L. Han, L. Li, J. Cheng, D. Yuan, J. Luo, *Cryst. Growth Des.*, 13 (2013) 5466-5472.
- [159] M. Zhang, Y.-P. Chen, H.-C. Zhou, *Cryst. Eng. Comm.*, 15 (2013) 9544.
- [160] P. Manna, B.K. Tripuramallu, S.K. Das, *Cryst. Growth Des.*, (2013) 131123060822000.



- [161] G.-X. Jin, J.-P. Ma, Y.-B. Dong, *J. Mol. Struct.*, 1052 (2013) 146-157.
- [162] B.R. Bijini, S. Prasanna, M. Deepa, C.M. Nair, K. Rajendra Babu, *Spectrochimica acta. Part A, Molecular and biomolecular spectroscopy*, 97 (2012) 1002-1006.
- [163] T.C. Stamatatos, E. Katsoulakou, V. Nastopoulos, C.P. Raptopoulou, E. Manessi-Zoupa, S.P. Perlepes, *Z Naturforsch B*, 58 (2003).
- [164] Z. Florjanczyk, W. Bury, E. Zygadlo-Monikowska, I. Justyniak, R. Balawender, J. Lewinski, *Inorg. Chem.*, 48 (2009) 10892-10894.
- [165] Q. Wei, D. Yang, T.E. Larson, T.L. Kinnibrugh, R. Zou, N.J. Henson, T. Timofeeva, H. Xu, Y. Zhao, B.R. Mattes, *J. Mater. Chem.*, 22 (2012) 10166.
- [166] S.-S. Chen, Z.-H. Chen, J. Fan, T.-a. Okamura, Z.-S. Bai, M.-F. Lv, W.-Y. Sun, *Cryst. Growth Des.*, 12 (2012) 2315-2326.
- [167] M. Kim, J.A. Boissonault, C.A. Allen, P.V. Dau, S.M. Cohen, *Dalton Trans*, 41 (2012) 6277-6282.
- [168] J.J. Perry Iv, P.L. Feng, S.T. Meek, K. Leong, F.P. Doty, M.D. Allendorf, *J. Mater. Chem.*, 22 (2012) 10235.
- [169] P.C. Guo, Z. Chu, X.M. Ren, W.H. Ning, W. Jin, *Dalton Trans*, 42 (2013) 6603-6610.
- [170] K. Jayaramulu, S.K. Reddy, A. Hazra, S. Balasubramanian, T.K. Maji, *Inorg. Chem.*, 51 (2012) 7103-7111.
- [171] R.G. Pearson, *J. Am. Chem. Soc.*, 85 (1963).
- [172] G. Peng, L. Ma, J. Cai, L. Liang, H. Deng, G.E. Kostakis, *Cryst. Growth Des.*, 11 (2011) 2485-2492.
- [173] L. Du, Z. Lu, K. Zheng, J. Wang, X. Zheng, Y. Pan, X. You, J. Bai, *J Am Chem Soc*, 135 (2013) 562-565.

- [174] B. Bhattacharya, R. Dey, D. Ghoshal, *J. Chem. Sci.*, 125 (2013).
- [175] W.-T. Chen, S.-M. Ying, Y.-P. Xu, Q.-Y. Luo, D.-S. Liu, *J. Struct. Chem.*, 52 (2011).
- [176] L. Wang, L. Duan, D. Xiao, E. Wang, C. Hu, *J. Coord. Chem.*, 57 (2004).
- [177] D.T. Tran, X. Fan, D.P. Brennan, P.Y. Zavalij, S.R.J. Oliver, *Inorg. Chem.*, (2005).
- [178] Y.-R. Lee, J. Kim, W.-S. Ahn, *Korean J. Chem. Eng.*, 30 (2013) 1667-1680.
- [179] [http://lib.convdocs.org/pars\\_docs/refs/123/122314/122314.html\\_123f9dc8.gif](http://lib.convdocs.org/pars_docs/refs/123/122314/122314.html_123f9dc8.gif), 2013.
- [180] C.-P. Li, M. Du, *Chem. Commun.*, 47 (2011) 5958-5972.
- [181] B. Supronowicz, A. Mavrandonakis, T. Heine, *J. Phys. Chem. C*, 117 (2013) 14570-14578.
- [182] M. Fischer, J.R. Gomes, M. Froba, M. Jorge, *Langmuir*, 28 (2012) 8537-8549.
- [183] M. Dincă, J.R. Long, *Angewandte Chemie (International ed. in English)*, 47 (2008) 6766-6779.
- [184] W.M. Bloch, C.J. Sumbly, *Chem. Commun.*, 48 (2012) 2534-2536.
- [185] B.-c. Tzeng, H.-t. Yeh, T.-y. Chang, G.-h. Lee, 2 (2009) 10-13.
- [186] M. Lanchas, D. Vallejo-Sanchez, G. Beobide, O. Castillo, A.T. Aguayo, A. Luque, P. Roman, *Chem. Commun.*, 48 (2012) 9930-9932.
- [187] C.-D. Wu, W. Lin, *Angew. Chem., Int. Ed.*, 44 (2005) 1958-1961.
- [188] M. Dinca, J.R. Long, *Angew. Chem. Int. Ed.*, 47 (2008) 6766.
- [189] N.L. Rosi, J. Eckert, M. Eddaoudi, D.T. Vodak, J. Kim, M. O'Keeffe, O.M. Yaghi, *Science*, 300 (2003) 1127-1129.
- [190] H. Furukawa, N. Ko, Y.B. Go, N. Aratani, S.B. Choi, E. Choi, A.O. Yazaydin, R.Q. Snurr, M. O'Keeffe, J. Kim, O.M. Yaghi, *Science*, 329 (2010) 424-428.
- [191] V.A. Laboratories, <http://amrita.vlab.co.in/?sub=2&brch=190&sim=606&cnt=1>

- [192] X.-S. Wang, S. Ma, K. Rauch, J.M. Simmons, D. Yuan, X. Wang, T. Yildirim, W.C. Cole, J.J. López, A.D. Meijere, H.-C. Zhou, *Chem. Mater.*, 20 (2008) 3145-3152.
- [193] M. Dincă, A. Dailly, Y. Liu, C.M. Brown, D.A. Neumann, J.R. Long, *J. Am. Chem. Soc.*, 128 (2006) 16876-16883.
- [194] Y.H. Liu, H.L. Tsai, Y.L. Lu, Y.S. Wen, J.C. Wang, K.L. Lu, *Inorg. Chem.*, 40 (2001) 6426-6431.
- [195] A.G. Wong-Foy, A.J. Matzger, O.M. Yaghi, *J. Am. Chem. Soc.*, (2006).
- [196] L. Wang, Y. Sun, H. Sun, *Faraday Discuss.*, 151 (2011) 143.
- [197] A.W. Thornton, K.M. Naim, A.J. Hill, M.R. Hill, *J. Am. Chem. Soc.*, (2009).
- [198] M.R. Hill, A.W. Thornton, K.M. Nairn, K. Sumida, A.J. Hill, 2010 International Conference on Nanoscience and Nanotechnology, (2010) 33-36.
- [199] T. Hussain, S. Chakraborty, R. Ahuja, *Chem. Phys. Chem.*, 14 (2013) 3463-3466.
- [200] K.L. Mulfort, T.M. Wilson, M.R. Wasielewski, J.T. Hupp, *Langmuir*, 25 (2009) 503-508.
- [201] Z.R. Herm, E.D. Bloch, J.R. Long, *Chem. Mater.*, (2013) 131126064322007.
- [202] Y.-S. Bae, R.Q. Snurr, *Microporous Mesoporous Mater.*, 132 (2010) 300-303.
- [203] M. Hirscher, B. Panella, B. Schmitz, *Microporous Mesoporous Mater.*, 129 (2010) 335-339.
- [204] Y.-S. Bae, R.Q. Snurr, *Microporous Mesoporous Mater.*, 135 (2010) 178-186.
- [205] B. Schmitz, I. Krkljus, E. Leung, H.W. Hoffken, U. Muller, M. Hirscher, *Chem. Sus. Chem.*, 3 (2010) 758-761.
- [206] J.W. Steed, *Coord. Chem. Rev.*, (2001) 171.
- [207] J.S. Bradshaw, R.M. Izatt, *Acc. Chem. Res.*, 30 (1997) 338.

- [208] Y. Inokuchi, O.V. Boyarkin, R. Kusaka, T. Haino, T. Ebata, T.R. Rizzo, *J Phys Chem A*, 116 (2012) 4057-4068.
- [209] M.F. Attallah, E.H. Borai, M.A. Hilal, F.A. Shehata, M.M. Abo-Aly, *Journal of hazardous materials*, 195 (2011) 73-81.
- [210] F.A. Shehata, M.F. Attallah, E.H. Borai, M.A. Hilal, M.M. Abo-Aly, *Applied radiation and isotopes : including data, instrumentation and methods for use in agriculture, industry and medicine*, 68 (2010) 239-249.
- [211] X. Luo, L. Liu, F. Deng, S. Luo, *J. Mater. Chem. A*, (2013) 8280.
- [212] <http://www.sigmaaldrich.com/catalog/product/aldrich/274984?lang=en&region=US>
- [213] G.W. Gokel, D.J. Cram, C.L. Liotta, H.P. Harris, F.L. Cook, *Org. Synth., Coll.* , 6 (1988) 301.
- [214] C.J. Pedersen, *J. Am. Chem. Soc.*, 92 (1970) 391.
- [215] J.J. Christensen, J.O. Hill, R.M. Izatt, *Science*, 174 (1971) 459.
- [216] K.I. Popov, A.G. Vendilo, V. Chistov, H. Rönkkömäki, M. Lajunen, V. Privalov, J. Dikareva, *Polyhedron*, 63 (2013) 50-54.
- [217] N. Alizadeh, *Spectrochimica acta. Part A, Molecular and biomolecular spectroscopy*, 78 (2011) 488-493.
- [218] Z.-H. Sun, F.-F. Pan, Triyanti, M. Albrecht, G. Raabe, *European Journal of Organic Chemistry*, 2013 (2013) 7922-7932.
- [219] F. Lázaro-Fernández, A. Sastre, T. Torres, *J. Chem. Soc., Chem. Commun.*, (1995) 419.
- [220] A.J. Doheny Jr., B. Ganem, *J. Chem. Educ.* , 4 (1980) 308.
- [221] P.G. J., *Inorg. Chem.*, 6 (1967) 503.
- [222] C.J. Pedersen, *J. Inclusion Phenom.*, 6 (1988) 337.

- [223] D. Braga, S. D'Agostino, F. Grepioni, M. Gandolfi, K. Rubini, *Dalton Trans*, 40 (2011) 4765-4777.
- [224] C. Fiolka, R. Striebinger, T. Walter, C. Walbaum, I. Pantenburg, *Zeitschrift für anorganische und allgemeine Chemie*, 635 (2009) 855-861.
- [225] V. Shivaiah, S.K. Das, *Inorg. Chem. Commun.*, (2005) 7313.
- [226] E. Luboch, A. Cygan, J.F. Biernat, *Inorg. Chim. Acta*, 102 (1983) 203.
- [227] M.J. Champion, P. Farina, W. Levason, G. Reid, *Dalton Trans*, 42 (2013) 13179-13189.
- [228] M.I. Saleh, E. Kusriani, H.K. Fun, B.M. Yamin, *Journal of Organometallic Chemistry*, 693 (2008) 2561-2571.
- [229] M.I. Saleh, E. Kusriani, B. Saad, R. Adnan, A.S. Mohamed, B.M. Yamin, *Journal of Luminescence*, 126 (2007) 871-880.
- [230] B. Neumüller, K. Dehnicke, *Zeitschrift für anorganische und allgemeine Chemie*, 632 (2006) 1681-1686.
- [231] M.A. Neuman, E.C. Steiner, R.v.F. P., F.P. Boer, *Inorg. Chem.*, 14 (1975) 735.
- [232] T.B. Rubtsova, O.K. Kireeva, B.M. Bulychev, *Polyhedron*, 11 (1992).
- [233] A. Jaenschke, J. Paap, U. Behrens, *Zeitschrift für anorganische und allgemeine Chemie*, 634 (2008) 461-469.
- [234] A.N. Chekhlov, *Koord. Khim.*, (2007) 578.
- [235] P.C. Junk, J.W. Steed, *J. Coord. Chem.*, 60 (2007) 1017.
- [236] K. Ruhlandt-Senge, U. Englisch, *Chem. Eur. J.*, 6 (2000) 4063.
- [237] J.S. Alexander, K. Ruhlandt-Senge, H. Hope, *Organometallics*, 22 (2003) 4933.
- [238] A.R. Katritzky, M.S. Kim, D. Fedoseyenko, K. Widyan, M. Siskin, M. Francisco, *Tetrahedron*, 65 (2009) 1111-1114.

- [239] Z. Lasemi, R. Hosseinzadeh, M. Tajbakhsh, M. Mohadjerani, *Bulg. Chem. Commun.*, 45 (2013) 379.
- [240] J.S. Showell, J.R. Russell, D. Swern, *J. Org. Chem.*, 27 (1962) 2853.
- [241] J. Cai, *Coordination Chemistry Reviews*, 248 (2004) 1061-1083.
- [242] G.K. Shimizu, R. Vaidhyanathan, J.M. Taylor, *Chem Soc Rev*, 38 (2009) 1430-1449.
- [243] G.A. Kraus, J.J. Lee, *Journal of Surfactants and Detergents*, 16 (2012) 317-320.
- [244] L. Zhang, J. Shi, A. Xu, B. Geng, S. Zhang, *Journal of Surfactants and Detergents*, 16 (2012) 183-190.
- [245] D.C. French, D.S. Crumrine, *J. Org. Chem.*, 55 (1990) 5494.
- [246] G.H. Ohrlein, W. Schwab, R. Ehrler, V. Jager, *Org. Synth.*, (2000).
- [247] K.R. Fewings, P.C. Junk, D. Georganopoulou, P.D. Prince, J.W. Steed, *Polyhedron*, 20 (2001) 643.

## CHAPTER 2

### Scope of the Thesis

#### 2.0 Summary of Content

Over the last few decades, important reasons for the study of Group II organometallics have emerged, mainly due to their particular interest as synthetic precursors<sup>[1-5]</sup> and functional materials.<sup>[6-8]</sup> Whilst the metals show high promise in these fields, research on their properties has not come without difficulties. These difficulties arise because the target compounds are challenged by the weak nature of the metal-ligand bond with increasing metal size, a mainly electrostatically controlled coordination environment, and a significant propensity to aggregate, associated with limited solubility.<sup>[9, 10]</sup> Thus, studying the properties of alkaline earth coordination complexes remains a challenging area of research.

The scope of this thesis is geared towards the analysis of the structure/function relationships in alkaline earth complexes, particularly as gas storage materials and synthetic precursors. Thus, this thesis is divided into two parts.

The first part is focused on alkaline earth metal organic framework (MOF) chemistry, and is based on one of the lightest metals in the periodic table, magnesium, with the aim to prepare lightweight, porous materials for gas storage. While a large amount of open-frameworks have been reported for transition metals,<sup>[11, 12]</sup> the expansion of MOF chemistry to magnesium is based on the affinity of magnesium towards hydrogen, offering the possibility of hydrogen storage in the pores. Further, hydrogen sorption to the metal sites provides the possibility of a larger storage capacity. Very few prior examples of magnesium-based MOFs have been reported and the number is especially small for those that remain intact after desolvation and exhibit permanent microporosity. This is discussed in **Chapter 3**, where the synthesis and

characterization of lightweight magnesium coordination complexes, based on the *para*-pyridinecarboxylic acid, is detailed.

While magnesium-based materials have been evaluated for hydrogen storage materials due to its lightweight character, the larger, heavier metals calcium, strontium and barium display larger metal diameters that allow for different structural properties. Because we are interested in a correlation of metal size with physical properties, we explored synthetic routes explored for magnesium chemistry, as outlined in **Chapter 3**. Then we used these routes to afford four novel heavy alkaline earth metal (Ca, Sr and Ba) coordination complexes, as summarized and discussed in **Chapters 4-5**.

The second part of this thesis, **Chapter 6**, reports our studies of the effect of 18-crown-6 coordination on the highly aggregated, anhydrous alkaline earth tosylates. These were reported to be excellent pre-cursors towards isolating heavy alkaline earth metal amides,<sup>[13, 14]</sup> yet their poor solubility in common organic solvents is an obstacle. The crystallographic features and physical properties of four novel 18-crown-6 stabilized alkaline earth tosylates are reported. This work provides a nice overview on the effect of various parameters, including non-covalent interactions, on the coordination chemistry of the target compounds.



## 2.1 Study on Metal Organic Frameworks: ligand choice, reaction solvent composition and metal size dependency

Alkaline earth metal-based MOFs containing the biocompatible metals magnesium and calcium in conjunction with phosphoric acids, have been previously studied in our group by Dr. Victoria Bampoh<sup>[15]</sup> as possible bone therapy additives. This work impressively demonstrated the correlation between reaction conditions and structural features<sup>[15]</sup>, as also observed in the literature,<sup>[16-20]</sup> Dr. Bampoh's work was geared to design systematic approaches towards the target compounds, on the basis of a) the ligand type and b) the solvent composition, and c) metal size dependency.

The choice of ligand type in our work is based on evidence that rigid, multi-topic ligands have afforded open-frameworks.<sup>[21-24]</sup> Specifically, ligands based on flat aromatic centers have been demonstrated to offer these properties.<sup>[25-27]</sup> Therefore, we decided to employ pyridinecarboxylic acids for the construction of higher dimensional networks (Figure 2.1). The MOF literature is heavily populated with examples involving carboxylate-based networks, and the study of ditopic ligands with both carboxylates and nitrogen binding points as MOF producers is new and promising.<sup>[28-31]</sup>

There are many powerful advantages in using pyridinecarboxylic acids as linkers in MOF chemistry: the multiple binding sites, consisting of an anionic carboxylate and Lewis basic nitrogen, offer coordination to two different ligand moieties. Furthermore, pyridinecarboxylic acids exist in the form of several isomers, with the pyridyl site in para, meta and ortho position, allowing the study of ligand geometry on overall solid architecture without changing the nature

of the ligand system. Furthermore, the ligands are soluble in water and a variety of organic solvents and are of low cost. There are significant considerations, especially in light of the desired technical application.

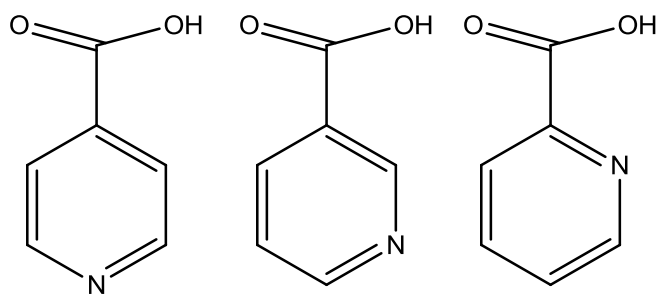


**Figure 2.1** para, meta and ortho-pyridinecarboxylic acid

It has been widely documented that solvent choice has a major impact on MOF architecture, and thus, a systematic study on solvent effect is essential in this work. This has been an area of interest since reports indicated that mixtures of polar organic solvents afford higher dimensional architectures (2D, 3D).<sup>[32, 33]</sup> Again, although prior work is available on transition metals, in contrast it is not clear of these effects would be apparent for the s-block metals. Solvent mixtures also seem to have an effect on the inclusion of different solvents in the cavities.<sup>[34]</sup> Thus, our systematic approaches include studying solvent mixtures and their different ratios ranging from water to mixtures of polar organic solvents (mainly EtOH, MeOH, CH<sub>3</sub>CN, DMF, THF), to study their effect on the resulting structures. Using these solvent choices, five new magnesium coordination complexes were obtained and characterized, as described in **Chapter 3**.

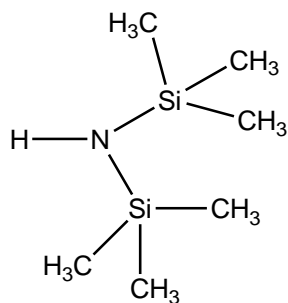
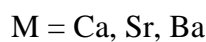
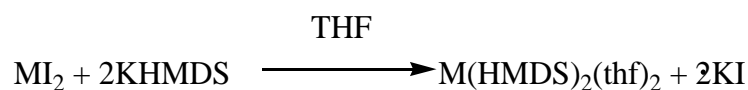
Literature reports document a clear correlation between metal size and the resulting coordination complex. Thus, we were interested in the study of metal dependency on network geometry. There are very few literature reports on heavy alkaline earth metal open-frameworks coordination compounds, likely because the large metal diameters increasing from calcium to barium promote aggregation under formation of condensed phases.

This is discussed in **Chapters 4-5**, where metal size dependency (calcium, strontium and barium) on the resulting coordination complexes was studied under variations of the solvent composition, in analogy to **Chapter 3**. This work afforded five new calcium, strontium and barium coordination polymers.

## 2.2 Crown ether stabilized alkaline earth tosylates: donor studies

Salt metathesis (Scheme 2.1) is one of the most effective routes towards the synthesis of alkaline earth amides, which can be used as precursors towards heavy alkaline earth organometallics.<sup>[10]</sup>

Whilst salt metathesis provides the amides in high yield and purity, the starting metal iodides ( $\text{CaI}_2$ ,  $\text{SrI}_2$  and  $\text{BaI}_2$ ) must be anhydrous and highly pure,<sup>[35]</sup> making them very expensive. Further, the incomplete precipitation of the resulting alkali halide under formation of “ate” complexes is a distinct possibility, imposing difficulties in the isolation of pure products.<sup>[36]</sup>



HMDS = Hexamethyldisilazane

### Scheme 2.1 Salt metathesis reaction

Two communications in the 1990's dealt with alternative starting materials to replace the expensive alkaline earth iodides. One proposed by Frankland *et al.*<sup>[13]</sup>, involved alkaline earth triflates ( $\text{CF}_3\text{SO}_3\text{H}$ , Figure 2.2) in reaction with alkali metal amides in THF, affording  $\text{Ca(HMDS)}_2(\text{thf})_2$  and  $\text{Sr(HMDS)}_2(\text{thf})_2$  in high yields.

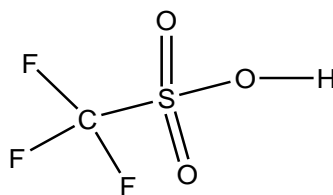
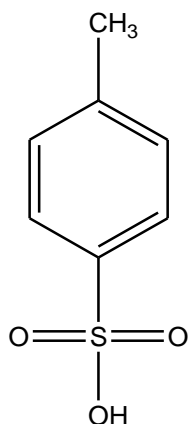


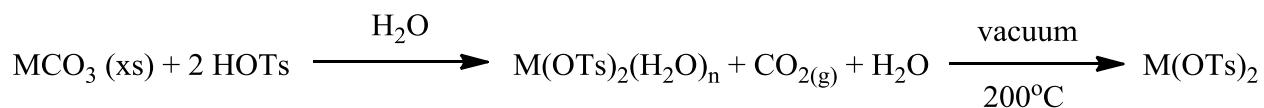
Figure 2.2 Triflic acid

Triflic acid, whilst being highly acidic ( $\text{p}K_a = -15$ ),<sup>[37]</sup> is still very expensive. The second communication explored the possibility of using the less expensive *p*-toluenesulfonic acid (HOTs, Figure 2.3)<sup>[14]</sup> precursors to obtain the target amides *via* salt metathesis.



**Figure 2.3** *p*-toluenesulfonic acid (HOTs,  $pK_a = -6.56$ )<sup>[38]</sup>

The attractiveness of *p*-toluenesulfonic acid as a cost-effective precursor further lies in the facile and inexpensive preparation of the alkaline earth tosylates through a bench-top acid base reaction without toxic side products. Whilst not as acidic as triflic acid, HOTs remains acidic enough to easily undergo aqueous acid-base chemistry with the corresponding alkaline earth carbonates under release of CO<sub>2</sub> gas. The anhydrous M(OTs)<sub>2</sub> are easily obtained by mild heating under dynamic vacuum for a few hours (Scheme 2.2). Conveniently, even though the following metathesis reactions require strict inert gas conditions, the M(OTs)<sub>2</sub> starting materials are air stable, facilitating handling and storage.



M= Mg, Ca, Sr, Ba

n = Mg: 6; Ca: 4; Sr: 1; Ba: 1

**Scheme 2.2** Synthesis of M(OTs)<sub>2</sub>

Surprisingly, little is known about the structural chemistry and physical properties of the alkaline earth metal tosylates. It is well documented however,<sup>[13, 14]</sup> that the anhydrous tosylates display very limited solubility, even in the presence of polar solvents such as THF. The low solubility is likely a consequence of significant aggregation upon dehydration.

In our work, initial studies involved refluxing the anhydrous tosylates in THF under inert conditions, yet this did not improve solubility. Thus we evaluated the role of the multidentate donor 18-crown-6<sup>[39-42]</sup> and its role in the structural chemistry of the alkaline earth metal tosylates.

Due to the limited solubility of the tosylates in organic solvents, the solvent of choice remained water. Reactions between the alkaline earth tosylates and 18-crown-6 in different ratios (metal/crown: 1:1, 1:2) were performed, obtaining four new crown stabilized alkaline earth tosylate coordination complexes exhibiting a range of ion association modes. This project provides fascinating insight into different mechanisms to obtain steric saturation in the large alkaline earth metal centers.

### 2.3 References

- [1] J.S. Alexander, K. Ruhlandt-Senge, *Eur. J. Inorg. Chem.*, (2002) 2761.
- [2] B.I. Nakhmanovich, Y.G. Urman, A.A. Arest-Yakubovich, *Macromol. Chem. Phys.*, 202 (2001) 1327.
- [3] S. Harder, F. Feil, A. Weeber, *Organometallics*, 20 (2001) 1044.
- [4] T.P. Hanusa, *Organometallics*, 21 (2002) 2559.
- [5] W. Teng, Doctoral Thesis, in: Department of Chemistry, Syracuse University.
- [6] W.D. Buchanan, D.G. Allis, K. Ruhlandt-Senge, *Chem. Commun.*, 46 (2010) 4449.
- [7] W.D. Buchanan, M.A. Guino-o, K. Ruhlandt-Senge, *Inorg. Chem.*, 49 (2010) 7144.
- [8] W.D. Buchanan, E.D. Nagle, K. Ruhlandt-Senge, 8 (2009) 263.
- [9] A. Torvisco, A.Y. O'Brien, K. Ruhlandt-Senge, *Coord. Chem. Rev.*, 11-12 (2011) 1268.
- [10] A.G. Goos, P.J. Rosado Flores, Y. Takahashi, K. Ruhlandt-Senge, *Alkaline Earth Metals: Organometallic Chemistry 2012*.
- [11] H.C. Zhou, J.R. Long, O.M. Yaghi, *Chem. Rev.*, 112 (2012) 673-674.
- [12] G. Xiaojun, S. Haiquan, *Materials Focus*, 1 (2012) 97.
- [13] A.D. Frankland, P.B. Hitchcock, M.F. Lappert, G.A. Lawless, *J. Chem. Soc., Chem. Commun.*, (1994) 2435.
- [14] A.D. Frankland, M.F. Lappert, *J. Chem. Soc. Dalton Trans.*, (1996) 4151.
- [15] V. Bampoh, Doctoral Thesis, in, Syracuse University, 2012.
- [16] C. McKinstry, E.J. Cussen, A.J. Fletcher, S.V. Patwardhan, J. Sefcik, *CrystGrowthDes*, 13 (2013) 5481-5486.
- [17] F. Yuan, J. Xie, H.-M. Hu, C.-M. Yuan, B. Xu, M.-L. Yang, F.-X. Dong, G.-L. Xue, *CrystEngComm*, 15 (2013) 1460.

- [18] X.-J. Kong, Y.-P. Ren, L.-S. Long, R.-B. Huang, L.-S. Zheng, M. Kurmoo, *CrystEngComm*, 10 (2008) 1309.
- [19] X.-M. Chen, M.-L. Tong, *Acc. Chem. Res.*, 40 (2007) 162.
- [20] T.A. Makal, A.A. Yakovenko, H.-C. Zhou, *J. Phys. Chem. Letters*, 2 (2011) 1682-1689.
- [21] L. Sarkisov, L.R. Martin, M. Haranczyk, B. Smit, *J. Am. Chem. Soc.*, 136 (2014) 2228.
- [22] L. Liu, X. Wang, Q. Zhang, Q. Li, Y. Zhao, *CrystEngComm*, 15 (2013) 841.
- [23] W. Yang, M. Guo, Y. Fei-Yan, S. Zhong-Ming, *Cryst. Growth Des.*, 12 (2012).
- [24] S. Henke, R. Schmid, J.-D. Grunwaldt, R.A. Fischer, *Chem. Eur. J.*, 16 (2010) 14296.
- [25] J.-J. Wang, M.-L. Yang, H.-M. Hu, G.-L. Xue, D.-S. Li, Q.-Z. Shi, *Z. Anorg. Allg. Chem.*, 633 (2007) 341.
- [26] X. Wang, J. Luan, H. Lin, C. Xu, G. Liu, J. Zhang, A. Tian, *CrystEngComm*, 15 (2013) 9995.
- [27] J.-Q. Liu, Y.-Y. Wang, Y.-N. Zhang, P. Liu, Q.-Z. Shi, S.R. Batten, *Eur. J. Inorg. Chem.*, 2009 (2009) 147-154.
- [28] A. Pichon, A. Lazuen-Garay, L.S. James, *CrystEngComm*, 8 (2006) 211.
- [29] S. Xiang, J. Huang, L. Li, J. Zhang, L. Jiang, X. Kuang, C.-Y. Su, *Inorg. Chem.*, 50 (2011) 1743.
- [30] M.C. Das, H. Xu, S. Xiang, Z. Zhang, H.D. Arman, G. Qian, B. Chen, *Chem. Eur. J.*, 17 (2011) 7817.
- [31] Y.-H. Zhou, Y.-P. Tian, *Bull. Korean Chem. Soc.*, 34 (2013) 2800-2802.
- [32] I. Senkovska, J. Fritsch, S. Kaskel, *Eur. J. Inorg. Chem.*, (2007) 5475.
- [33] C. Dey, T. Kundu, B. Biswal, A. Mallick, R. Banerjee, *Acta. Cryst. B70*, (2014) 3.



- [34] X.-R. Hao, X.-L. Wang, K.-Z. Shao, G.-S. Yang, Z.-M. Su, G. Yuan, *CrystEngComm*, 14 (2012) 5596.
- [35] M. Westerhausen, *Inorg. Chem.*, 30 (1991) 96.
- [36] M.M. Gillett-Kunnath, J.G. MacLellan, C.M. Forsyth, P.C. Andrews, G.B. Deacon, K. Ruhlandt-Senge, *Chem. Commun.*, (2008) 4490-4492.
- [37] R.D. Howells, J.D. McGown, 77 (1977) 69.
- [38] D.C. French, D.S. Crumrine, *J. Org. Chem.*, 55 (1990) 5494.
- [39] U. Englich, K. Ruhlandt-Senge, *Z. Anorg. Allg. Chem.*, 627 (2001) 851.
- [40] D.C. Green, U. Englich, K. Ruhlandt-Senge, *Angew. Chem. Int. Ed.*, 38 (1999) 354.
- [41] U. Englich, K. Ruhlandt-Senge, F. Uhlig, *J. Organomet. Chem.*, 613 (2000) 139.
- [42] S. Chadwick, U. Englich, B.C. Noll, K. Ruhlandt-Senge, *Inorg. Chem.*, 37 (1998) 4718.

## CHAPTER 3

Novel magnesium coordination networks based on the *p*-pyridinecarboxylic acid ligand**3.0 Introduction**

With a remarkable growth in the number and applications of metal organic frameworks (MOFs), the vast majority of known compounds are transition metal based carboxylates.<sup>[1]</sup> In contrast, little is known about main-group-based MOFs, with even less information on s-block metal based species. There are significant differences between main group and transition metal MOF's, the most relevant of which is the lack of geometrical control, due to the filled or energetically unavailable d-orbitals. Thus, detailed synthetic knowledge, achieved by extensive work over two decades,<sup>[2-4]</sup> and a well-defined coordination chemistry, as made possible by d-orbital participation results in an extensive library of structural patterns, is not available for the main group MOFs. This is especially the case for s-block MOFs, where the large metal sizes commonly result in large coordination numbers, and geometries are mainly dictated by electrostatic interactions. Further, the weak metal ligand bonds often provide multiple coordination environments which are all quite similar in energy, making a prediction of geometrical parameter especially challenging. However, the recent dissemination of a number of potential applications has spurred the interest in s-block MOFs. Of special interest are lithium and magnesium based MOFs for gas storage, because of their low weight and their significant affinity towards hydrogen.<sup>[5]</sup>

For both metals, the use of multitopic linkers has been documented, and ligands with two different hard/soft binding sites have afforded 3D networks.<sup>[6-8]</sup> In particular, *p*-

pyridinecarboxylic acid (Hin) (Figure 3.1a) and its isomers are of interest, as systematic studies based on substitution pattern and different binding modes (Figure 3.1b) are easily possible. For the alkali metals, work by Abrahams *et al.*<sup>[9]</sup> afforded the 3-dimensional [Li(in)]•0.5 DMF, which exhibits a microporous structure with gas adsorption properties. For the heavier group II metals, calcium and strontium,<sup>[10]</sup> picolinic acid and isonicotinic acid afforded hydrogen bonded networks. The Ca isonicotinate species displays layers associated *via*  $\pi$ --- $\pi$  stacking and hydrogen bonding,<sup>[11]</sup> whereas the Sr congener contains an unusual dissociated [in]<sup>-</sup> ligand.<sup>[11]</sup>

The effect of solvent composition on resulting frameworks is a topic of much discussion. In the transition metal sphere, studies involving the role of solvent in structural assembly have arisen before. Specific examples of structures for transition metals include frameworks by Chen *et al.*<sup>[12]</sup>, who reported on solvent dependent Mn(II) structures based on tetrachloroterephthalates, in which solvent combinations (pyridine/water, EtOH/MeOH, dioxane/H<sub>2</sub>O, MeOH/DMF) afforded 1-dimensional (pyridine/water; EtOH/MeOH), 2-dimensional (dioxane/H<sub>2</sub>O) and 3-dimensional (MeOH/DMF) frameworks. For Mg(II) frameworks, Mazaj *et al.*<sup>[13]</sup>, using trimesic acid, investigated the control of crystallization processes by tuning solvent composition. Their system consisted of EtOH/water in various compositions (EtOH/H<sub>2</sub>O = 0:4; 1:4; 1.8:2.2; 4:0), with stable structures ranging from 0D (0:4), 1D (1:4), 2D (1.8:2.2) and 3D (4:0).

Further examples include Banerjee *et al.*,<sup>[14]</sup> who isolated four different Mg(II) frameworks that were based on 3,5-pyridinecarboxylic acid under different solvent compositions. Thus, we see that it is important to develop systematic studies in order to pinpoint conditions that lead to functional MOFs.

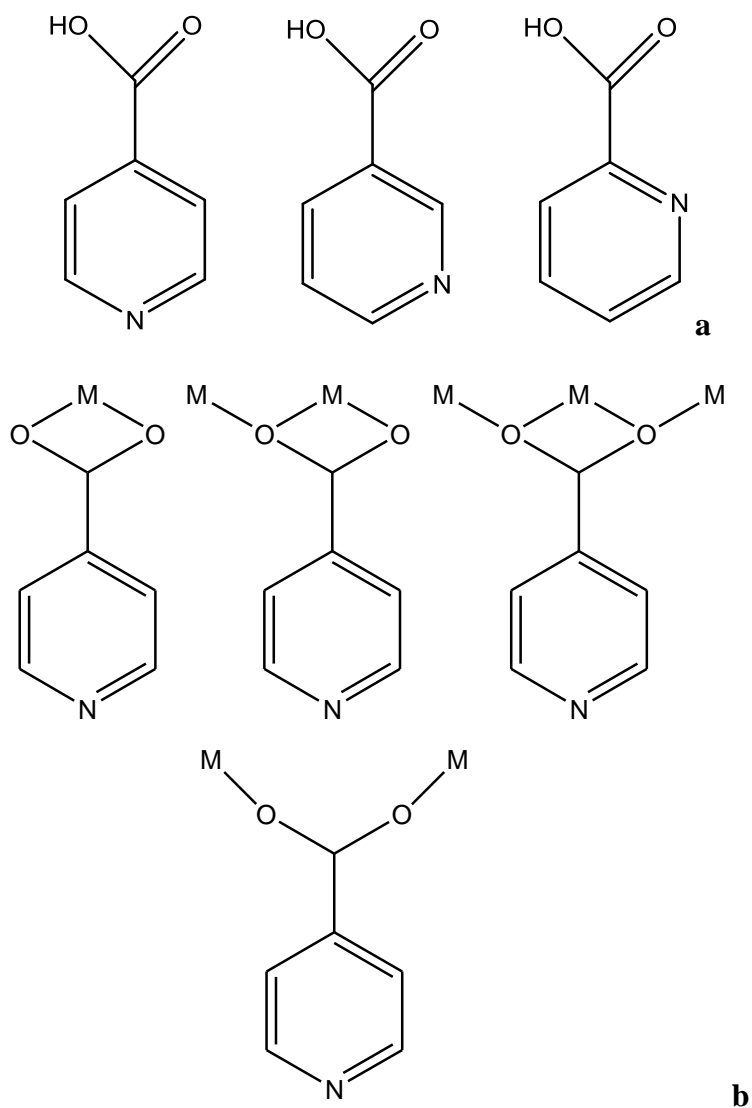


**Figure 3.1** (a) From left to right *p*-pyridinecarboxylic acid (Hin), *m*-pyridinecarboxylic acid (Hnic) and *o*-pyridinecarboxylic acid (b) binding modes in pyridinecarboxylic acid, nitrogen coordination not shown

In our work we describe several magnesium *p*-pyridinecarboxylic acid (Hin) networks, showing that small changes in reaction conditions lead to significant changes in network geometry. These include a family with three different guest molecules (**1a - c**), a hydrogen

bonded network (2), and a zwitterionic compound, where the anion plays a major role in the propagation of the network (3).

### 3.1 Experimental

#### 3.1.1 General physical measurements

All chemicals were obtained commercially and used without further purification (purity of  $\text{Mg}(\text{NO}_3)_2 \cdot 6\text{H}_2\text{O}$  – 98%, Hin – 98%). IR measurements were carried with KBr pellets using a Nicolet IR200 FT-IR spectrophotometer between  $4000\text{ cm}^{-1}$  to  $400\text{ cm}^{-1}$ . Melting point determinations (uncalibrated) were made using capillary tubes in a Mel-Temp II melting point apparatus.

TGA (Thermogravimetric Analysis) measurements were performed on a TGA Q500 series instrument (TA Instruments-Waters LLC) under an  $\text{N}_2$  balance/sample purge flow of 40 mL/min and 60 mL/min, respectively. The samples (wt. 6-20 mg) were loaded onto a platinum pan and heated using a ramp method, from room temperature to  $750\text{ }^\circ\text{C}$  (ramp rate:  $10\text{ }^\circ\text{C}/\text{min}$ ). Temperature dependent powder X-ray diffraction experiments were performed on a Bruker D8 Series II Advanced diffractometer equipped with a point detector and a target producing  $\text{CuK}\alpha$  ( $1.54\text{ \AA}$ ) radiation. A scan range was chosen between  $10\text{-}70\text{ }^\circ 2\theta$ , with a 1 sec/step scanspeed in increments of 0.04 steps. The temperature experiments were performed on a Parr TTK450 temperature stage, equipped with a liquid nitrogen cooling system, under vacuum from  $25\text{-}300\text{ }^\circ\text{C}$ . Compounds **1a** and **b** were characterized by the physisorption of  $\text{N}_2$  (Airgas, 99.999%) at  $77\text{ K}$  (Micromeritics ASAP 2020). Prior to  $\text{N}_2$  dosing, samples were gassed out under vacuum at  $298\text{ K}$  for 24 h to avoid any structural collapse due to elevated temperatures. Surface areas were

determined by BET; total pore volumes were estimated from the total quantity of nitrogen condensed on the samples at a relative pressure of 0.995.

All single crystal X-ray data were collected on a Bruker Kappa diffractometer using an APEX 2 CCD detector and MoK $\alpha$  radiation (0.7107 Å). Crystals were cooled using a Cryocool LN-3 low temperature device (Cryoindustries of America, Inc.) The crystals were submerged in highly viscous hydrocarbon oil (Infineum), mounted on a MITEGEN® mount and placed in the low temperature stream on the diffractometer, similar to what has been described previously.<sup>[15]</sup> Data collection parameters and refinement details have been described elsewhere in detail.<sup>[15, 16]</sup> The crystal structures were solved using direct methods and subsequent refinement was accomplished by the full-matrix least-squares method on  $F^2$ .<sup>[17]</sup> All non-hydrogen atoms were refined anisotropically. Absorption corrections were performed using the SADABS program.<sup>[18]</sup> Hydrogen atoms were calculated to fixed positions. SQUEEZE parameters in PLATON were utilized to determine the approximate solvent void volume after removal of solvent electron density for **1a-c**.<sup>[19]</sup>

The non-centrosymmetric spacegroups in **1a** and **1b** were confirmed using the program PLATON.<sup>[19]</sup> For **1a**, the disordered DMF molecule was refined over split positions as follows: 0.57588 and 0.42412.

### 3.1.2 Synthesis

**General procedure:** Compounds **1a-c**, **2** and **3** were synthesized using solvothermal/hydrothermal conditions in Carius tubes (4 mL). The solvents (or mixtures thereof) (DMF, ACN, THF and H<sub>2</sub>O) were chosen for their ability to dissolve Mg(NO<sub>3</sub>)<sub>2</sub>·6H<sub>2</sub>O and the Hin ligand. Reactions were performed in the temperature range of 120-135 °C, using different donor ratios, as summarized in Scheme 1.

**{[Mg(in)<sub>2</sub>]<sub>2</sub>·DMF}<sub>∞</sub> (1a):** 0.3 mmol (88.5 mg) of Mg(NO<sub>3</sub>)<sub>2</sub>·6H<sub>2</sub>O and 0.6 mmol (77.9 mg) of Hin in a 1:3 (4 mL) DMF/MeOH mixture were combined. The Carius tube was sealed under vacuum and reacted solvothermally at 135°C. After 2 days, colorless block-shaped crystals suitable for X-ray crystallography were isolated from the clear, colorless mother liquor. Mp: decomposes >475°C. Yield (non-optimized): 93.2 mg, 31%. IR (cm<sup>-1</sup>): 2976 (br, w); 2781 (w); 2440 (w); 1543 (w); 1471 (w); 1384 (s); 1233 (w); 1024 (m); 885 (w); 867 (s); 784 (w); 681 (w).

**{[Mg(in)<sub>2</sub>]<sub>2</sub>·ACN}<sub>∞</sub> (1b):** 0.5 mmol (128.2 mg) of Mg(NO<sub>3</sub>)<sub>2</sub>·6H<sub>2</sub>O and 1 mmol (123.1 mg) of Hin in a 2:2 (4 mL) ACN/DMF mixture were combined. The Carius tube was sealed under vacuum and kept at 135°C. Overnight, colorless block-shaped crystals suitable for X-ray crystallography were obtained from the clear, colorless mother liquor. Mp: decomposes > 400 °C. Yield (not optimized): 86.6 mg, 30%. IR (cm<sup>-1</sup>): 3048 (w); 2462 (w); 1986 (w); 1627 (br, s); 1558 (s); 1497 (s); 1425 (br, s); 1216 (m); 1090 (m); 1017 (m); 850 (s); 786 (s); 713 (s); 682 (s); 601 (m); 562 (m).

**{[Mg(in)]·0.5THF}<sub>∞</sub> (1c):** 1 mmol (256.4 mg) of Mg(NO<sub>3</sub>)<sub>2</sub>·6H<sub>2</sub>O and 2 mmol (246.2 mg) of Hin in a 2:2 MeOH/THF mixture were combined. The Carius tube was sealed under vacuum and reacted solvothermally at 135°C. Overnight, colorless block-shaped crystals suitable for X-ray crystallography were obtained from the clear, colorless mother liquor. Mp: decomposes > 400 °C. Yield (not optimized): 56.8 mg, 21%. IR (cm<sup>-1</sup>): 2723 (w); 2352 (w); 1983 (w); 1613 (m); 1555 (m); 1455 (s); 1376 (s); 1216 (w); 1155 (w); 1064 (w); 1015 (w); 878 (w); 846 (m); 783 (m); 711 (m); 676 (m).

**{[Mg(in)<sub>2</sub>(H<sub>2</sub>O)]·EtOH}<sub>∞</sub> (2):** 0.5 mmol (128.2 mg) of Mg(NO<sub>3</sub>)<sub>2</sub>·6H<sub>2</sub>O and 1 mmol (123.1 mg) of Hin in 4 mL of EtOH were combined. The Carius tube was sealed under vacuum and reacted solvothermally at 135°C. Overnight, colorless block-shaped crystals suitable for X-ray crystallography were obtained from the clear, colorless mother liquor. Mp: decomposes > 400 °C. Yield (not optimized): 118 mg, 17%. IR (cm<sup>-1</sup>): 2724 (w); 2672 (w); 2413 (w); 2305 (w); 1972 (m); 1884 (w); 1612 (w); 1469 (m); 1453 (s); 1380 (s); 1155 (w); 971 (w); 884 (w); 776 (w); 722 (s).

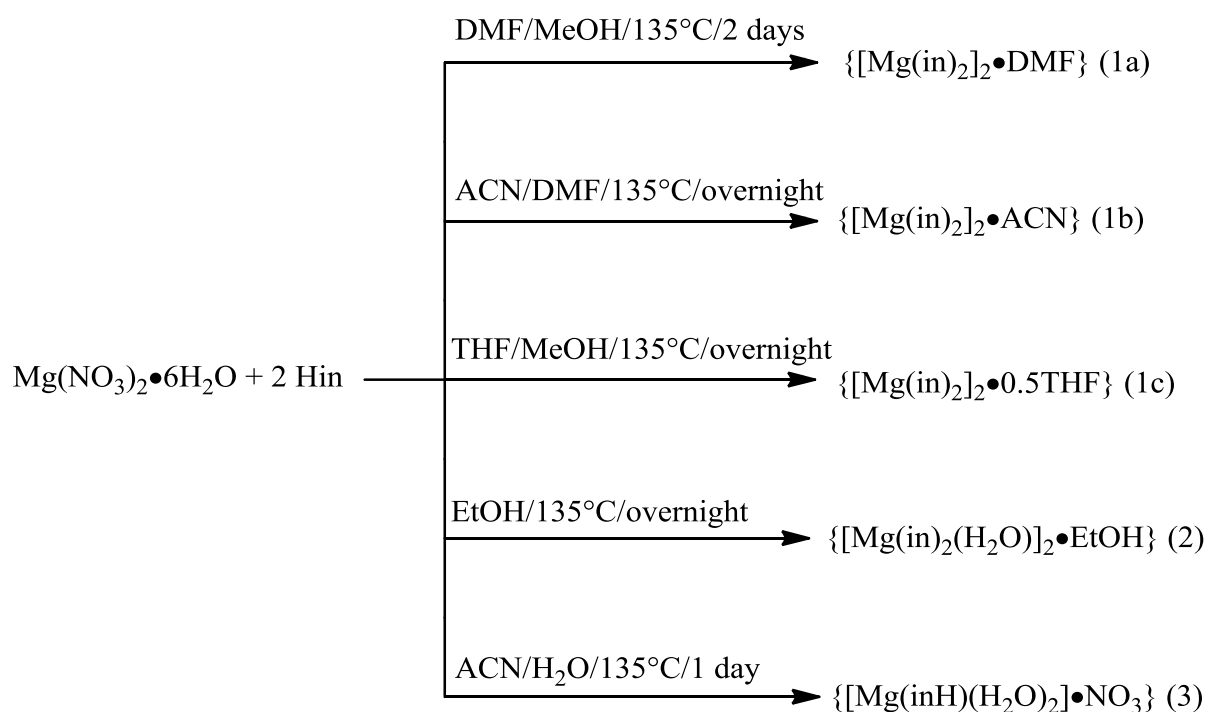
**{[Mg(inH)(OH<sub>2</sub>)<sub>2</sub>][NO<sub>3</sub>]}<sub>∞</sub> (3):** 0.5 mmol (128.6 mg) of Mg(NO<sub>3</sub>)<sub>2</sub>·6H<sub>2</sub>O and 1 mmol (123.1 mg) of Hin were combined in a mixture of 3:1 (4 mL) CH<sub>3</sub>CN/H<sub>2</sub>O. The mixture was kept at 120 °C in the sealed Carius tube. After 1 day, colorless block-shaped crystals suitable for X-ray crystallography were obtained from the clear, colorless, mother liquor. Mp: decomposes >452°C. Yield % (not optimized): 188 mg, 40%. IR (cm<sup>-1</sup>): 3398 (br, s); 2396 (w); 2344 (w); 1635 (s); 1560 (w); 1388 (s); 1048 (m); 1002 (m); 969 (w); 860 (w); 825 (m); 688 (w).



## 3.2 Results and Discussion

### 3.2.1 Synthesis

The target compounds were prepared by acid base chemistry, involving the treatment of magnesium nitrate with the organic ligand (Scheme 3.1). Since reaction conditions have a profound effect on the composition of the resulting frameworks,<sup>[20-23]</sup> reagent stoichiometry and reaction conditions were systematically varied.



**Scheme 3.1** Synthesis of **1a-c**, **2** and **3**

**1a:** DMF/MeOH ratio: 1:3

**1b:** ACN/DMF ratio: 2:2

**1c:** THF/MeOH ratio: 2:2

**2:** EtOH ratio: 4

**3:** ACN/H<sub>2</sub>O ratio: 3:1

As shown previously, the coordinating ability of the donors plays a significant role in the structural dimensionality of the resulting network,<sup>[24]</sup> prompting us to systematically investigate the solvent dependency on the formation of the target compounds (Table 2.1).

The compound family **1a - c** was obtained by introducing solvent mixtures in various ratios. Optimal conditions for the crystallization for **1a-c**, **2** and **3** were found at temperatures of 120 °C (**3**) and 135 °C (**1a-c** and **2**), as described in the experimental section. If the temperature was raised above 150°C, decomposition of the reagents was generally observed.

As a side note, soaking **1a** for 1 week in fresh ACN or THF did not produce **1b** or **1c**, as verified *via* single crystal X-ray diffraction analysis of the soaked samples. The samples also did not uptake small molecules such as cyclohexane and benzene.

Compounds **1a-c** and **2** are soluble in water, yet insoluble in other solvents. Water molecules coordinate to the metal center more effectively than less polar solvents,<sup>[25]</sup> which is why **2** and **3** crystallize as hydrogen bonded networks.

**Table 3.1** Solvent systems in the synthesis of **1a - c** and **2**

Solvent	Ratio	Compound
DMF	na	-
EtOH	na	<b>2</b>
MeOH/DMF	3:1, 1:3	<b>1a</b>
ACN/DMF	3:1, 2:2	<b>1b</b>
EtOH/DMF	3:1	<b>1a</b>
MeOH/THF	3:1	<b>1c</b>
MeOH/DMF/ACN	2:1:1	<b>1b</b>
EtOH/DMF/ACN	1:1:2	<b>1a</b>

Interestingly, whilst compound **2** was synthesized in EtOH as a solvent, a water molecule is coordinated to the metal center, resulting in a different structure as compared to the other compounds. It is rationalized that ethanol contains enough water to lead to the formation of a hydrogen-bonded, 2-dimensional sheet network, as explained in the structural characterization section. Further, repeating the reaction using dry ethanol resulted in the isolation of the water species ( $\{[\text{Mg}(\text{in})_2]_2 \cdot \text{H}_2\text{O}\}$ ) as reported by Liu *et al.* (detailed below).<sup>[26]</sup>

Compound **3** was prepared from a 3:1 ratio of acetonitrile/water, resulting in a zwitterionic species. The zwitterion nature of isonicotinic acid in solution has been studied

before, and it has been found that at low pH the predominant form of isonicotinic acid is the zwitterion.<sup>[27-30]</sup> This possibly led to the formation of a zwitterion species, instead of a neutral species.

## 3.2.2 Structural characterization of 1a-c, 2 and 3

Table 3.2 Structural characterization for compounds 1a - c, 2 and 3

Compound	<b>1a</b>	<b>1b</b>	<b>1c</b>	<b>2</b>	<b>3</b>
Empirical formula	$C_{27}H_{23}Mg_2N_5O_9$	$C_{26}H_{21}Mg_2N_5O_8$	$C_{12}H_8MgN_2O_4$	$C_{28}H_{30}MgN_4O_{12}$	$C_{12}H_{16}MgN_4O_{14}$
Formula weight	610.12	580.10	268.51	663.18	464.60
Crystal system	Monoclinic	Monoclinic	Monoclinic	Monoclinic	Triclinic
Space group	$P2_1$	$P2_1$	$P2_1/c$	$P2_1/c$	P-1
T (K)	86(2)	90(2)	90(2)	90(2)	90(2)
Unit cell dimensions ( $\text{\AA}$ , $^\circ$ )					
a	9.876(2)	9.864(11)	4.9198(16)	10.708(3)	6.122(8)
b	12.996(3)	13.084(16)	12.874(4)	11.903(3)	8.104(2)
c	10.706(2)	10.566(12)	11.004(4)	12.844(4)	9.376(3)
$\alpha, \gamma$	90	90	90	90	89.557(5); 88.521(5)

---

$\beta$	100.64(3)	101.699(2)	99.705(6)	110.02(7)	86.613(5)
Volume ( $\text{\AA}^3$ )	1350.5(5)	1335.5(3)	687.0(4)	1538.28(8)	464.1(2)
Z	2	2	2	2	1
Calculated density ( $\text{g/cm}^{-3}$ )	1.498	1.433	1.298	1.432	1.662
Absorption coefficient ( $\text{mm}^{-1}$ )	0.155	0.150	0.139	0.148	0.182
$\theta$ range	2.49 to 35.75°	1.97 to 26.37°	2.46 to 30.64°	2.15 to 26.37°	2.18 to 26.95°
Unique reflections	12009	5329	2088	2857	5657
Total reflections	35575	10389	8209	19219	2001
Goodness-of-fit on $F^2$	0.981	1.430	1.028	1.033	1.029
$R_1$ , $wR_2$ (all data)	$R_1 = 0.0676$ , $wR_2 = 0.1206$	$R_1 = 0.0455$ , $wR_2 = 0.1671$	$R_1 = 0.0623$ , $wR_2 = 0.1684$	$R_1 = 0.0450$ , $wR_2 = 0.1425$	$R_1 = 0.0544$ , $wR_2 = 0.0956$
$R_1$ , $wR_2$ (Final)	$R_1 = 0.0430$ , $wR_2 = 0.1079$	$R_1 = 0.0418$ , $wR_2 = 0.1598$	$R_1 = 0.0528$ , $wR_2 = 0.1506$	$R_1 = 0.0414$ , $wR_2 = 0.1381$	$R_1 = 0.0357$ , $wR_2 = 0.0890$
F(0 0 0)	630	600	276	692	240

---

The compounds **1a - c** display isostructural network geometries, with different guest molecules in the cavities. Because of the isostructural nature, only **1a** is shown. **1a** and **b** crystallize in the monoclinic non-centrosymmetric space group  $P2_1$ , while **1c** crystallizes in the centrosymmetric spacegroup  $P2_1/c$ . **1a** and **b** display distorted octahedral geometries with O-Mg-O angles ranging from  $87.207(8)$  to  $178.427(10)^\circ$  (**1a**) and  $87.710(4)$  to  $176.988(5)$  for (**1b**).

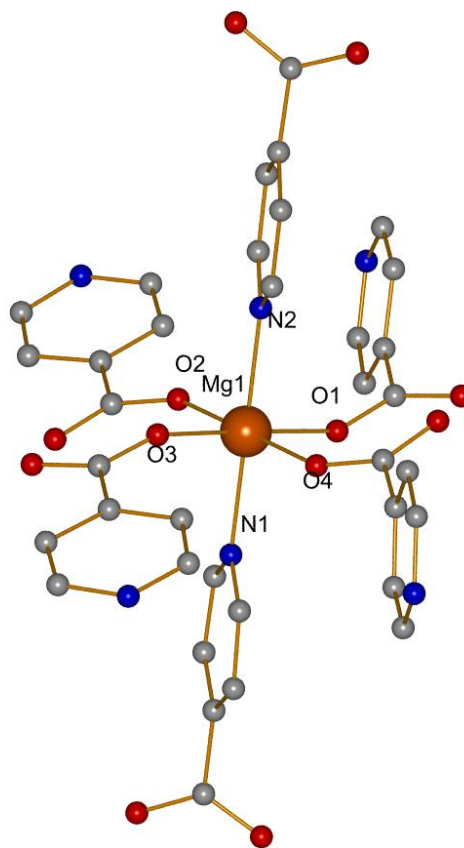
In both **1a** and **1b**, the asymmetric units display two rather similar independent magnesium centers coordinated equatorially by four oxygen atoms [Mg-O distances **1a**:  $2.046(8)$  (avg) Å, **1b**:  $2.060(11)$  Å (avg)] from four different ligands.

The axial positions in **1a** and **b** are occupied by two pyridyl nitrogens [Mg-N distances **1a**:  $2.215(5)$  Å (avg), **1b**:  $2.189(8)$  (avg) Å]. The N-Mg-N angles for **1a** and **b** are  $179.809(11)^\circ$  and  $178.425(7)^\circ$  respectively.

For **1c**, the asymmetric unit displays one half-occupied magnesium center. Like **1a** and **b**, the magnesium center displays a distorted octahedral geometry and is equatorially coordinated by four oxygens (three of which are symmetry generated). The Mg-O distances average  $2.051(9)$  Å, whilst O-Mg-O angles range from  $87.268(6)$  to  $180^\circ$ . As in **1a** and **b**, **1c** is coordinated axially by two nitrogen atoms (one which is symmetry generated). The Mg-N values are close [Mg-N  $2.206(5)$  and  $2.207(5)$  Å], with a N-Mg-N angle of  $180^\circ$ . Figure 3.3 shows the magnesium coordination environment in **1a-c**. A summary of pertinent bond lengths and angles for **1a - c** is presented in Table 3.3. These are within reported values for other compounds.<sup>[31, 32]</sup>

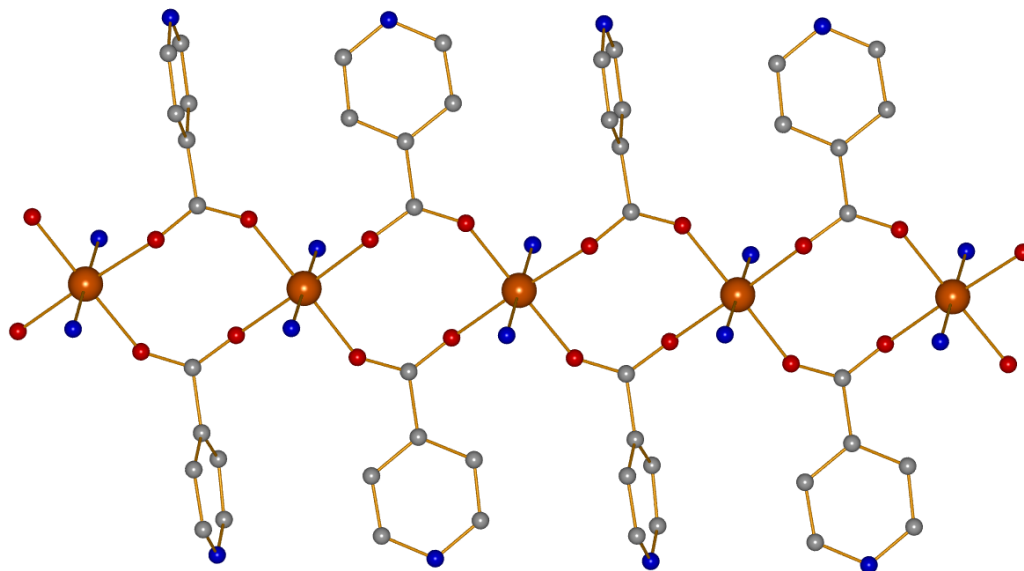
Due to the isostructural relationship between **1a**, **b** and **c**, structural propagation in **1a - c** is achieved in a similar fashion. Chains are formed *via* carboxylate moieties bridging neighboring magnesium centers, as shown in Figure 3.4a. Another set of chains is formed through the axial pyridyl nitrogen atoms, providing further propagation, as shown in Figure 3.4b.

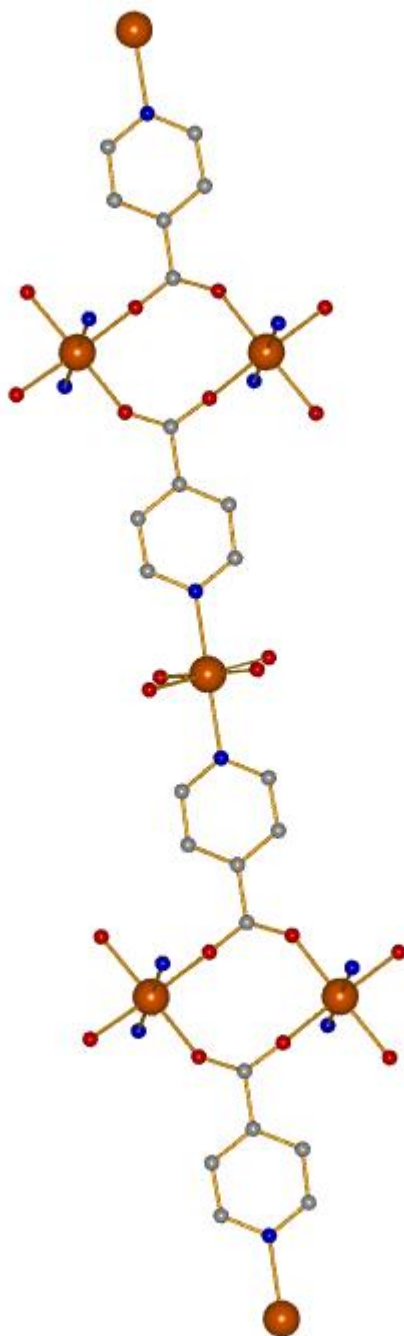
The combination of these two chains results in  $[\text{MgO}_4\text{N}_2]$  nodes to afford three-dimensional rhombohedral shaped channels, as shown in Figure 3.5.



**Figure 3.3** Six coordinate magnesium center in **1a**, **1b** and **1c** exhibit similar geometries, the magnesium center in **1c** sitting in a half occupancy position.



**a**

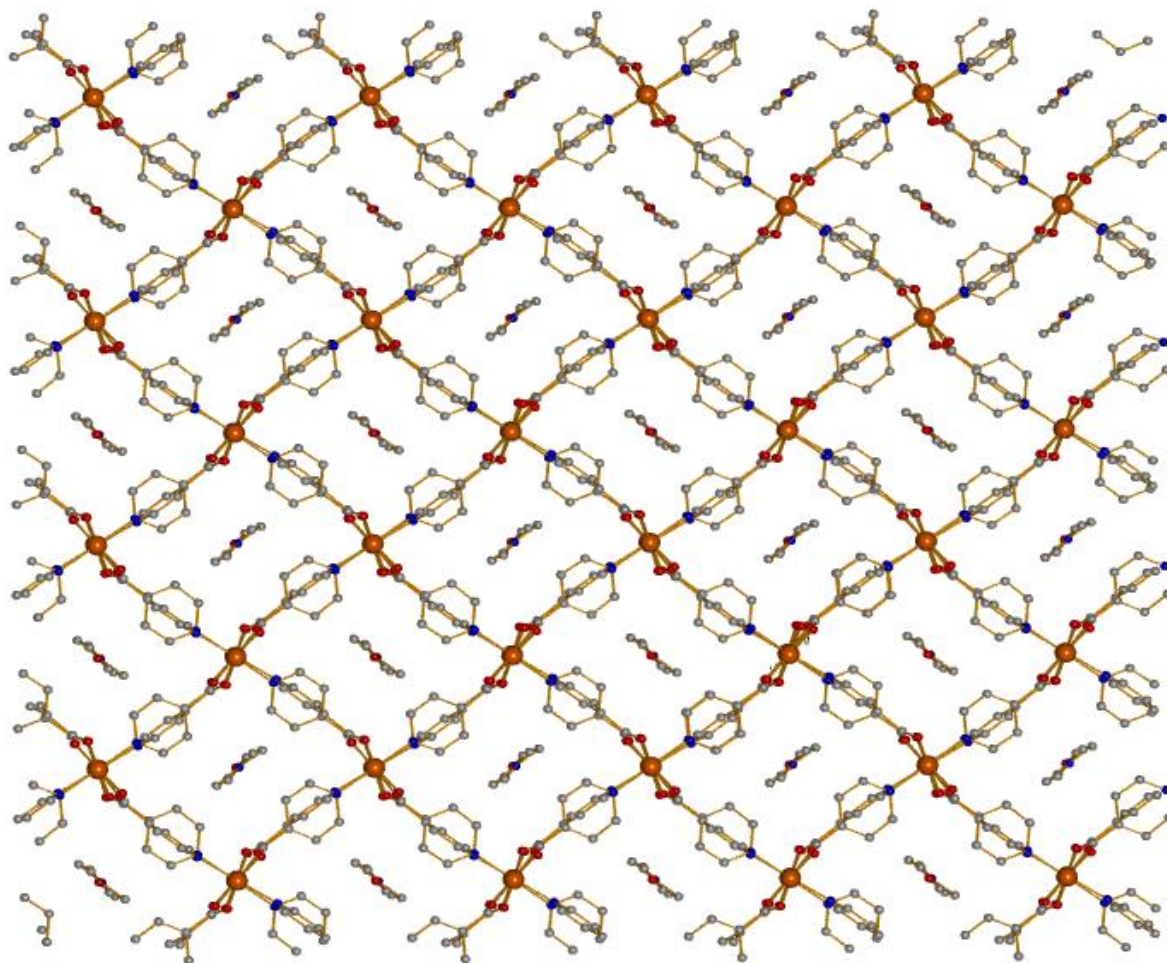
**b**

**Figure 3.4** Representation of the formation of the 3-dimensional network in compounds **1a - c**: (a) 1-dimensional chains afforded by bridging carboxylates; (b) axial propagation by pyridyl nitrogens. Hydrogen atoms have been removed for clarity.

**Table 3.3** Summary of selected bond lengths (Å) and angles (°) in **1a – c**

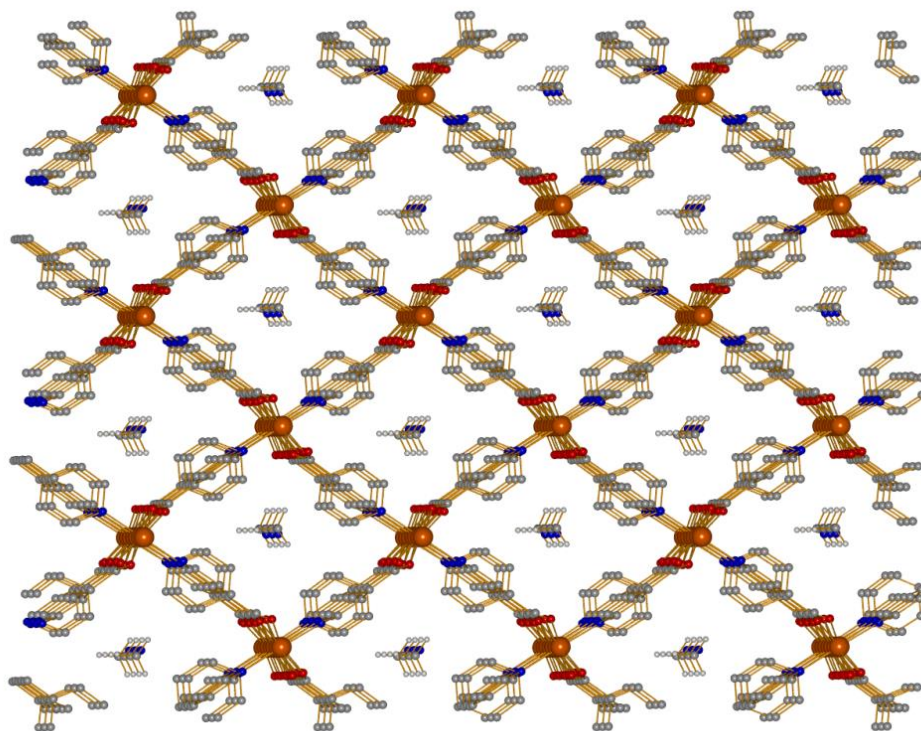
	<b>1a</b>	<b>1b</b>	<b>1c</b>
Mg(1)-O(1)	2.051(2)	2.073(2)	2.052(4)
Mg(1)-O(2)	2.038(2)	2.031(3)	2.050(5)
Mg(1)-O(3)	2.032(2)	2.058(3)	2.052(4)*
Mg(1)-O(4)	2.062(2)	2.077(3)	2.050(5)*
Mg(1)-N(1)	2.214(2)	2.185(4)	2.207(5)*
Mg(1)-N(2)	2.216(3)	2.194(4)	2.206(5)*
O(1)-Mg(1)-O(2)	87.413(7)	89.424(4)	87.268(6)
O(1)-Mg(1)-O(3)	178.058(9)	176.988(5)	180.000(1)*
O(1)-Mg(1)-N(1)	87.207(8)	92.481(5)	92.103(7)*
O(1)-Mg(1)-N(2)	92.946(7)	88.012(5)	87.897(6)*
N(1)-Mg(1)-N(2)	179.81(1)	178.425(7)	180.000(8)*
O(2)-Mg(1)-O(3)	94.271(8)	93.384(5)	92.732(7)*
O(2)-Mg(1)-O(4)	178.43(1)	178.816(6)	180.000(1)*
O(2)-Mg(1)-N(1)	91.31(1)	88.222(5)	92.006(6)*
O(2)-Mg(1)-N(2)	88.578(9)	92.279(6)	87.994(6)*
O(3)-Mg(1)-O(1)	178.058(9)	176.988(5)	180.000(1)*
O(3)-Mg(1)-O(4)	87.087(7)	87.710(4)	87.268(6)*
O(3)-Mg(1)-N(1)	91.784(8)	88.649(5)	87.897(6)*
O(3)-Mg(1)-N(2)	88.066(9)	90.786(5)	92.103(7)*
O(4)-Mg(1)-O(1)	91.216(8)	89.491(5)	92.732(7)*
O(4)-Mg(1)-N(1)	87.846(8)	90.350(5)	92.006(6)*
O(4)-Mg(1)-N(2)	92.27(1)	88.158(5)	87.994(6)*

\*Corresponding symmetry generated Mg-O distance or O-Mg-O, O-Mg-N, N-Mg-N angle around Mg(1) for **1c**. O(3), O(4), N(1) and N(2) in **1c** are symmetry generated in the structure.



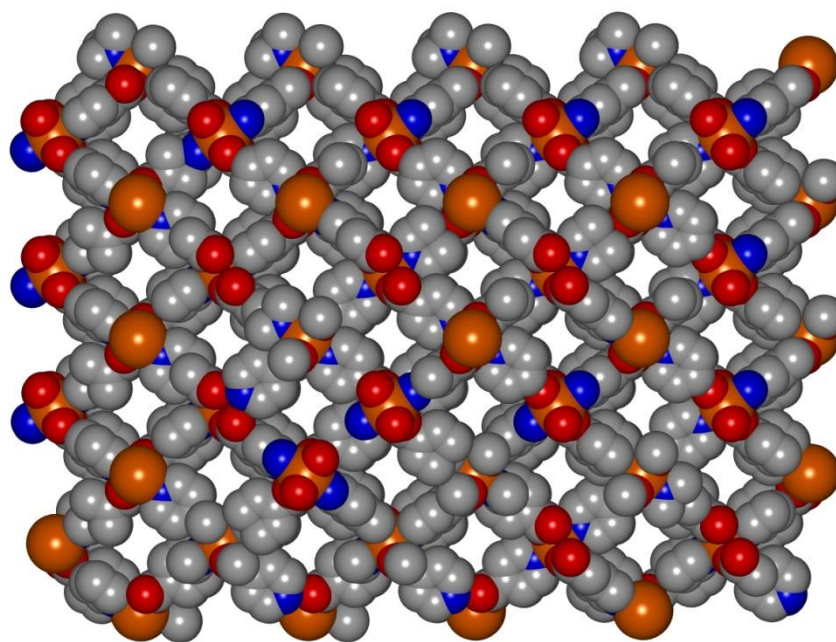
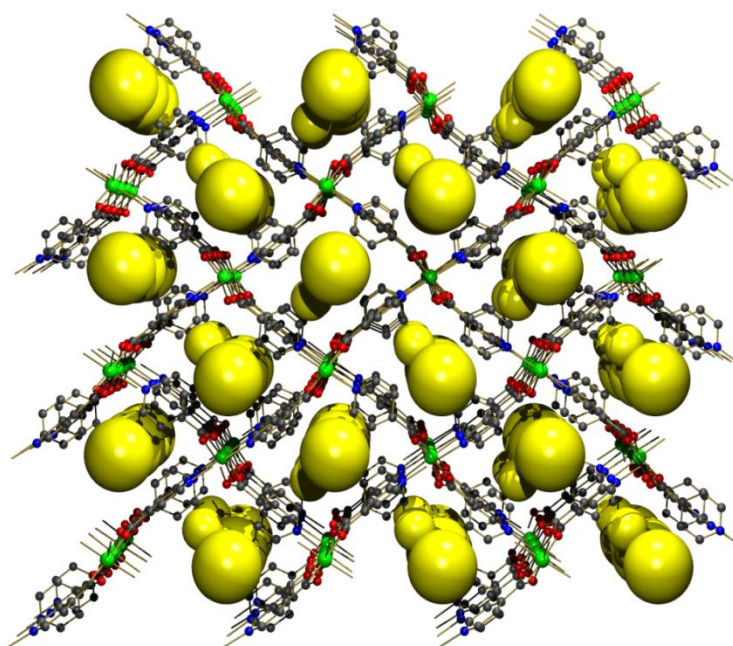
**Figure 3.5** Rhombohedral shaped cavities in **1a** showing disordered DMF. The channel geometry in **1b** and **c** is similar, with guests ACN (**1b**) and THF (**1c**) occupying the channels.. Hydrogen atoms removed for clarity.

In addition, compounds **1a-c** exhibit channels of differing sizes. Window sizes for **1a-c** were obtained by measuring Mg---Mg distances and are summarized in Table 3.4. Different guest molecules are observed in **1a-c** (Figure 3.6). Void space calculation, using the PLATON software, determined that **1a** shows one disordered DMF molecule in the asymmetric unit [ $316.9 \text{ \AA}^3$  (23.5%)], whilst **b** shows an ordered acetonitrile [ $69.2 \text{ \AA}^3$  (5.2%)]. Disorder refinement attempts for the guest molecule in **1c** were unsuccessful. Since the compound was isolated from a MeOH/THF mixture, SQUEEZE calculations were performed to elucidate the presence of MeOH or THF in the channels. The SQUEEZE calculation returned a volume of  $74.4 \text{ \AA}^3$  (10.8 % of the total unit cell volume), finding  $28 e^-$  in the voids, and these were assigned as 0.5 THF molecules. Figure 3.7 shows an example the space filling and calculated solvent plot of **1a**.



**Figure 3.6** Channel view of **1b** with acetonitrile guest molecules. Hydrogen atoms on ligands removed for clarity. Donor substitution in **1a-c** results in a slight channel size change.



**a****b**

**Figure 3.7** (a) Space filling plot for **1a** showing channel spaces (b) Calculated solvent plot in **1a**, yellow spheres represent DMF molecules.

The calculated void space volumes are considerably lower than those reported by Banerjee *et al.*<sup>[14]</sup>, who reported that three 3-dimensional structures based on Mg(II) in conjunction with 3,5-pyridinedicarboxylate demonstrated theoretical volumes ranging from 617 Å<sup>3</sup> to 2084 Å<sup>3</sup>.

Furthermore, Liu *et al.*<sup>[33]</sup> reported a structure with the formula  $\{[\text{Mg}(\text{in})_2]_2 \cdot \text{H}_2\text{O}\}_\infty$  with an isostructural motif to **1a-c**, in which instead a water molecule locates in the channels, obtaining similar window sizes to that of **1b**. Structural propagation is achieved in the same way as **1a-c**. This particular structure was isolated from DMF, whereas compounds **1a-c** were isolated from mixtures of MeOH/DMF. In our case, using DMF as the sole reaction solvent resulted in clear colorless solutions.

Window sizes in **1a-c** are larger than that of the reported  $[\text{Li}(\text{in})] \cdot 0.5\text{DMF}$ <sup>[9]</sup> which exhibits rectangular channels with a value of 4 Å x 5.5 Å. This result is possibly due to the different coordination geometry around the metal (for the reported Li<sup>+</sup> species: 4-coordinated, tetrahedral geometry; our Mg species: 6-coordinated, octahedral geometry).<sup>[34]</sup>

There is a noticeable increase in window size as the solvent molecule size decreases (DMF < THF < ACN). This result is consistent with the findings of Senkovska *et al.*<sup>[32, 35]</sup> for Mg frameworks, in which the guest molecule size was also correlated with increasing window size.

**Table 3.4** Window sizes for **1a-c**, and  $\{[\text{Mg}(\text{in})_2]_2 \cdot \text{H}_2\text{O}\}^{[33]}$ 

Compound	Window Size (Mg--- Mg distances)	Unit Cell Volume	Void volumes (Void vol./Total vol. x 100)
$\{[\text{Mg}(\text{in})_2]_2 \cdot \text{DMF}\}$ ( <b>1a</b> )	10.70 Å x 8.50 Å	1350.5 Å <sup>3</sup>	316.9 Å <sup>3</sup> (23.5 %)
$\{[\text{Mg}(\text{in})_2]_2 \cdot \text{ACN}\}$ ( <b>1b</b> )	13.08 Å x 8.46 Å	1335.5 Å <sup>3</sup>	69.2 Å <sup>3</sup> (5.2 %)
$\{[\text{Mg}(\text{in})_2]_2 \cdot \text{THF}\}$ ( <b>1c</b> )	11.00 Å x 8.56 Å	687.6 Å <sup>3</sup>	74.4 Å <sup>3</sup> (10.8 %),
$\{[\text{Mg}(\text{in})_2]_2 \cdot \text{H}_2\text{O}\}$	11.30 Å x 8.59 Å	1377.9 Å <sup>3</sup>	Not reported (24.3%)

Few frameworks with *p*-pyridinecarboxylic acid and Mg have been reported, the first example reported being a hydrogen bonded network.<sup>[25]</sup> As opposed to **1a-c**, in this example the 6-coordinate Mg center was coordinated axially by a pyridyl nitrogen, an oxygen from a carboxylate and equatorially by four waters. The waters formed an extended hydrogen bonded network. This clearly evidences the diversity of coordination motifs that *p*-pyridinecarboxylic acid can provide.

Compound **2** crystallizes in the monoclinic space group  $P2_1/c$ . Unlike **1a-c**, the asymmetric unit contains one fully occupied magnesium center. The magnesium center displays a six coordinate geometry consisting of two axial pyridyl nitrogen atoms [Mg-N 2.21(3) (avg) Å] with an N-Mg-N angle of 177.66(6)°. Three of the four equatorial oxygens stem from the ligand carboxylate [Mg-O: 2.042(4) (avg)], the fourth from a coordinated water with a Mg-O<sub>w</sub> distance of 2.083(1) Å. O-Mg-O angles range from (including the water position) 84.79(5)° to 172.32(5)°, and O-Mg-O<sub>w</sub> angles range from 84.99(5)-177.63(5)°, as shown in Figure 3.8. The N-Mg-O angles range from 88.75(5)-94.53(5)°, whilst the N-Mg-O<sub>w</sub> angle has a value of 89.15(5)°.



Table 3.5 summarizes selected bond lengths and angles for **2**. The bond lengths and angles are within published values.<sup>[36, 37]</sup>

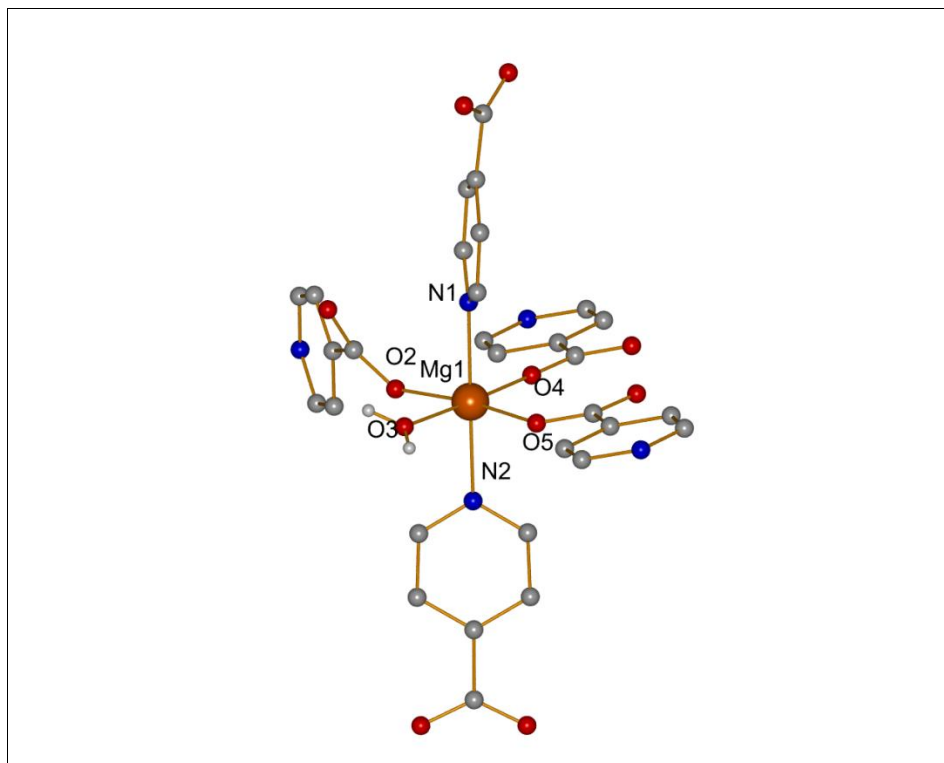


**Figure 3.8** The 6-coordinate metal environment in compound **2**. In contrast to compounds **1a - c**, one position, O3w is water. Hydrogen atoms, except for those on water, have been removed for clarity.

**Table 3.5** Selected bond lengths (Å) and angles (°) for **2**

Mg(1)-O(2)	2.0739(13)	O(2)-Mg(1)-N(1)	94.53(5)
Mg(1)-O(3) <sub>w</sub>	2.0834(13)	N(2)-Mg(1)-N(1)	177.66(6)
Mg(1)-O(4)	2.0095(13)	O(4)-Mg(1)-O(2)	89.99(5)
Mg(1)-O(5)	2.0437(13)	O(4)-Mg(1)-O(3) <sub>w</sub>	177.83(6)
Mg(1)-N(1)	2.229(2)	O(2)-Mg(1)-O(3) <sub>w</sub>	88.32(5)
Mg(1)-N(2)	2.191(2)	O(5)-Mg(1)-N(2)	88.75(5)
O(4)-Mg(1)-O(5)	96.786(1)	O(3) <sub>w</sub> -Mg(1)-N(2)	89.15(5)
O(5)-Mg(1)-O(2)	172.32(5)	O(5)-Mg(1)-N(1)	89.19(5)
O(5)-Mg(1)-O(3) <sub>w</sub>	84.99(5)	O(3)-Mg(1)-N(1)	89.56(5)
O(4)-Mg(1)-N(1)	89.21(5)		
O(4)-Mg(1)-N(2)	92.13(6)		

Whilst in **1a-c** an integral part of the three-dimensional propagation is achieved through magnesium bridging carboxylate chains (Figure 3.4a), the presence of an equatorial water donor (O3<sub>w</sub>) in the terminal position in compound **2** prevents this propagation, resulting in 2-dimensional sheets assembled *via* hydrogen bonding from the water (O3<sub>w</sub>) to the non-coordinated carboxylate oxygens O1 (H---A distance 1.97(3) Å, <DHA 169.3(3) °). This is in contrast of the 3-dimensional network observed for **1a-c**.

The ethanol molecule's oxygen O6 (not pictured) is also involved in one hydrogen bond to the other hydrogen in the metal bound water (H---A distance 1.89(3) Å, <DHA 166.0(2) °). Figure 3.9 details **2**, as viewed through the b-axis, where hydrogen bond associated 2-dimensional sheets can be observed. Like **1a-c**, propagation for **2** is also achieved through chains

formed by axial nitrogens coordinated to metal centers as shown in Figure 3.10a, in which one of the carboxylate oxygens in **1a-c** is replaced by water in **2**.

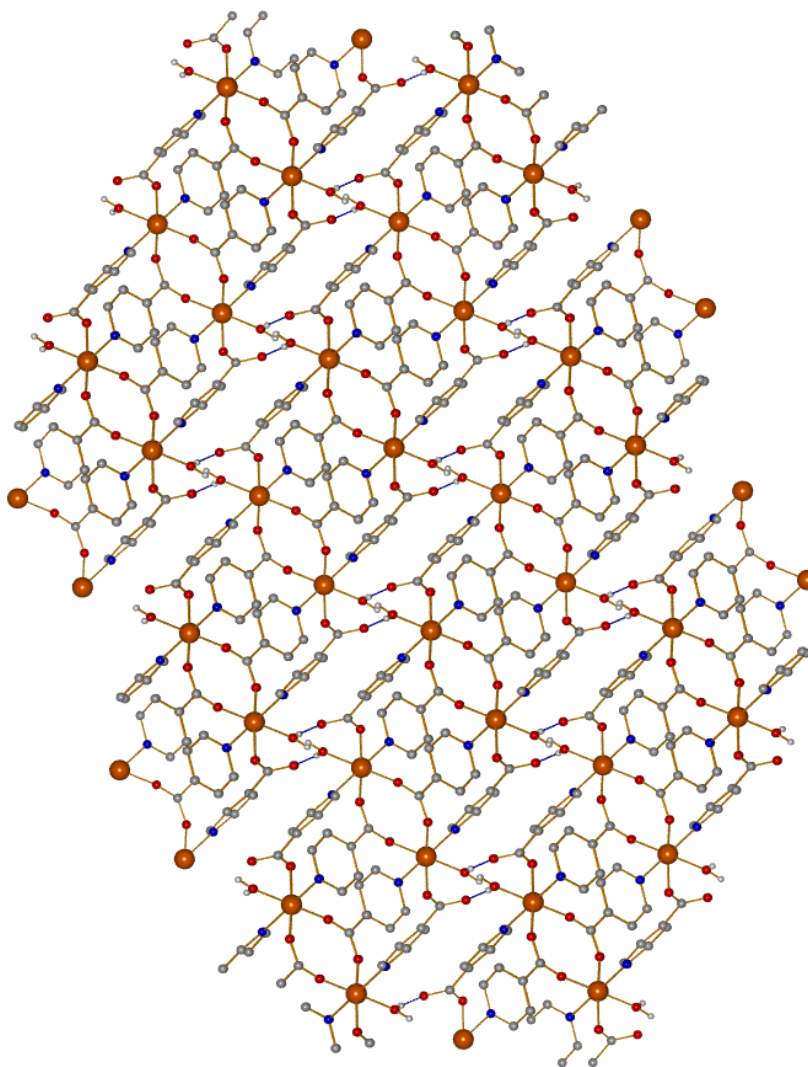


**Figure 3.9** Compound **2** as seen through b-axis. In **2**, the presence of a water molecule affords 2-dimensional sheets which are associated *via* hydrogen bonds. EtOH molecule not shown for clarity. Hydrogen atoms on the pyridyl rings removed for clarity.

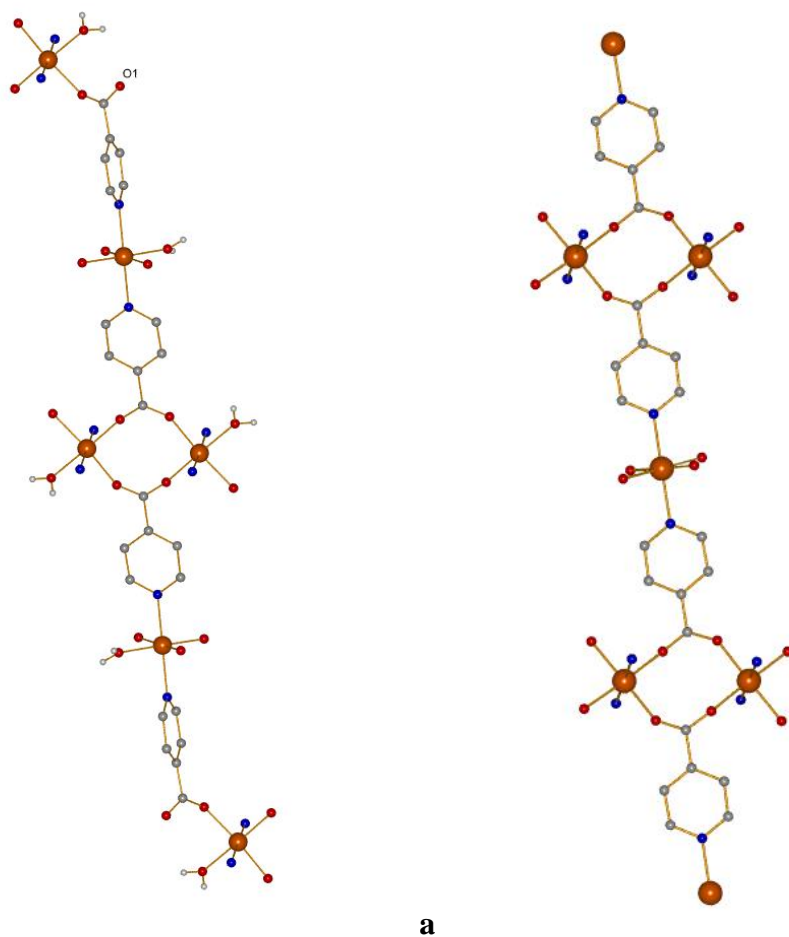


**Figure 3.10** Side by side comparison of (a) axial coordination by pyridyl nitrogens in **2** and (b) axial coordination by pyridyl nitrogens in **1a**. Much like **1a-c**, axial coordination by pyridyl nitrogens affords 1-dimensional chains. No propagation is observed through O1. Hydrogen atoms on the pyridyl rings have been removed for clarity.

Interestingly, in **2**, though the structural propagation is similar to **1a-c**, the presence of the terminal water molecule reduces the dimensionality from a fully 3-dimensional network (**1a-c**) to a hydrogen bound 2-dimensional coordination polymer. This is comparable to other structures, in which terminally coordinated solvent molecules have yielded 2-dimensional motifs.<sup>[38-40]</sup>

Likewise, although rhombohedral channels are formed in **1a-c**, compound **2** exhibits channel-like motifs. These spaces are filled with hydrogen bound ethanols of crystallization. Figure 3.11 displays square shaped intermolecular spaces formed from the association of these 2-dimensional sheets *via* hydrogen bonds. Further, in the case of **2**, a solvent-accessible volume of [359 Å<sup>3</sup> (23.3%)] was calculated *via* PLATON after removal of the coordinated water and ethanol of crystallization.

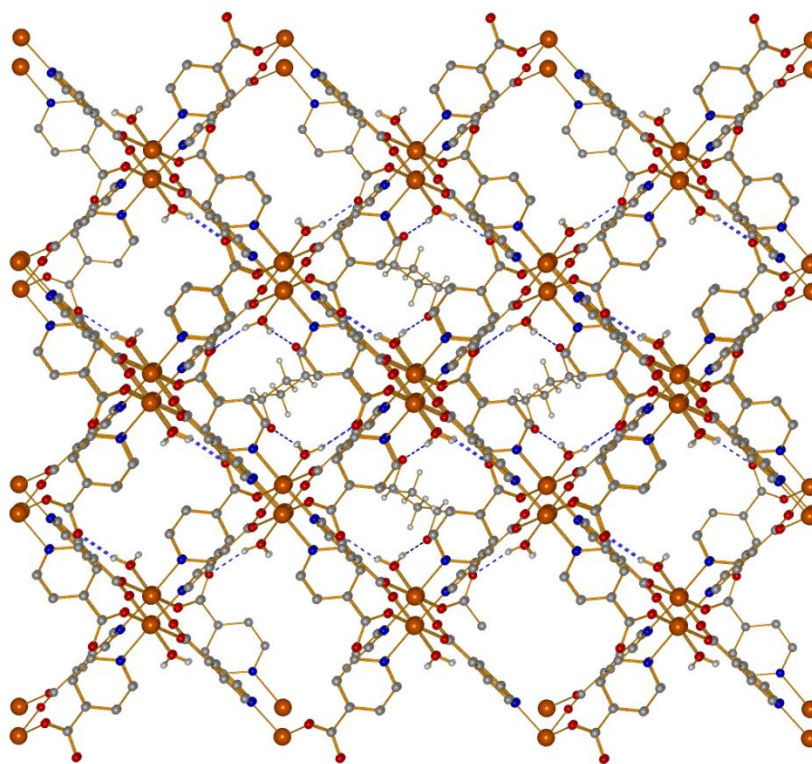


**Figure 3.11** Square shaped spaces in **2**. Also shown are hydrogen bonds which associate the 2-dimensional sheets into a 3-dimensional hydrogen bonded coordination polymer.

Compound **3** crystallizes in the triclinic space group P-1. The magnesium center is located on a center of symmetry, and thus only half of the metal environment is symmetry independent. The metal environment is six-coordinate, comprised of four water molecules in the equatorial plane (two symmetry generated) [Mg-O<sub>w</sub> 2.075(3) Å (avg)], in addition to carboxylate in the axial position [Mg-O 2.032(1) Å] (Figure 3.12). Table 3.6 summarizes bond lengths and angles for **3**, which are within reported values.<sup>[41, 42]</sup>

Interestingly, the Hin ligand is in the form of a zwitterion, with the pyridyl nitrogen being protonated (the proton was located in a difference map) whereas the carboxylate moieties are deprotonated. Thus, the magnesium center presents itself as a dicationic species, with charges balanced by the nitrate anion in the asymmetric unit.

**Table 3.6** Selected bond lengths (Å) and angles (°) for **3**

---

---

Mg(1)-O(1)	2.032(1)
Mg(1)-O(3) <sub>w</sub>	2.083(2)
Mg(1)-O(4) <sub>w</sub>	2.067(2)
O(1)-Mg(1)-O(1)'	180.000(1)
O(1)-Mg(1)-O(3) <sub>w</sub>	88.503(8)
O(1)-Mg(1)-O(4) <sub>w</sub>	89.183(1)
O(1)-Mg(1)-O(3) <sub>w</sub> '	91.497(8)
O(1)-Mg(1)-O(4) <sub>w</sub> '	90.817(8)
O(3) <sub>w</sub> -Mg(1)-O(4) <sub>w</sub> '	94.581(7)
O(3) <sub>w</sub> '-Mg(1)-O(3) <sub>w</sub> '	89.21(5)

---

---

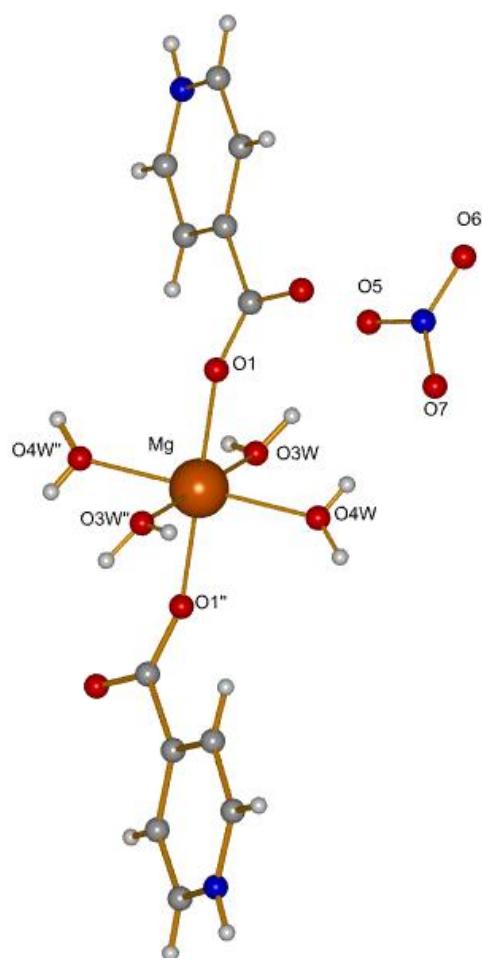


**Figure 3.12** Magnesium coordination environment in compound **3**. As the asymmetric unit contains only one half-occupied magnesium, only one nitrate is shown.

There is no evidence of  $\pi$ --- $\pi$  stacking. Instead main structural propagation is achieved through hydrogen bonding. The metal bound waters hydrogen-bind to the nitrate anions and neighboring carboxylates, forming an intricate pattern of chains. Chains are also formed through hydrogen bond interactions coming from the hydrogen at the pyridyl nitrogen site to the nitrate anions. The combination of these chains expands the structure into a complex 2-dimensional sheet network (Figure 3.13).

To our knowledge no examples of alkaline earth zwitterions based on the isonicotinic acid ligand have been reported. The chemistry of supramolecular zwitterion complexes involving pyridinecarboxylic acids and metals is not well known, yet studies involving lanthanides and transition metals<sup>[43, 44]</sup> have been reported. In these the unbound counterions act as charge balancers and often as connectors to expand the hydrogen bonded networks.

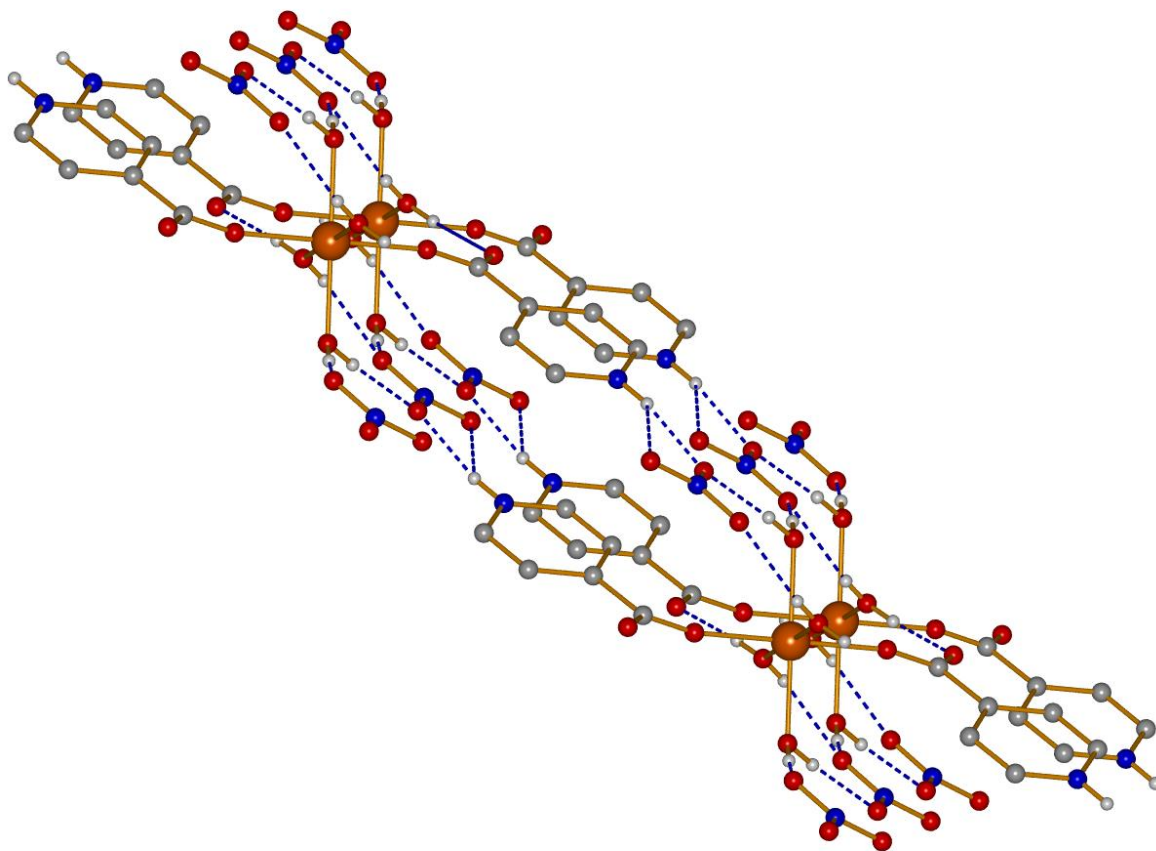


**Figure 3.13** A chain formed by hydrogen bonding from water to nitrates and carboxylates. The combination of these chains forms a 2-dimensional sheet supported by hydrogen bonds.



### 3.3 Thermal Analysis and Structural Integrity of **1a-c**, **2** and **3**

A TGA study was performed on **1a-c**, **2** and **3**, to observe their thermal properties. The compounds, except **1b** and **3** are stable at temperatures higher than 300 °C after initial solvent loss (Figure 3.14). Table 3.7 summarizes the results from the TGA.

**Table 3.7** TGA data for compounds **1a-c**, **2** and **3**

Compound	$\Delta T$	% $W_{\text{exp}}$	% $W_{\text{calc}}$	Loss
{[Mg(in) <sub>2</sub> ] <sub>2</sub> ·DMF} ( <b>1a</b> )	30-190 °C	11.2%	11.9%	DMF
{[Mg(in) <sub>2</sub> ] <sub>2</sub> ·ACN} ( <b>1b</b> )	30-130 °C	7.0%	7.1%	ACN
{[Mg(in)]·0.5THF} ( <b>1c</b> )	30-250°C	12.0%	11.8%	0.5 THF
{[Mg(in) <sub>2</sub> (H <sub>2</sub> O)]·EtOH} <sub>∞</sub> ( <b>2</b> )	30-106°C	5.5%	6.9%	EtOH
{[Mg(inH)(OH <sub>2</sub> ) <sub>2</sub> ][NO <sub>3</sub> ]} <sub>∞</sub> ( <b>3</b> )	30-140°C	13.5%	15.5%	4 H <sub>2</sub> O

$\Delta T$ : temperature range; %  $W_{\text{exp}}$ : % experimental weight loss; %  $W_{\text{calc}}$ : % theoretical weight calculated; Loss: calculated guest solvents.

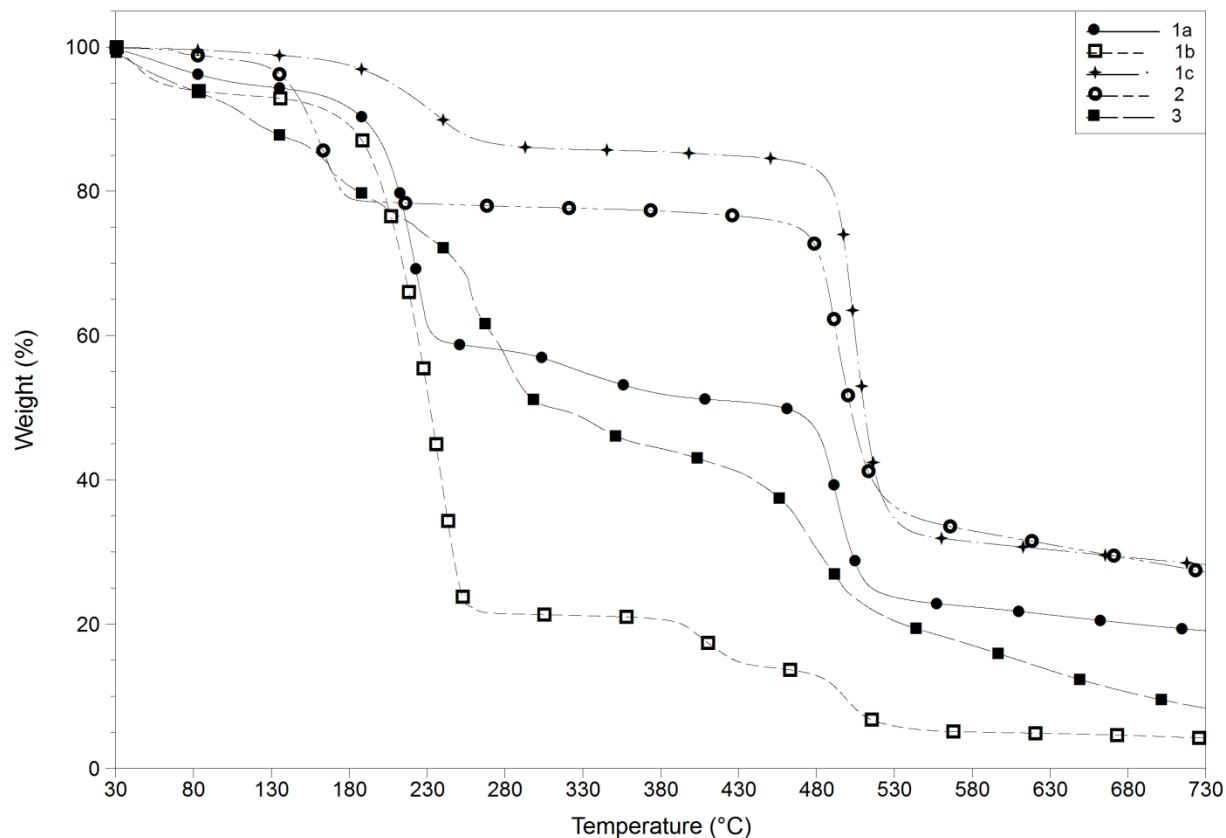
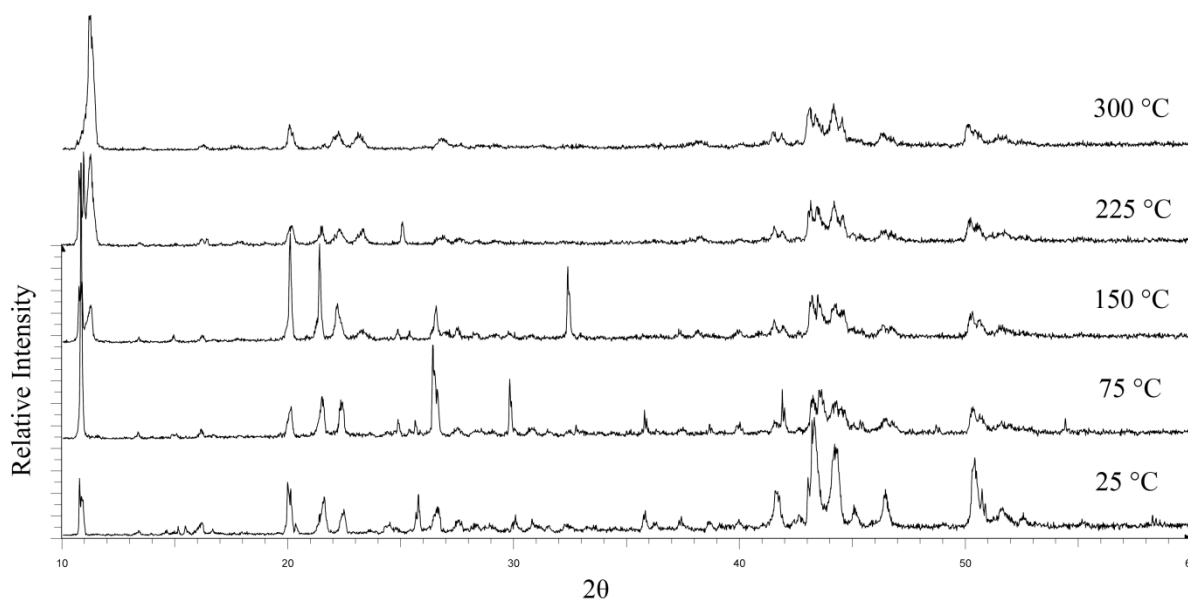
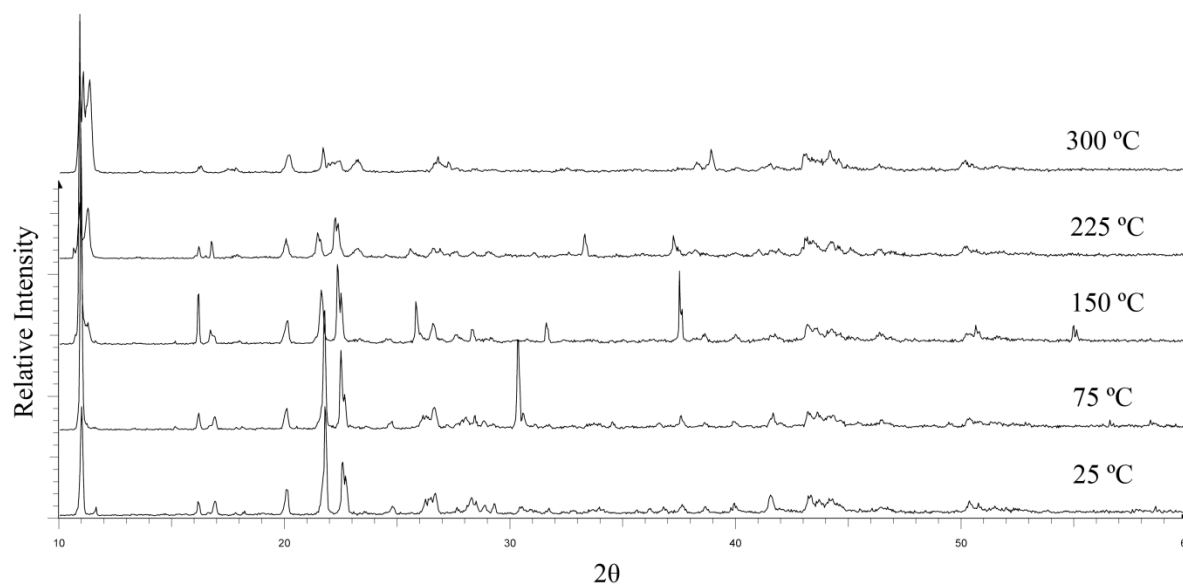


**Figure 3.14** Overlay of TGA of **1a-c**, **2** and **3** shows initial loss of lattice solvents followed by decomposition  $>400^{\circ}\text{C}$ .

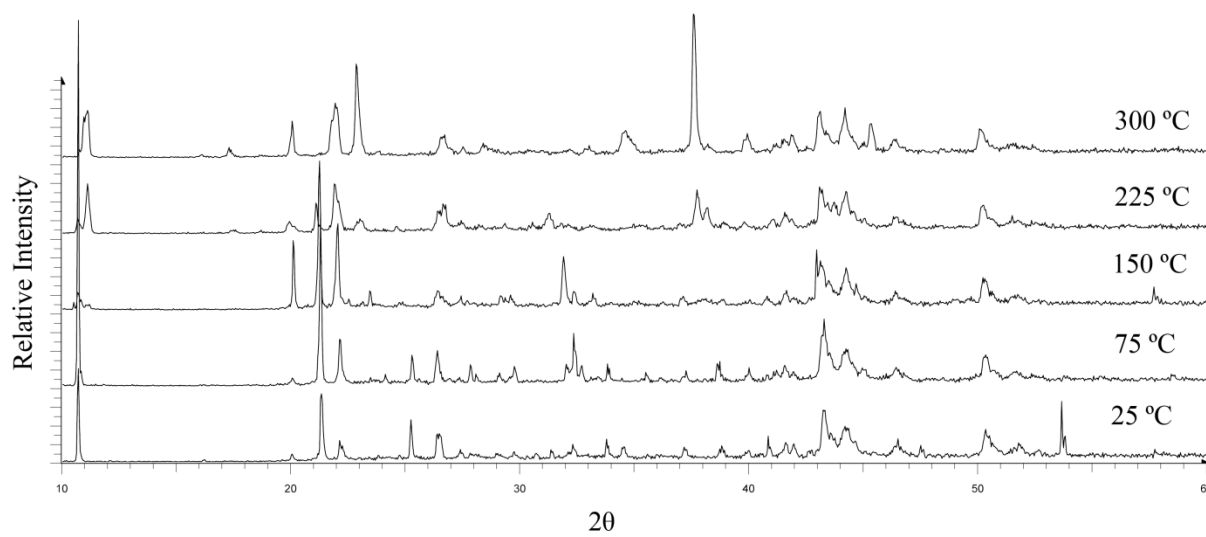
To determine the thermal stability of the compounds after desolvation, variable temperature powder X-ray diffraction experiments, from room temperature to  $300^{\circ}\text{C}$ , were performed on the open-frameworks **1a-c**. The room temperature and simulated diffraction patterns of **1a-c** are very similar, because of the isostructural nature of the compounds. Upon heating **1a-c** to  $300^{\circ}\text{C}$ , several unknown phases are observed at  $150$  and  $225^{\circ}\text{C}$ , yet the structural integrity of the framework remains intact (Figure 3.15a-c) after desolvation. The identity of these phases could not be determined.



(a)



(b)



(c)

**Figure 3.15** Thermodiffractogram of (a) **1a** and (b) **1b** and (c) **1c** from 25-300 °C, the overall structures remain intact after desolvation

Further, since **1a** exhibited the highest calculated void space volume of the three isostructural frameworks ( $316 \text{ \AA}^3$ , 23.3%), preliminary adsorption studies were performed to determine permanent porosity. The BET surface studies using  $\text{N}_2$  indicated that **1a** is non-porous, as evidenced by low surface area obtained ( $13 \text{ m}^2\text{g}^{-1}$ ). This correlates with other compounds reported to be non-porous with low BET surface areas,<sup>[13, 14]</sup> and the low void space volume calculated from PLATON.

### 3.4 Conclusions

Five novel coordination complexes based on Mg(II), in conjunction with isonicotinic acid, were successfully isolated and characterized. The use MeOH/DMF mixtures resulted in the synthesis of three isostructural 3-dimensional frameworks with 1D rhombohedral shaped channels of varying size (**1a-c**)

Compounds **1a-c** were subjected to variable temperature PXRD and determined to retain integrity at high temperatures. Since compound **1a** displayed the largest pore volume calculations from PLATON, N<sub>2</sub> adsorption studies were performed determining non-porosity due to the low BET surface area (13 m<sup>2</sup>g<sup>-1</sup>).

Compounds **2** and **3** crystallized as hydrogen bonded networks. The use of ethanol as a solvent made possible the synthesis of a 2-dimensional hydrogen bonded coordination network (**2**) with similar structural features to **1a-c**, in which one of the carboxylates is replaced by a water molecule which is involved in structural propagation through hydrogen bonding. Compound **3**, was crystallized as hydrogen bonded zwitterion from an ACN/H<sub>2</sub>O mixture, in which the protonated pyridyl nitrogen participates in intricate hydrogen bonding and the unbound nitrate balances the charge on the magnesium center.

### 3.5 References

- [1] C.N.R. Rao, S. Natajaran, R. Vaidhyanathan, *Angew. Chem. Int. Ed.*, (2004) 1466.
- [2] M. Dinca, A.F. Yu, J.R. Long, *J. Am. Chem. Soc.*, (2006) 8904.
- [3] Z. Yan, M.-L. Tong, X.-M. Chen, *New. J. Chem.*, (2004) 1412.
- [4] D. Frahm, F. Hoffmann, M. Froba, *CrystEngComm*, 15 (2013) 9429.
- [5] T.A. Maark, S. Pal, *International Journal of Hydrogen Energy*, 35 (2010) 12846-12857.
- [6] M.A. Sharif, H. Aghabozorg, E. Motyeian, *Acta Cryst. Sect. E.*, 63 (2007) m2235.
- [7] D. Banerjee, J. Finkelstein, A. Smirnov, P.M. Forster, L.A. Borkowski, S.J. Teat, J.B. Parise, *Growth (Lakeland)*, (2011) 2572-2579.
- [8] D. Banerjee, S.J. Kim, L.A. Borkowsky, W. Xu, J.B. Parise, *Cryst. Growth Des.*, 10 (2010) 709.
- [9] F.B. Abrahams, M.J. Grannas, T.A. Hudson, R. Robson, *Angew. Chem. In. Ed.* , 49 (2010).
- [10] Y.C. Chen, K.B. Wang, Y. Wang, *Polyhedron*, 29 (2010).
- [11] Y.C. Chen, K.B. Wang, Y. Wang, *Polyhedron*, 29 (2010) 669.
- [12] S.-C. Chen, Z.-H. Zhang, K.-L. Huang, Q. Chen, M.-Y. He, A.-J. Cui, L. Chao, Q. Liu, M. Du, 8 (2008) 3437.
- [13] M. Mazaj, T. Birsa Čelič, G. Mali, M. Rangus, V. Kaučič, N. Zabukovec Logar, *CrystGrowthDes*, 13 (2013) 3825-3834.
- [14] D. Banerjee, J. Finkelstein, A. Smirnov, P.M. Forster, L.A. Borkowski, S.J. Teat, J.B. Parise, *Cryst. Growth Des.*, 11 (2011) 2572-2579.
- [15] S. Chadwick, K. Ruhlandt-Senge, *Chem. Eur. J.*, 4 (1998) 1768.
- [16] S. Chadwick, U. Englich, B.C. Noll, K. Ruhlandt-Senge, *Inorg. Chem.*, 37 (1998) 4718.
- [17] G.M. Sheldrick, XShell 6.3.1, in, *Siemens Analytical X-ray Instruments*, Madison, Wisconsin: 1994.

- [18] G.M. Sheldrick, SADABS, Program for Empirical Absorption Correction of Area Detector Data, in, University of Gottingen, Gottingen, 1996.
- [19] A.L. Spek, *Acta Cryst.*, D65 (2009) 148-155.
- [20] C.-P. Li, M. Du, *Chemical communications* (Cambridge, England), 47 (2011) 5958-5972.
- [21] F.A. Almeida Paz, J. Klinowski, M.F.S. Vilela, J.P.C. Tomé, J.A.S. Cavaleiro, J. Rocha, *Chem. Soc. Rev.*, 41 (2012) 1088.
- [22] L.S. James, *Chem. Soc. Rev.*, 32 (2003) 276.
- [23] J. He, Y. Zhang, Q. Pan, J. Yu, H. Ding, R. Xu, *Microporous and Mesoporous Materials*, 90 (2006) 145.
- [24] P.L. Cheng, M. Du, *Chem. Commun.*, 47 (2011) 5958.
- [25] B.M. Cingi, C.A. Villa, C. Guastini, D. Viterbo, *Gazzeta Chimica Italiana*, 104 (1974) 1087.
- [26] T. Liu, D. Luo, D. Xu, H. Zeng, Z. Lin, *Dalton Trans*, 42 (2013) 368-371.
- [27] J.-C. Hallé, J. Lelievre, F. Terrier, *Can. J. Chem.*, 74 (1996) 613.
- [28] H.H. Jaffé, *J. Am. Chem. Soc.*, 77 (1955) 4445.
- [29] M.H. Abraham, W.E. Acree, *J. Chem. Thermodynamics*, 61 (2013) 74-78.
- [30] P.I. Nagy, K. Takács-Novak, *J. Am. Chem. Soc.*, 119 (1997) 4999.
- [31] V. Koteswara Rao, M. Zeller, S.R. Lovelace-Cameron, *Acta Cryst.*, 68 (2012) m1291-1292.
- [32] I. Senkowska, J. Fritsch, S. Kaskel, *Eur. J. Inorg. Chem.*, 2007 (2007) 5475-5479.
- [33] T. Liu, D. Luo, D. Xu, H. Zeng, Z. Lin, *Dalton Trans.*, 42 (2013) 368.
- [34] B.F. Abrahams, M.J. Grannas, T.A. Hudson, R. Robson, *Angewandte Chemie International Edition*, 49 (2010) 1087-1089.
- [35] I. Senkowska, S. Kaskel, *Eur. J. Inorg. Chem.*, 2006 (2006) 4564-4569.
- [36] Y.-P. He, Y.-X. Tan, J. Zhang, *Cryst. Growth Des.*, 201 (2013) 6.

- [37] Q. Zhang, H. Hao, H. Zhang, S. Wang, J. Jin, D. Sun, *Eur. J. Inorg. Chem.*, (2013) 1123.
- [38] Y. Chen, D. Zhang, D. Li, *Solid State Sci.*, 12 (2010) 461.
- [39] G. Wu, Z.-M. Wang, X.-T. Ge, X.-L. Wang, Q.-F. Zhang, *Z Naturforsch B*, 65b (2010) 27.
- [40] A. Karmakar, C.L. Oliver, *Z Kristallogr.* , 228 (2013) 330-334.
- [41] A. Mallick, S. Saha, P. Pachfule, S. Roy, R. Banerjee, *J. Mater. Chem.*, 20 (2010) 9073.
- [42] M.C. Das, S.K. Ghosh, C.E. Sañudo, P. Bharadwaj, *Dalton Trans.*, 9 (2008) 1644.
- [43] X.H. Huang, W.B. Pan, X.H. Xu, R.H. Zeng, *Acta Cryst.* , E (2008) m1098.
- [44] E.A. Mainicheva, D.G. Samsonenko, O.A. Geras'ko, V.P. Fedin, *Koord. Khim.*, 35 (2009) 920.



## CHAPTER 4

Synthesis, characterization and crystal structure of the 3-dimensional hydrogen bonded coordination complex  $\{[\text{Ba}(\text{in})(\text{H}_2\text{O})_6][\text{in}]\}_\infty$ 

## 4.0 Introduction

Previous reports have shown that the use of linkers containing mixed donor atoms may afford a range of coordination environments (See **Chapter 2**, Figure 2.1), depending on the metal centers.<sup>[1,2]</sup> Carboxylate-pyridine combinations in a ligand system afforded previous 3D transition metal MOFs, including a porous, metal organic framework based on Mn.<sup>[3]</sup> Other examples include the isostructural complexes  $[\text{Zn}(\text{in})_2(\text{H}_2\text{O})_4]$  and  $[\text{Cd}(\text{in})_2(\text{H}_2\text{O})_4]$ ,<sup>[4]</sup> in which the ligand coordinates through its carboxylate and nitrogen donor atoms. Remarkably, the increase in metal size from Zn to Cd has no effect on the overall structural features.

In contrast to the extensive work on transition metal MOFs, little is known about the s-, p- and f- block analogs. Alkaline earth metal analogs, based on the isonicotinic acid ligand system, include  $\{[\text{Mg}(\text{in})_2(\text{H}_2\text{O})_4]\}$  in which the ligand coordinates through its *para* nitrogen and one of the carboxylate oxygens. Further association is provided by an extensive network of hydrogen bonding through the four waters coordinated to the metal center. The magnesium center is six coordinated and can be regarded as a distorted octahedron. Recently, calcium  $\{[\text{Ca}(\text{in})_2(\text{H}_2\text{O})_4]\}$  and strontium  $\{[\text{Sr}(\text{in})(\text{H}_2\text{O})_6][\text{in}]\}$  coordination networks, based on the isonicotinic acid ligand, have also been reported.<sup>[7]</sup> In contrast to the magnesium species, and expressing the increase in metal size, both carboxylate oxygens and the ligand's *para* nitrogen participate in coordination to the Ca(II) center. In this example the calcium center is seven coordinate with a capped octahedral

geometry. Similar to the magnesium analog, the 3-dimensional network structure is afforded by extensive hydrogen bonding through its four waters and  $\pi$ --- $\pi$  stacking.

In line with the trend observed upon descending group II, the strontium complex displays an eight coordinate metal center, in which two of the coordination sites are occupied by the carboxylate moieties, in addition to six water molecules. The carboxylates bind in a  $\mu_2$ - $\eta^1:\eta^1$  fashion. The overall metal environment can be described as dodecahedral. Interestingly, one ligand binds to the metal center while the other is non-metal bound. The  $[\text{Sr}(\text{in})(\text{H}_2\text{O})_6]_\infty$  layers associate *via* hydrogen bonding and  $\pi$ --- $\pi$  stacking (3.502(3) – 3.611(3) Å) interactions with the unassociated ligands to afford a 3D framework. The arrangement of coordinated and unassociated ligands is not observed for the magnesium and calcium species. A related eight coordinate barium environment is observed in the anhydrous, heteroleptic poly[ $\mu_4$ -isonicotinato- $\mu_3$ -nitrate-barium(II)] ( $[\text{Ba}(\text{in})(\text{NO}_3)]_n$ ).<sup>[8]</sup> By analogy to the strontium compound, the  $[\text{in}]^-$  ligand bridges the metal centers; however, the presence of the non-coordinated  $\text{NO}_3^-$  anion results in significantly different structural features.

This chapter reports studies geared to further illuminate the influence of metal radius on the overall structural features of isonicotinate-based heavy alkaline earth MOF's by the preparation and characterization of a homoleptic barium isonicotinate complex.

## 4.1 Experimentals

### 4.1.1 General and physical measurements

All chemicals were obtained commercially and used without further purification (purity of  $\text{BaCO}_3$  – 98%, 4-pyridinecarboxylic acid – 99%). Reactions were carried out in distilled water. IR measurements were carried out as mineral oil mulls in KBr discs in a Nicolette IR200 FT-IR

spectrophotometer between  $4000\text{ cm}^{-1}$  to  $500\text{ cm}^{-1}$ . TGA measurements were performed on a TGA Q500 series instrument (TA Instruments-Waters LLC) under an  $\text{N}_2$  balance/sample purge flow of  $40\text{ mL/min}$  and  $60\text{ mL/min}$ , respectively. The sample (wt.  $7.9640\text{ mg}$ ) was loaded onto a platinum pan and heated using a ramp method from room temperature to  $750\text{ }^\circ\text{C}$ . All crystal data were collected using a Bruker SMART system with a 3-circle goniometer and a APEX-CCD detector. Data were collected using  $\text{MoK}\alpha$  radiation at  $103(2)\text{ K}$  using a low temperature device built by H. Hope (UC Davis).

The crystals were submerged in highly viscous hydrocarbon oil (Infineum), mounted on a glass fiber and placed in the low temperature stream on the diffractometer, as described in detail previously.<sup>[9]</sup> Data collection parameters and refinement details have been described in detail.<sup>[9]</sup> The crystal structure was solved using direct methods, with subsequent refinement by full-matrix least-squares method on  $F^2$ .<sup>[10]</sup> All non-hydrogen atoms were refined anisotropically. Hydrogen atoms, except those of water molecules, were calculated to fixed positions using restraints. Water hydrogens were located directly in the difference map. An absorption correction was performed using the SADABS program.<sup>[11]</sup> Centroid to centroid distances representing  $\pi\text{---}\pi$  contacts were calculated using the OLEX2 crystallographic suite.<sup>[12]</sup> Powder diffractometry experiments were recorded in a Bruker D8 Advance, equipped with a copper source and a NaI scintillation counter. Crystallographic data (excluding structure factors) for the structure reported in this paper have been deposited with the Cambridge Crystallographic Data Center as a supplementary publication, no. CCDC 794948. Copies of the data can be obtained free of charge on application to CCDC, 12 Union Road, Cambridge C21EZ, UK (fax:(+44) 1223-336-033; e-mail: [deposit@ccdc.cam.ac.uk](mailto:deposit@ccdc.cam.ac.uk)).

#### 4.1.2 Synthesis of 4

$\{[\text{Ba}(\text{in})(\text{H}_2\text{O})_6][\text{in}]\}_\infty$  (**4**): A slight excess of  $\text{BaCO}_3$  (493.3 mg, 2.5 mmol) and inH (492.8 mg, 4 mmol) were combined in 25 mL of distilled water. The resulting slurry ( $\text{BaCO}_3$  is insoluble under these conditions) was stirred and kept under reflux conditions for 24 hours, after which the colorless suspension was filtered hot using a Whatman no. 9 filter. The resulting clear, colorless mother liquor was allowed to cool down to room temperature and within a few days, colorless block-shaped crystals suitable for X-ray crystallography were collected.  $M_p$  = above 400 °C. Yield (non-optimized): 23.38 %. IR ( $\text{cm}^{-1}$ ): 3415.43 (s), 2351.74 (w), 1600.23 (w), 1549.45 (w), 1057.93 (w).

## 4.2 Structural Characterization of 4

Table 4.1 Crystallographic data and structural refinement for 4

	<b>4</b>
Empirical formula	C <sub>12</sub> H <sub>20</sub> BaN <sub>2</sub> O <sub>10</sub>
Formula weight	489.64
Crystal system	Monoclinic
Space group	P2 <sub>1</sub> /c
T (K)	103(2)
Unit cell dimensions (Å, °)	
a	6.2592(18)
b	44.289(12)
c	7.2754(15)
α, γ	90
β	118.890(18)
Volume (Å <sup>3</sup> ), Z	1765.8(8), 4
Calculated density (Mg/m <sup>-3</sup> )	1.842(8)
Absorption coefficient (mm <sup>-1</sup> )	2.303
2θ range	0.92 to 28.33°
Unique reflections	4373
Total reflections	17527
Goodness-of-fit on F <sup>2</sup>	1.358
R <sub>1</sub> , wR <sub>2</sub> (all data)	R <sub>1</sub> = 0.0473, wR <sub>2</sub> = 0.0780
R <sub>1</sub> , wR <sub>2</sub> (Final)	R <sub>1</sub> = 0.0435, wR <sub>2</sub> = 0.0763
F(0 0 0)	968

Crystallographic analysis revealed that **4** crystallizes in the monoclinic P2<sub>1</sub>/c space group and is isostructural with the previously reported strontium compound.<sup>[7]</sup> The target complex displays a 3D framework *via* a network of hydrogen bonding between metal-coordinated water molecules and π---π interactions between the parallel aromatic rings. The structure contains an uncoordinated isonicotinate that is instrumental in the formation of the 3D network through non-covalent interactions. Of particular importance to the formation of the 3D network is the π---π stacking between these non-metal bound ligands, with contacts between (3.532(3) and 3.648(3) Å). The metal centers are eight coordinate, with six of the coordination sites belonging to water

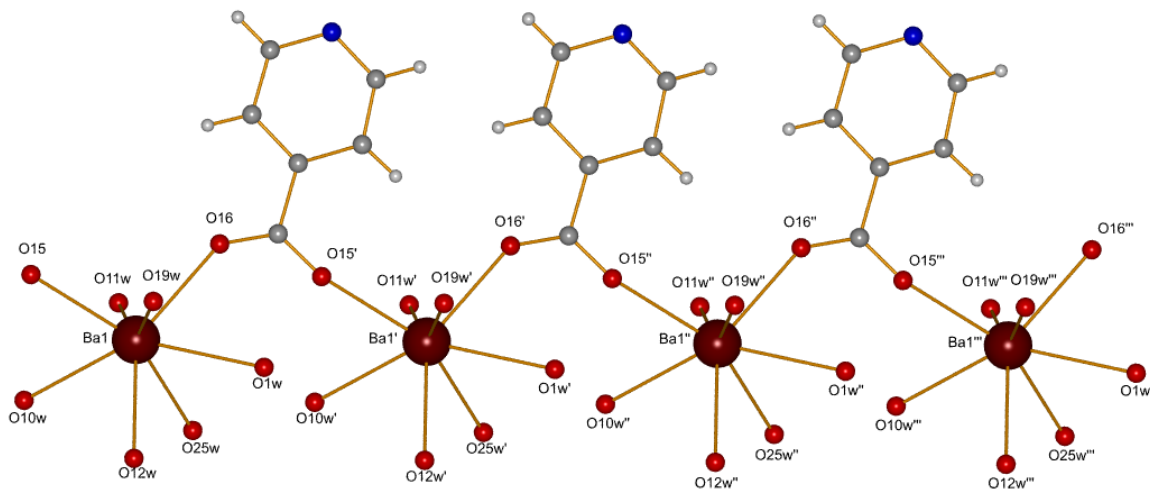
molecules, and Ba-water distances ranging from 2.766(3) – 2.838(3) Å. These distances agree with literature values.<sup>[13, 14]</sup> The eight coordinated metal center adopts a distorted dodecahedral geometry, with two coordination sites occupied by two carboxylate oxygens from two different isonicotinate ligands. These bridge the metal centers in a  $\mu_2\text{-}\eta^1:\eta^1$ - coordination mode and Ba-O distances of 2.684(3) Å and 2.689(3) Å, resulting in a 1D zigzag-like chain, as shown in Figure 4.1. The zig-zag chains are connected by hydrogen bonding (see table 4.3, Figure 4.2) and  $\pi\text{---}\pi$  interactions from the metal-bound ligands (3.642(2) Å) into 2D layers, as shown in Figure 4.3. All  $\pi\text{---}\pi$  stacking values are in agreement with literature values.<sup>[15]</sup> Despite the significant increase in ionic radius from strontium to barium (1.27 Å to 1.43 Å,  $\Delta$  0.16 Å)<sup>[16]</sup>, the overall structural features for the strontium and barium complexes are quite similar, with the expected bond length increases due to the increased metal radius. The larger metal radius also results in an increase in structural flexibility, as expressed by the slightly larger range of O-Ba-O angles (66.61(9) – 150.07(10) °), in contrast to (67.0(1) – 148.0(1) °) reported for the strontium congener. Furthermore, comparison of the powder diffraction patterns of the hydrated and dehydrated compounds demonstrated loss of crystalline form upon removal of coordinated waters.

**Table 4.2** Selected bond lengths (Å) and angles (°) for **4**

Ba(1)-O(16)	2.684(3)	O(25)W-Ba(1)-O(1)w	68.98(10)
Ba(1)-O(15)	2.689(3)	O(15)-Ba(1)-O(19)w	70.12(11)
Ba(1)-O(12)w	2.766(3)	O(16)-Ba(1)-O(19)w	85.08(11)
Ba(1)-O(11)w	2.791(3)	O(11)W-Ba(1)-O(1)w	116.13(10)
Ba(1)-O(19)w	2.811(3)	O(16)-Ba(1)-O(10)w	140.03(10)
Ba(1)-O(1)w	2.813(3)	O(15)-Ba(1)-O(10)w	71.55(10)
Ba(1)-O(10)w	2.838(3)		
O(15)W-Ba(1)-O(16)	102.69(9)		

**Table 4.3** Selected hydrogen bonding distances ( $\text{\AA}$ ) for **4**

D-H...A	d(D...A)
O(25)-H(62)...N(3)	2.769
O(11)-H(70)...N(2)	2.756
O(10)-H(64)...O(25)	2.825
O(1)-H(61)...O(8)	2.770
O(25)-H(63)...O(8)	2.852

**Figure 4.1** Zig-zag 1D chains. Water hydrogens and hydrogen bonding removed for clarity.

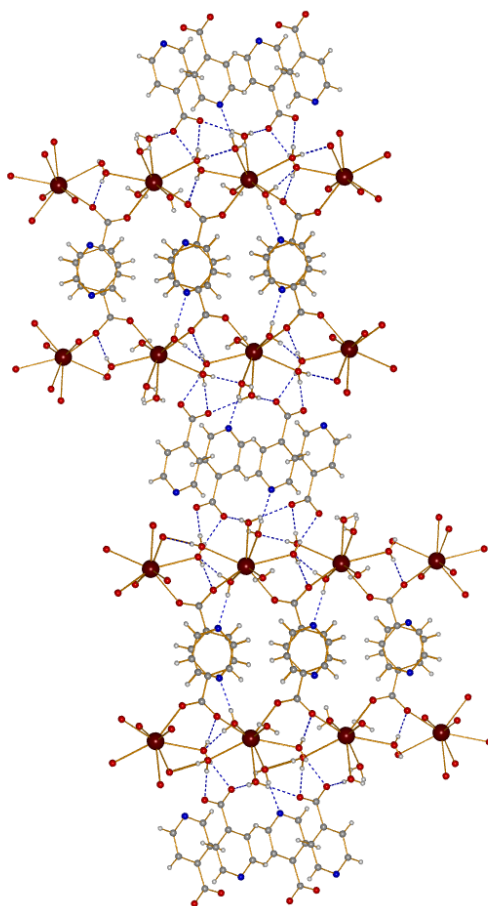


**Figure 4.2** 3D network showing hydrogen bonds (dashed lines) based on 1D chains connected into 2D sheets by non-covalent interactions.



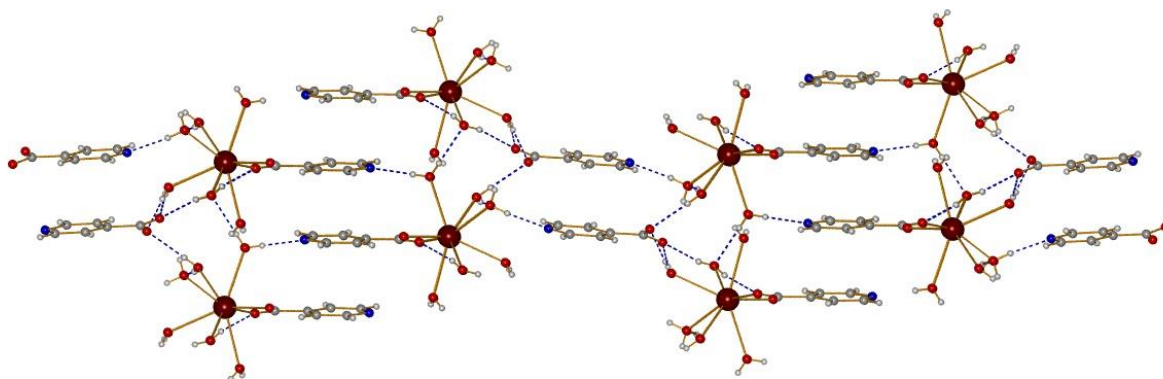


**Figure 4.3** 2D layers associated *via*  $\pi$ --- $\pi$  interactions and hydrogen bonding to form a 3D framework

### 4.3 Thermogravimetric analysis of 4

Thermogravimetric analysis (Figure 4.4) was performed to determine the thermal behavior of the title complex. The profile shows a decrease of 21.61 wt% until 124 °C, corresponding to the loss of six coordinated water molecules (calc. 22.06%). The compound appears to be stable until 490 °C, where a further 22.41 wt% drop is observed, coinciding with the start of decomposition into an uncharacterized black residue.

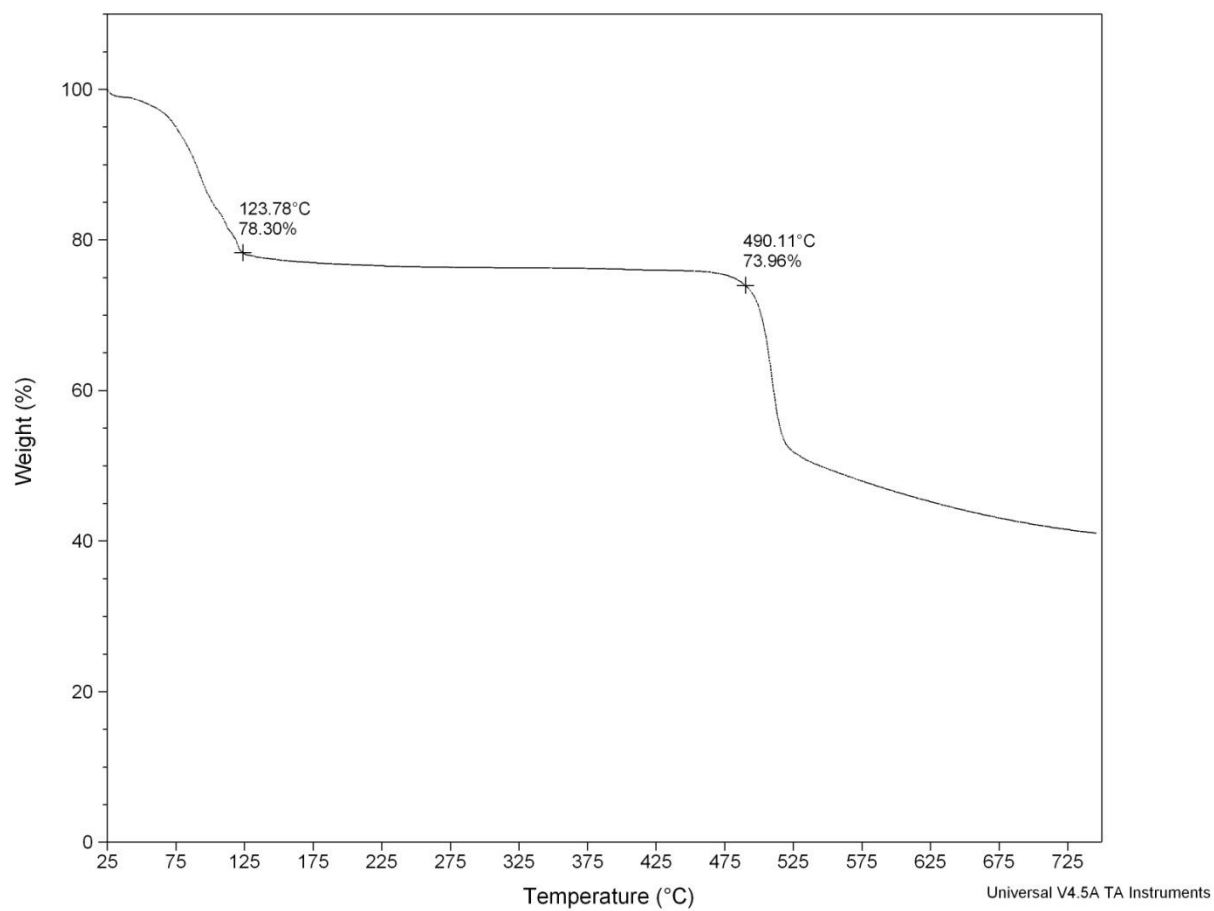


**Figure 4.4** TGA plot for **4** that shows stepwise loss of water molecules (~124 °C), thermal stability and consequent decomposition (490 °C).

#### 4.4 Conclusions

In summary, a novel barium coordination polymer **4**, which exhibits an unusual ion association mode with one metal-coordinated and one unassociated ligand, has been synthesized *via* simple acid base chemistry. Unexpectedly, the compound is isostructural with the strontium congener. The barium centers coordinate in a  $\mu_2\text{-}\eta^1:\eta^1$ -bridging motif to the ligand's carboxylate oxygens, resulting in zigzag 1D chains. These chains are formed into 2D layers *via* hydrogen bonding and  $\pi\text{---}\pi$  interactions. The separated counteranion enables linkage of the layers *via* an extensive network of hydrogen bonding and  $\pi\text{---}\pi$  interactions, affording a 3D framework. This work clearly demonstrates that a change in metal size does not necessarily result in a change in structural features. This observation strongly suggests the continued need for individual analysis of solids, as the prediction of the respective solid state structures is not yet possible.

#### 4.5 References

- [1] James, L. S., *Chem. Soc. Rev.* **2003**, 32, 276-288
- [2] Janiak, C., *Dalton. Trans.* **2003**, 14, 2781-2804
- [3] Wei, Q.; Nieuwenhuyzen, M.; James, L.S., *Microporous and Mesoporous Materials* **2004**, 73, 97-100.
- [4] Cingi, B. M.; Gaetani, M. A.; Guastini, C.; Musatti, A.; Nardelli, M., *Gazzetta Chimica Italiana* **1971**, 11, (101), 815-824.
- [5] Abrahams, F. B.; Grannas, M. J.; Hudson, T. A.; Robson, R., *Angew. Chem. In. Ed.* **2010**, 49, 1087-1089
- [6] Cingi, B. M.; Villa, C. A.; Guastini, C.; Viterbo, D., *Gazzetta Chimica Italiana* **1974**, 104, 1087-1093.
- [7] Chen, Y. C.; Wang, K. B.; Wang, Y., *Polyhedron* **2010**, 29, 669-674.
- [8] Schuy, A.; Ruschewitz, U., *Acta Cryst.* **2006**, E62, m992-m993.
- [9] Chadwick, S.; Ruhlandt-Senge, K., *Chem. Eur. J.* **1998**, 4, 1768.
- [10] G. M. Sheldrick, *SHELXTL Version 5, Siemens Analytical X-ray Instruments, Madison, WI, 1994.*
- [11] G. M. Sheldrick, SADABS, Program for Empirical Absorption Correction of Area Detector Data, University of Göttingern, 1996.
- [12] Dolomanov, O. V.; Bourhis, L. J.; Gildea, R. J.; Howard, J. A. K.; Puschmann, H., *J. Appl. Cryst.* **2009**, 42, 339-341.
- [13] Shuai, Q.; Chen, S.; Gao, S., *Struct. Chem.* **2007**, (18), 689-695.
- [14] Williams, C. A.; Blake, A. J.; Wilson, C.; Hubberstey, P.; Schröder, M., *Cryst. Growth Des.* **2008**, 8, (3), 911-922.

- [15] Jorgensen, W. L.; Severance, D. L., *J. Am. Chem. Soc.* **1990**, (112), 4768-4774.
- [16] Emsley, J., *The Elements*, 2<sup>nd</sup> ed.; Oxford University Guides; 1991.

## CHAPTER 5

**Heavy alkaline earth metal coordination networks based on the *para*- and *meta* pyridinecarboxylic acid****5.0 Introduction**

The family of alkaline earth metals provides a textbook example of the variation of physical and chemical properties that depend on metal size. Compounds based on the lighter metals beryllium and magnesium display significantly different properties than the heavier counterparts, calcium, strontium and barium. To a large extent, this can be attributed to a size effect, as the bond character changes dramatically upon descending group II. While molecular beryllium species possess a significant degree of covalency, this tendency is minimal in corresponding barium compounds. The increasing ionicity in the metal-ligand bonds can be attributed to a metal coordination environment that is predominantly dictated by electrostatic interactions and size considerations. Furthermore, because of the large size of the heavy alkaline earth metals, the predominantly ionic bonds tend to be weak. Thus, many factors may contribute to the steric saturation of a large metals center, making it very difficult to predict structural features for the heavy metals.

Synthesis of coordination polymers based on the heavy alkaline earth metals is slowly emerging. These polymers are studied for their feasibility to separate gas mixtures, particularly mixtures containing CO<sub>2</sub>,<sup>[1, 2]</sup> in addition to their potential in catalysis.<sup>[3-5]</sup> Considering these promising results, further studies in the isolation of higher-dimensional metal organic frameworks, based on the heavier metals, is warranted.

Because dense, non-porous and hydrogen-bonded network structures are commonly reported for Ca, Sr and Ba<sup>[6-10]</sup>, stable microporous materials are virtually unknown. The tendency towards the formation of condensed structures is caused by the significant ionic character of the metal-ligand bond; further, the large metal size requires high coordination numbers to achieve coordinative saturation, frequently resulting in uncontrolled aggregation.<sup>[11]</sup> To counter this effect, linear, multi-topic linkers have been identified to for their potential to provide three-dimensional, highly regular, open network structures.

Examples reported to date include isostructural calcium and strontium species based on the the linear 4,4'-sulfonylbenzoate acid (SBA).<sup>[12]</sup> The compounds were prepared using using microwave synthesis and display a microporous character. The properties of the calcium compound were evaluated for gas separation by Banerjee *et al.*,<sup>[1]</sup> who reported high CO<sub>2</sub>/N<sub>2</sub> selectivity.

A recent barium example is based on the benzene-1,3,5-trisbenzoic acid (HBTB) ligand,<sup>[13]</sup> which affords a 1D microporous species in which the nine-coordinate barium center connects to ligand oxygen atoms forming a honeycomb type structure with pores measuring 8 x 13 Å<sup>2</sup>. The channels are assembled by weak  $\pi$ --- $\pi$  interactions (3.8 Å) between the BTB layers. This example was reported to be the first 1D barium microporous material exhibiting permanent microporosity. Other examples are based on the arenesulfonate ligand<sup>[14]</sup> and have been reported to afford higher dimensional structures.

This chapter summarizes our efforts to prepare and characterize calcium, strontium and barium species based on the the *para*- and *meta* pyridinecarboxylic acid (Hin and Hnic, respectively). On the basis of our prior success in using *para* pyridinecarboxylic acid for the

synthesis of well-defined magnesium MOFs in **Chapter 3**, we here expand this work to the heavier metals. To evaluate the effect of ligand geometry we also examined the metal substituted ligand. Further, this work allows the direct comparison of the magnesium compounds with the heavier congeners, giving a unique insight into the effect of metal size. Thus, this chapter will present the synthesis of four different coordination networks along with their structural features and thermal stability.

## 5.1 Experimental

### 5.1.2 General and Physical Measurements

All chemicals were obtained commercially and used without further purification (purity of  $\text{Ca}(\text{NO}_3)_2 \cdot 4\text{H}_2\text{O}$ – 98%,  $\text{SrCl}_2 \cdot 6\text{H}_2\text{O}$  – 99%,  $\text{BaCl}_2 \cdot 2\text{H}_2\text{O}$  – 98%, Hin and Hnic– 98%).

IR measurements were carried out as KBr pellets or in a Nujol mull using a Nicolet IR200 FT-IR spectrophotometer between  $4000\text{ cm}^{-1}$  to  $400\text{ cm}^{-1}$ . TGA measurements were performed on a TGA Q500 series instrument (TA Instruments-Waters LLC) under an  $\text{N}_2$  balance/sample purge flow of 40 mL/min and 60 mL/min, respectively. The samples (wt. 6-20 mg) were loaded onto platinum pans and heated using a ramp method from room temperature to  $750\text{ }^\circ\text{C}$  (ramp rate:  $10\text{ }^\circ\text{C}/\text{min}$ ). Melting point determinations (uncalibrated) were made using capillary tubes in a Mel-Temp II melting point apparatus.

All single crystal X-ray data were collected on a Bruker Kappa diffractometer using an APEX 2 CCD detector and  $\text{MoK}\alpha$  radiation ( $0.7107\text{ \AA}$ ). Crystals were cooled using a Cryocool LN-3 low temperature device (Cryoindustries of America, Inc.) The crystals were submerged in highly viscous hydrocarbon oil (Infineum), mounted on a MITEGEN® mount and placed in the low temperature stream on the diffractometer, similar to what has been described previously.<sup>[15]</sup>



Data collection parameters and refinement details have been described elsewhere in detail.<sup>[15, 16]</sup>

The crystal structures were elucidated using direct methods, with subsequent refinement by full-matrix least-squares method on  $F^2$ .<sup>[17]</sup> All non-hydrogen atoms were refined anisotropically.

Absorption corrections were performed using the SADABS program.<sup>[18]</sup> Hydrogen atoms, except those on water molecules were calculated to fixed positions. Hydrogen atoms were fixed using restraints.

### 5.1.3 Synthesis of 5-8

**General procedure:** Compounds **5-8** were synthesized using solvothermal/hydrothermal conditions in thick-walled glass tubes (Carius tubes) with a fill volume of 4 mL. The solvents (or mixtures thereof) (MeOH, DMF and CH<sub>3</sub>CN) were chosen because of their ability to dissolve the metal salts and the organic ligands. Reactions were performed in the temperature range of 100-135 °C, using different donor ratios, as summarized in Scheme 5.1.

**[[Ca(nic)<sub>2</sub>]]<sub>∞</sub> (5):** 2 mmol (492.5 mg) of Ca(NO<sub>3</sub>)<sub>2</sub>·4H<sub>2</sub>O and 6 mmol (739.4 mg) of Hnic in a 3:1 (4 mL) MeOH/DMF mixture were combined in a sealed Carius tube and reacted solvothermally at 135°C. Overnight, colorless block-shaped crystals suitable for X-ray crystallography were isolated from the clear, colorless mother liquor. Mp: decomposes >475°C. Yield (non-optimized): 93.2 mg, 54%. IR (cm<sup>-1</sup>): 3434 (s, br); 3067 (w); 2780 (w); 2439 (w); 1974 (w); 1926 (w); 1565 (s); 1499 (s); 1474 (w); 1406 (s); 1384 (s); 1198 (m); 1164 (w); 1117 (w); 1042 (w); 1094 (w); 1031 (w); 848 (s); 768 (s); 699 (s); 635 (m); 540 (s).

**[[Ca(in)(CH<sub>3</sub>CN)(OH<sub>2</sub>)]]<sub>∞</sub> (6):** 0.5 mmol (111.9 mg) of Ca(NO<sub>3</sub>)<sub>2</sub>·4H<sub>2</sub>O and 1 mmol (125.7 mg) of Hin in a 3:1 (4 mL) CH<sub>3</sub>CN/MeOH mixture were combined in a sealed Carius tube and reacted solvothermally at 120 °C. After 3 days, colorless block-shaped crystals suitable for X-ray crystallography were isolated out of the clear, yellow mother liquor. Mp: decomposes >472°C. Yield % (non-optimized): 59.5 mg, 34%. IR (cm<sup>-1</sup>): 3410 (br, w); 3052 (w); 2956 (w); 2344 (w); 2260 (w); 1734 (s); 1604 (s, br); 1558 (w); 1409 (w); 1327 (w); 1292 (w); 1123 (s); 880 (m); 761 (m); 708 (m); 680 (m).

**[Sr(in)<sub>2</sub>]<sub>∞</sub> (7):** 1 mmol (265.9 mg) of SrCl<sub>2</sub>·6H<sub>2</sub>O and 2 mmol (246.5 mg) of Hin in a 3:1 (4 mL) MeOH/DMF mixture were combined in a sealed Carius tube and reacted solvothermally at 135 °C. Overnight, colorless block-shaped crystals suitable for X-ray crystallography were isolated from the clear, colorless mother liquor. Mp: decomposes >300°C. Yield (not optimized): 128 mg, 19%. IR (cm<sup>-1</sup>): 3063 (w); 2983 (m); 2782 (m); 2441 (w); 2344 (w); 1983 (w); 1590 (s); 1542 (s); 1396 (s); 1215 (m); 1153 (w); 1059 (m); 1003 (m); 873 (m); 853 (m); 773 (s); 688 (s).

**[Ba(in)(Cl)]<sub>∞</sub> (8):** 0.3 mmol (71.9 mg) of BaCl<sub>2</sub>·2H<sub>2</sub>O and 0.6 mmol (75.4 mg) of Hin in a 3:1 (4 mL) MeOH/DMF mixture were combined in a sealed Carius tube and reacted solvothermally at 100 °C. Overnight, colorless block-shaped crystals suitable for X-ray crystallography were isolated out of the clear, colorless, mother liquor. Mp: decomposes >300°C. Yield % (non-optimized): 61 mg, 69%. IR (cm<sup>-1</sup>): 2979 (s, br); 2842 (w); 2761 (s); 2440 (m); 2344 (w); 1960 (w); 1735 (w); 1686 (w); 1637 (m); 1541 (m); 1473 (w); 1409 (s); 1219 (w); 1081 (w); 1025 (m); 1001 (w); 867 (w); 771 (s); 678 (s).

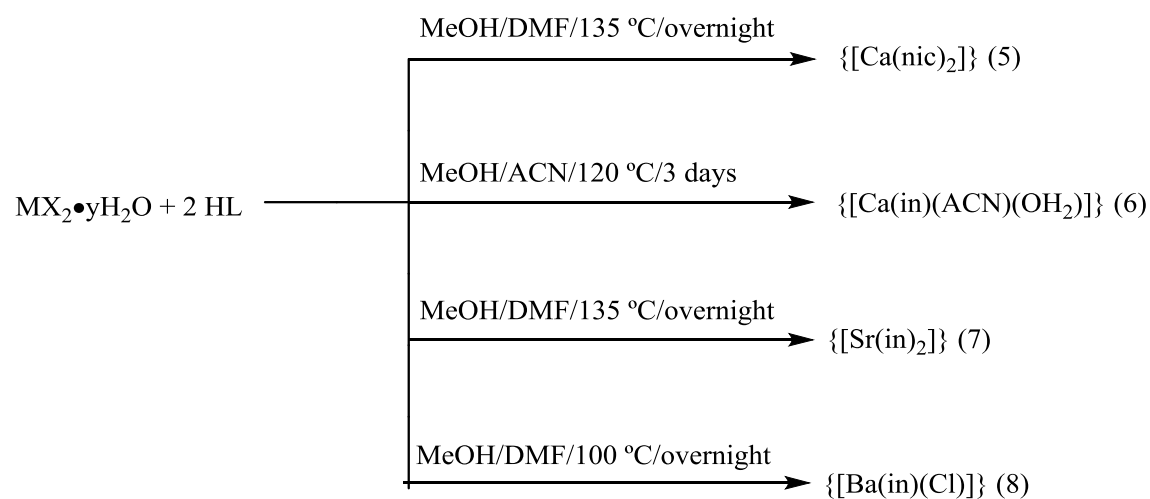
## 5.2 Results and Discussion

### 5.2.1 Synthesis Discussion

The target compounds were prepared by acid-base chemistry, involving the treatment of the metal salts with the organic ligands (Scheme 5.1). Since reaction conditions have a profound effect on the composition of the resulting frameworks,<sup>[19-22]</sup> reagent stoichiometry and reaction conditions were systematically varied.

The compound family **5-8** was obtained by introducing solvent mixtures in various ratios. Optimal conditions for the crystallization of **5-8** were found at temperatures of 100 °C (**8**), 120 °C (**6**) and 135 °C (**5, 7**), as described in the experimental section. If the temperature was raised above 150°C, decomposition of the reagents was generally observed. Mixtures of polar organic solvents afforded 3-dimensional frameworks, in accordance with previous reports.<sup>[23]</sup>

Compounds **5, 7** and **8** crystalize as 3D networks, whereas **6** is a hydrogen bonded coordination polymer. For **5**, the *m*-pyridinecarboxylic acid ligand (in a 3:1 MeOH/DMF mixture at 135 °C) afforded a 3-dimensional network, whilst **6** is produced from *p*-pyridinecarboxylic acid (in a 3:1 MeOH/ACN mixture at 120 °C), affording a hydrogen bonded coordination polymer. Compounds **7** and **8** are based on *p*-pyridinecarboxylic acid. They were obtained from 3:1 MeOH/DMF mixtures at 135 °C and 120 °C respectively. Experiments based on different metal salts showed that reactions employing strontium and barium nitrates yielded insoluble powders, although interestingly, calcium nitrate afforded good quality crystals. For strontium and barium, the chlorides provided crystalline material. This could be due to the higher solubility of strontium and barium chlorides in methanol.<sup>[24]</sup>



M = Ca (**5,6**); Sr (**7**); Ba (**8**)

X = Ca:  $\text{NO}_3^-$ ; Sr:  $\text{Cl}^-$ ; Ba:  $\text{Cl}^-$

Y = Ca: 4; Sr: 6; Ba: 2

L = Ca: Hnic; Sr: Hin; Ba: Hin

Solvent ratios: (**5, 7, 8**) MeOH/DMF: 3:1; (**6**) MeOH/ACN: 3:1

**Scheme 5.1** Synthesis of **5-8**

## 5.2.2 Structural Characterization

Table 5.1 Structural characterization for 5-8

Compound	<b>5</b>	<b>6</b>	<b>7</b>	<b>8</b>
Empirical formula	C <sub>32</sub> H <sub>42</sub> CaN <sub>2</sub> O <sub>16</sub>	C <sub>14</sub> H <sub>15</sub> CaN <sub>3</sub> O <sub>5</sub>	C <sub>12</sub> H <sub>8</sub> N <sub>2</sub> SrO <sub>4</sub>	C <sub>6</sub> H <sub>4</sub> BaNO <sub>2</sub> Cl
Formula weight	284.28	345.37	331.82	294.89
Crystal system	Monoclinic	Orthorhombic	Orthorhombic	Triclinic
Space group	P2 <sub>1</sub> /c	Pnma	Pbcn	P-1
T (K)	90(2)	90(2)	90(2)	86(2)
Unit cell dimensions (Å, °)				
a	8.9979(16)	9.6826(10)	16.365(2)	5.6117(5)
b	16.872(3)	17.9498(18)	10.0238(2)	7.3704(7)
c	9.0236(15)	8.7683(3)	14.443(2)	9.7216(9)
α, γ	90	90	90	85.482(2); 88.766(2)
β	119.3(4)			73.971(2)
Volume (Å <sup>3</sup> )	1193.8(4)	1523.9(3)	2369.2(5)	385.3(7)
Z	4	4	8	2
Calculated density (g/cm <sup>-3</sup> )	1.582	1.505	1.861	2.542
Absorption coefficient (mm <sup>-1</sup> )	0.188	0.441	4.563	5.443
θ range	2.41 to 25.64°	2.27 to 31.67°	2.38 to 27.14°	2.19 to 27.49°
Unique reflections	1685	2633	2601	1744
Total reflections	10126	23103	16035	5951
Goodness-of-fit on F <sup>2</sup>	0.987	1.022	1.018	1.137
R <sub>1</sub> , wR <sub>2</sub> (all data)	R <sub>1</sub> = 0.0390, wR <sub>2</sub> = 0.1186	R <sub>1</sub> = 0.0478, wR <sub>2</sub> = 0.1304	R <sub>1</sub> = 0.0171, wR <sub>2</sub> = 0.0378	R <sub>1</sub> = 0.0099, wR <sub>2</sub> = 0.0263
R <sub>1</sub> , wR <sub>2</sub> (Final)	R <sub>1</sub> = 0.0318, wR <sub>2</sub> = 0.1136	R <sub>1</sub> = 0.0462, wR <sub>2</sub> = 0.1387	R <sub>1</sub> = 0.0117, wR <sub>2</sub> = 0.0394	R <sub>1</sub> = 0.0101, wR <sub>2</sub> = 0.0264
F(0 0 0)	584.0	720	1312	272

Compound **5** crystallizes in the monoclinic spacegroup  $P2_1/c$ . The structure displays a six coordinate calcium center surrounded by four oxygens coming from carboxylate groups on the the nicotinic acid ligand [Ca-O 2.298(5) (avg) Å, O-Ca-O 93.26(6)-167.64(7) °], and two pyridyl nitrogens, arranged almost perpendicular to the metal center in a *cis* fashion [Ca-N distances 2.541(2) and 2.531(2) Å, O-Ca-N angles 83.55(6)-177.71(6) °, N-Ca-N angle 99.59(7) °], (Figure 5.1). Table 5.2 summarizes selected bond lengths and angles for **5**.

**Table 5.2** Selected bond lengths (Å) and angles (°) for **5**

Ca(1)-O(1)	2.2737(16)	O(2)-Ca(1)-O(3)	165.64(7)
Ca(1)-O(2)	2.3287(15)	O(2)-Ca(1)-O(4)	91.44(6)
Ca(1)-O(3)	2.2895(15)	O(2)-Ca(1)-N(1)	86.79(6)
Ca(1)-O(4)	2.2978(19)	O(2)-Ca(1)-N(2)	84.39(6)
Ca(1)-N(1)	2.541(2)	O(3)-Ca(1)-O(4)	96.80(6)
Ca(1)-N(2)	2.531(2)	O(3)-Ca(1)-N(1)	85.23(7)
O(1)-Ca(1)-O(2)	97.68(6)	O(3)-Ca(1)-N(2)	85.20(6)
O(1)-Ca(1)-O(3)	93.26(6)	O(4)-Ca(1)-N(1)	177.71(6)
O(1)-Ca(1)-O(4)	95.26(6)	O(4)-Ca(1)-N(2)	81.66(7)
O(1)-Ca(1)-N(1)	83.55(6)	N(1)-Ca(1)-N(2)	99.59(7)
O(1)-Ca(1)-N(2)	176.36(6)		

The extended structure of **5** is achieved by metal coordination through the carboxylate oxygens and the pyridyl nitrogen in the nicotinic acid (Figure 5.2a). The first form of propagation involves the carboxylate moieties bridging the  $[CaO_4N_2]$  units in  $\mu_2\text{-}\eta^1\text{:}\eta^1$  - coordination modes (Figure 5.2b). The second form involves coordination of the pyridyl nitrogens to neighboring metal centers in the adjacent  $[CaO_4N_2]$  units forming zig-zag chains. These chains are also observed extending from the N-donor atoms, which coordinate to the metals. The combination of these two modes creates a complex and dense extended 3-dimensional network.

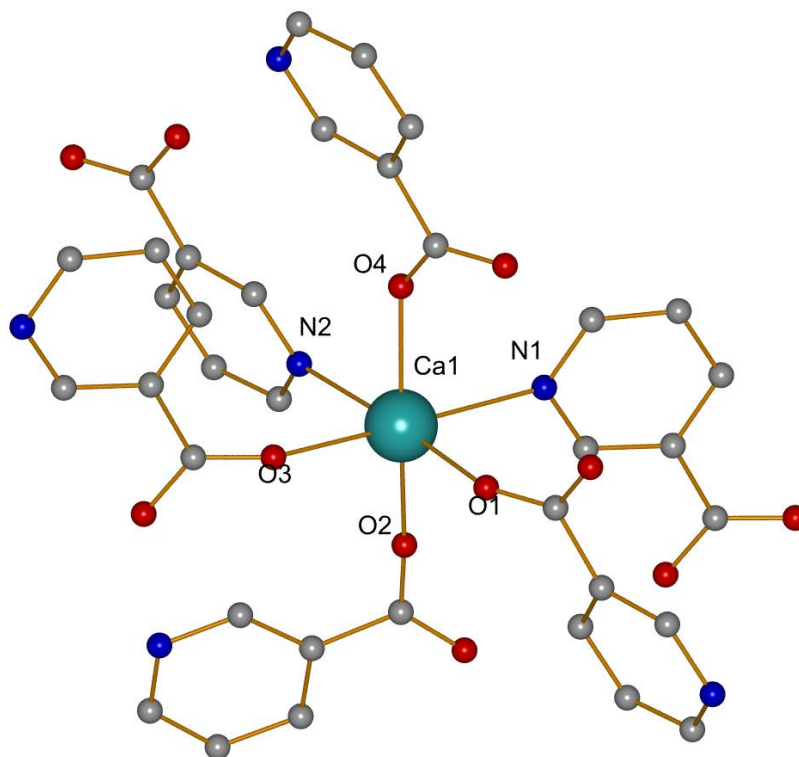
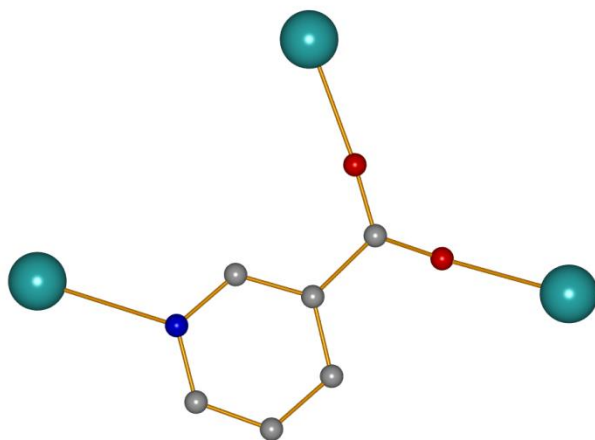
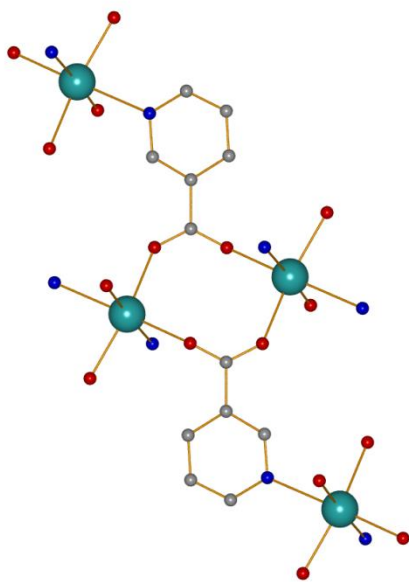


**Figure 5.1** The 6-coordinate calcium center in **5** with four oxygens and two *cis* coordinated nitrogen atoms. Hydrogen atoms have been removed for clarity.



a



b



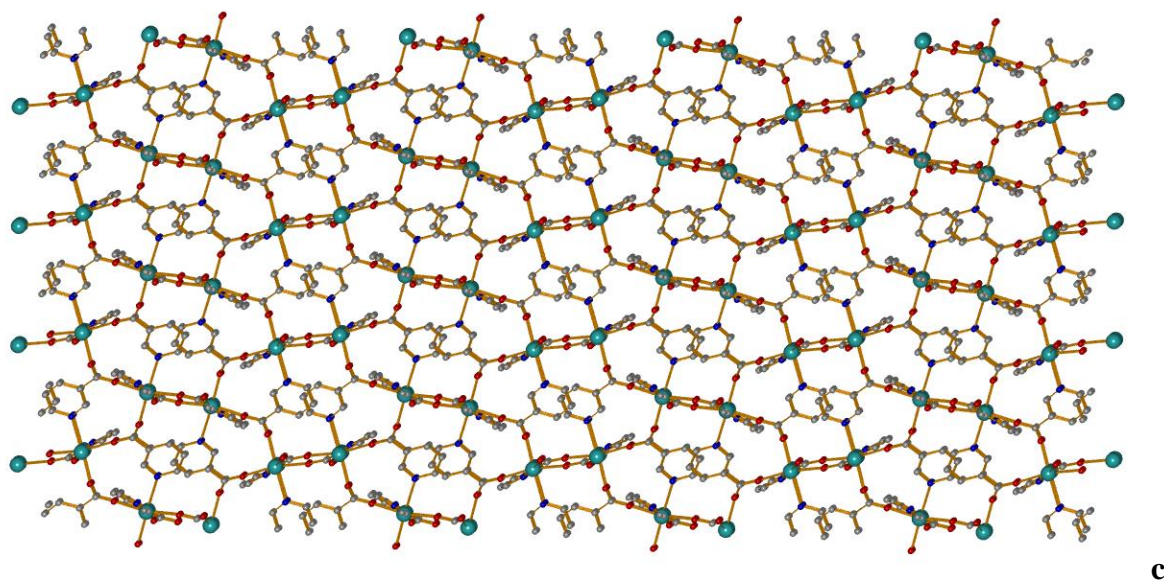


**Figure 5.2** (a) Structural propagation in **5** is achieved through metal-ligand coordination; (b) carboxylate moieties bridge adjacent calcium centers; (c) an intricate pattern of zig-zag chains combine to develop a dense three dimensional framework as seen through the c-axis.

The coordination environment of **5** is similar to that of the magnesium congener  $\{[\text{Mg}(\text{nic})_2]\}$ , reported by Liu *et al.*,<sup>[25]</sup> where the 6-coordinate magnesium center is surrounded by four carboxylate oxygens and two pyridyl nitrogens. By analogy to compound **5**, the pyridyl nitrogens coordinate to the metal in a *cis* fashion.

Compound **6** crystallizes in the orthorhombic spacegroup Pnma. The structure displays a six-coordinate calcium center located in a center of symmetry. The coordination sphere of the calcium center is comprised of five oxygen molecules, four of which are carboxylate oxygens coming from the isonicotinic acid ligand [Ca-O distances 2.308(2) Å (avg)]. These are located in the equatorial plane. Indicating the octahedral geometry, O-Ca-O angles involving the carboxylate moieties are observed at 85.46(4) ° and 174.52(4) ° for the *cis* and *trans* angles of

O(1) and O(1)'-Ca-O(2), respectively. One water molecule is located in one of the *trans* positions, [Ca-O<sub>w</sub> 2.3343(9) Å, O-Ca-O<sub>w</sub> values being 85.49(4) ° and 96.90(3) °]. Completing the coordination environment is an acetonitrile co-ligand in the second trans position [Ca-N distance 2.557(2) Å, O-Ca-N angles being 85.22(3) ° and 92.18(4) ° and 176.71(5) ° for O<sub>w</sub>-Ca-N], as shown in Figure 5.3. Bond distances and angles are summarized in Table 5.3.

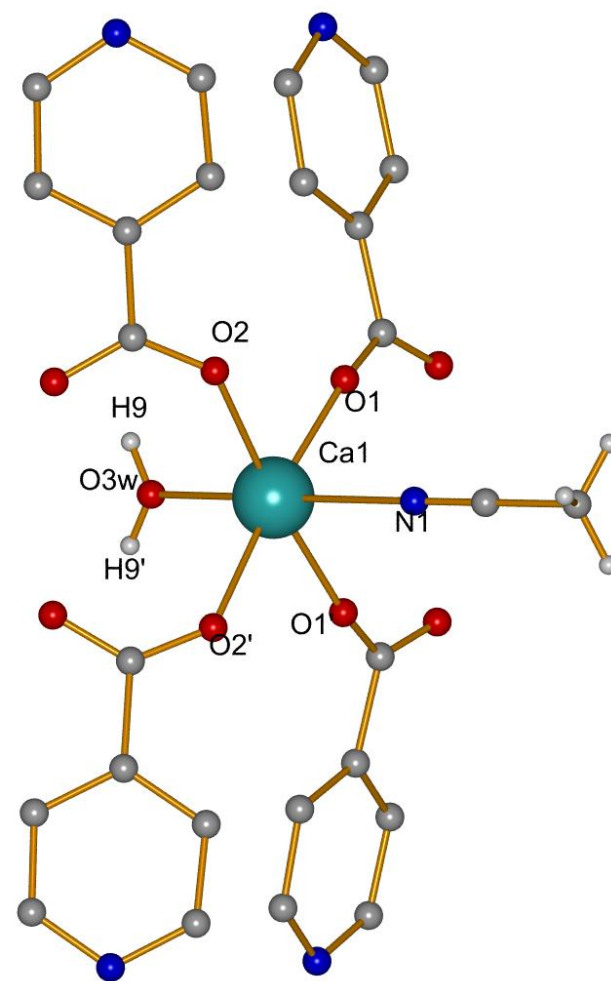


**Figure 5.3** Coordination environment around the calcium center in **6**, showing the center of symmetry. Aromatic hydrogen atoms on pyridyl ring have been removed for clarity.

**Table 5.3** Selected bond lengths (Å) and angles (°) for **6**

Ca(1)-O(1)	2.2844(9)
Ca(1)-O(2)	2.3310(9)
Ca(1)-O(3)w	2.3343(13)
Ca(1)-N(1)	2.557(6)
O(1)-Ca(1)-O(2)	85.46(4)
O(1)-Ca(1)-O(2)	174.52(4)
O(1)-Ca(1)-O(3)w	85.49(4)
O(2)-Ca(1)-O(3)w	96.90(3)
O(1)-Ca(1)-N(1)	92.18(4)
O(2)-Ca(1)-N(1)	85.22(3)
O(3)w-Ca(1)-N(1)	176.71(5)

The structural propagation of **6** is based on 1D chains formed by the carboxylate - calcium  $\mu_2\text{-}\eta^1:\eta^1$  -bridging mode (Figure 5.4). Further propagation is achieved through hydrogen bonding involving the pyridyl rings as proton acceptors of medium strength hydrogen bonding [H9---N2 distance 1.987(2) Å, <DHA angle of 140.94(4) °] with the metal bound water molecules, affording a 3-dimensional framework supported by hydrogen bonds (Figure 5.5).

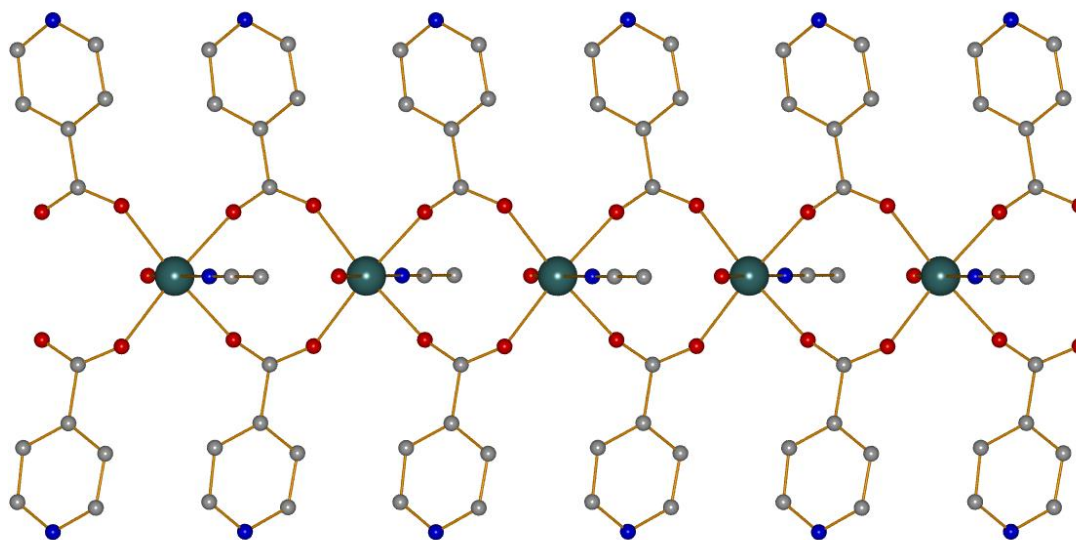


**Figure 5.4** The one-dimensional chain structure of **6**, showing the  $\mu_2.\eta^1:\eta^1$ -calcium-ligand bridging mode. Hydrogen atoms has been removed for clarity.

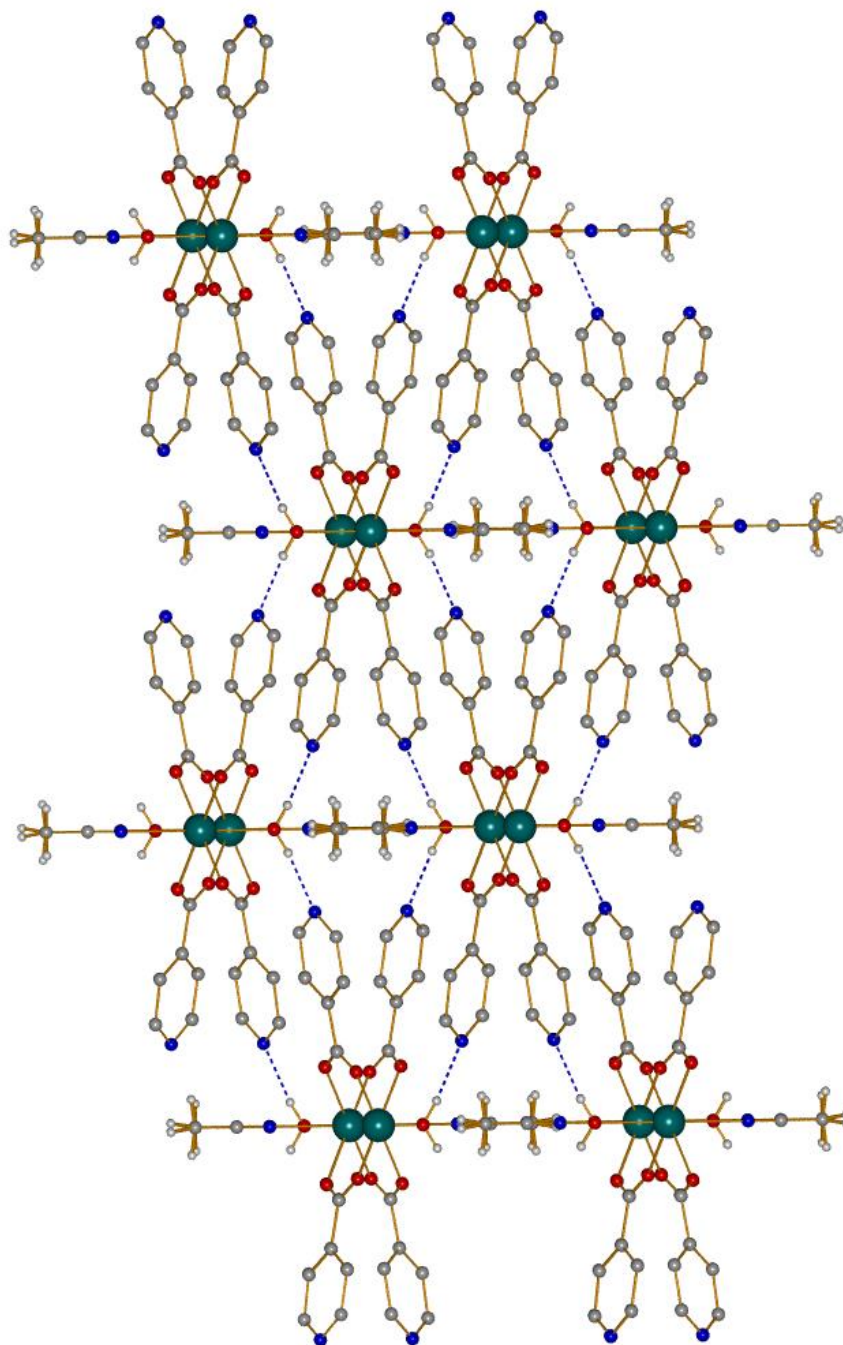


**Figure 5.5** The hydrogen bonded network in **6**, showing the hydrogen bonding between the metal bound water molecules and neighboring pyridyl ligands. Hydrogen atoms, except those of water and acetonitrile have been removed for clarity.

Compound **7** crystallizes in the orthorhombic spacegroup Pbcn. The complex shows a 7-coordinate strontium, in which five oxygens from the carboxylate ligands [Sr-O distances 2.590(5) Å (avg), with O-Sr-O angles ranging from 48.76(3)-125.35(3) °] and two nitrogens [Sr-N distance 2.782(3) and 2.738(4) Å, O-Sr-N angles ranging from 71.81(4)-157.65(4) °] perpendicular to the strontium metal in *cis* fashion complete (N-Sr-N: 84.49(4) °) the coordination sphere into SrO<sub>5</sub>N<sub>2</sub> polyhedra (Figure 5.6). Table 4 shows selected bond lengths and angles for **7**.

Two types of carboxylate binding modes were observed. In one case, the carboxylate moieties associate neighboring strontium metals through bridging and chelating in  $\mu_2\text{-}\eta^2\text{:}\eta^1$  coordination modes, forming [Sr<sub>2</sub>(in)<sub>2</sub>] units. Further, neighboring [Sr<sub>2</sub>(in)<sub>2</sub>] units are associated by carboxylates bridging in a  $\mu_2\text{-}\eta^1\text{:}\eta^1$  -fashion. The combination of these two motifs forms infinite one dimensional chains, as shown in Figure 5.7.



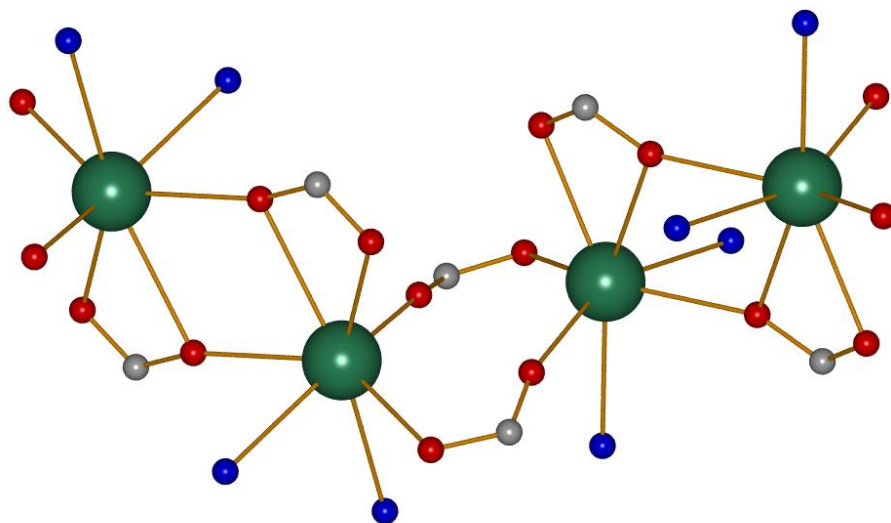


**Figure 5.7** The one-dimensional bridging motif in **7**, comprised of the association of  $\mu_2\text{-}\eta^2\text{:}\eta^1$ -bound  $[\text{Sr}_2(\text{in})_2]$  units through  $\mu_2\text{-}\eta^1\text{:}\eta^1$ -bridging carboxylates. The phenyl groups in the ligands have been removed for clarity.

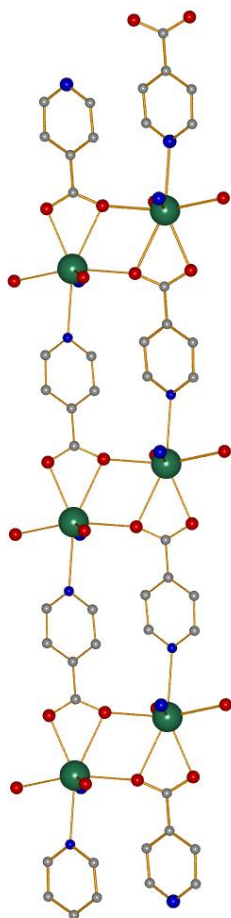


**Table 5.4** Selected bond lengths (Å) and angles (°) for **7**

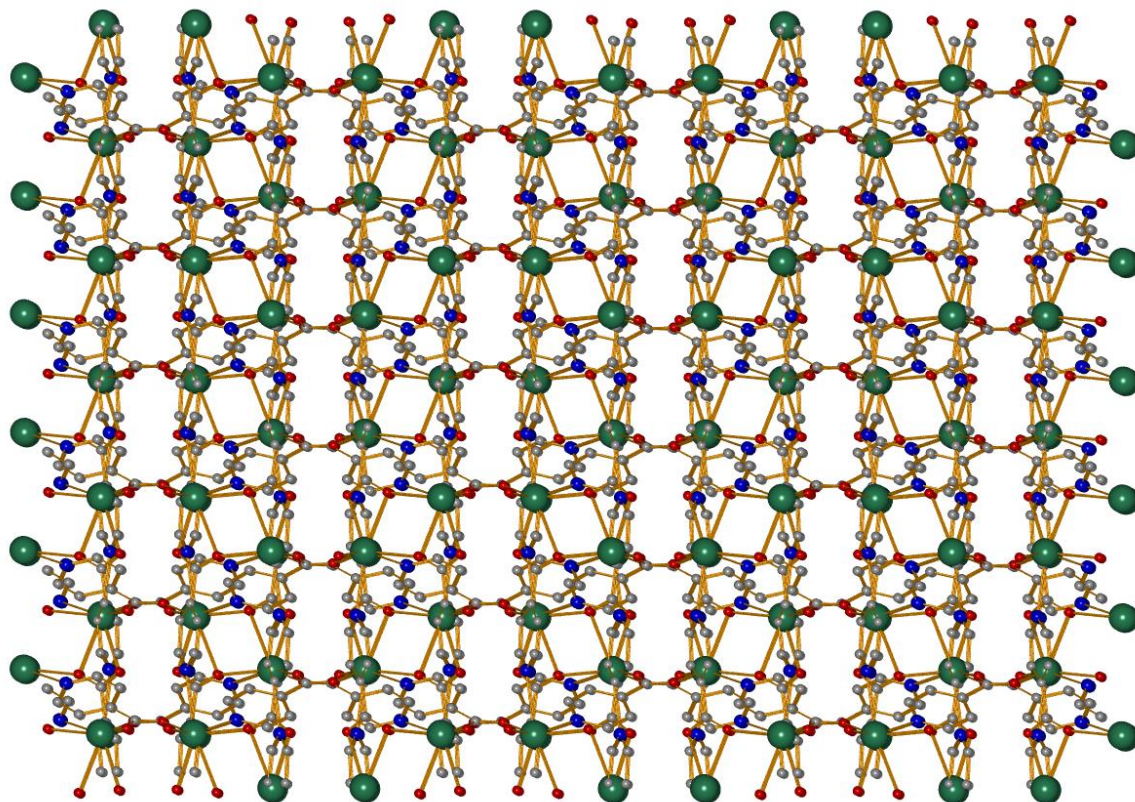
Sr(1)-O(1)	2.580(2)	O(2)-Sr(1)-O(4)	125.35(3)
Sr(1)-O(2)	2.527(1)	O(2)-Sr(1)-N(1)	71.81(4)
Sr(1)-O(3)	2.487(1)	O(2)-Sr(1)-N(2)	76.78(4)
Sr(1)-O(4)	2.764(1)	O(3)-Sr(1)-O(2)	119.09(4)
Sr(1)-N(1)	2.782(3)	O(3)-Sr(1)-O(4)	90.52(3)
Sr(1)-N(2)	2.738(4)	O(3)-Sr(1)-N(1)	157.07(4)
O(1)-Sr(1)-O(2)	79.11(4)	O(3)-Sr(1)-N(2)	79.18(4)
O(1)-Sr(1)-O(3)	101.92(4)	O(4)-Sr(1)-N(1)	98.87(4)
O(1)-Sr(1)-O(4)	48.76(3)	O(4)-Sr(1)-N(2)	157.65(4)
O(1)-Sr(1)-N(1)	99.98(4)	N(1)-Sr(1)-N(2)	84.49(4)
O(1)-Sr(1)-N(2)	152.70(4)		

Further spatial propagation of **7** is achieved through the pyridyl nitrogens, such that the chains are propagated into a second dimension (Figure 5.8) under formation of carboxylate linked pillars as shown through the a-axis in Figure 5.9. The pillars are composed of wave-like chains which associate into a 3D framework with oval shaped channels as shown in Figure 5.10a-b. Window channel size measures 15.15 x 10.59 Å, as determined by Sr---Sr distances.

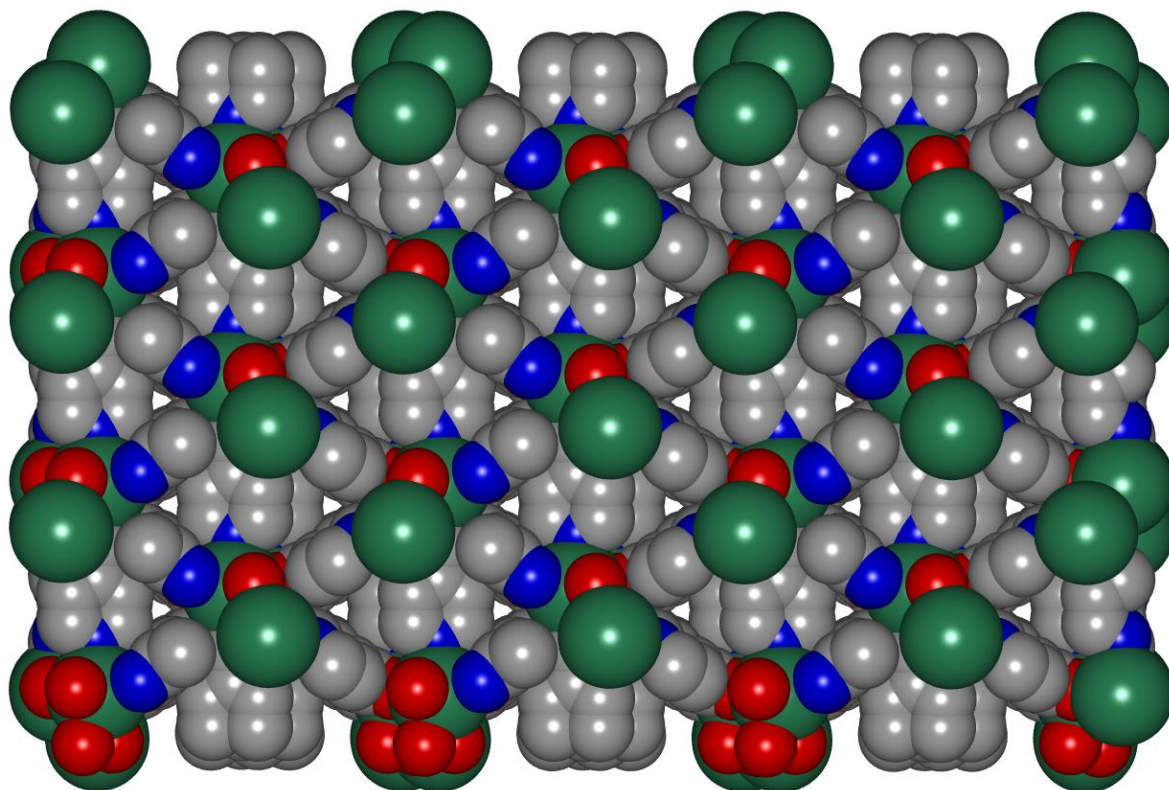
A peculiar feature of **7** is that the access to the significantly sized channels is blocked by pyridyl rings, preventing the functioning of the channels as hosts. A space-filling model shows that the channels are fully blocked by the pyridyl rings (Figure 5.10a).

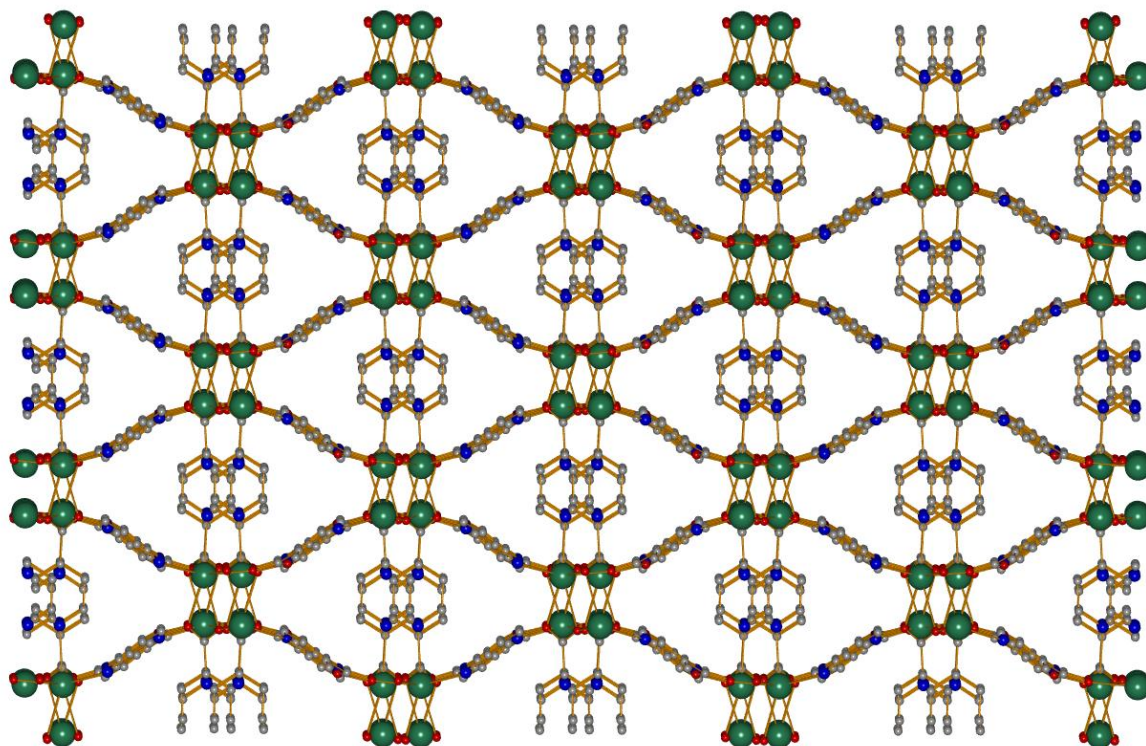


**Figure 5.8** Chains formed through pyridyl metal coordination in **7**. Hydrogen atoms have been removed for clarity.



**Figure 5.9** A side view of **7**. Sheets formed from the combination of carboxylate generated chains and coordinated pyridyl nitrogens in **7**.

**a**



b

**Figure 5.10** (a) Space filling model of the channels in **7**, the pyridyl rings block the channels. (b) Ball and stick model of oval shaped channels blocked by pyridyl rings in **7**.

Compound **8** crystallizes as a condensed structure in the triclinic spacegroup P-1. The structure displays a seven coordinate barium center and is coordinated by four carboxylate oxygen atoms (two symmetry generated) [Ba-O distances are 2.782(4) (avg) Å, O-Ba-O angles range from 74.35(4)-104.63(3) °], a nitrogen atom from the pyridyl ring [Ba-N distance 2.927(13) Å, O-Ba-N angles range from 70.93(3)-137.20(4) °] and two chlorine atoms (one symmetry generated) [Ba-Cl distance 3.19(5) Å, O-Ba-Cl and N-Ba-Cl angles 76.80(3)-



153.50(2) ° and 117.95(3) °, respectively] as seen in Figure 5.11. Table 5.5 summarizes selected bond lengths and angles for **8**.

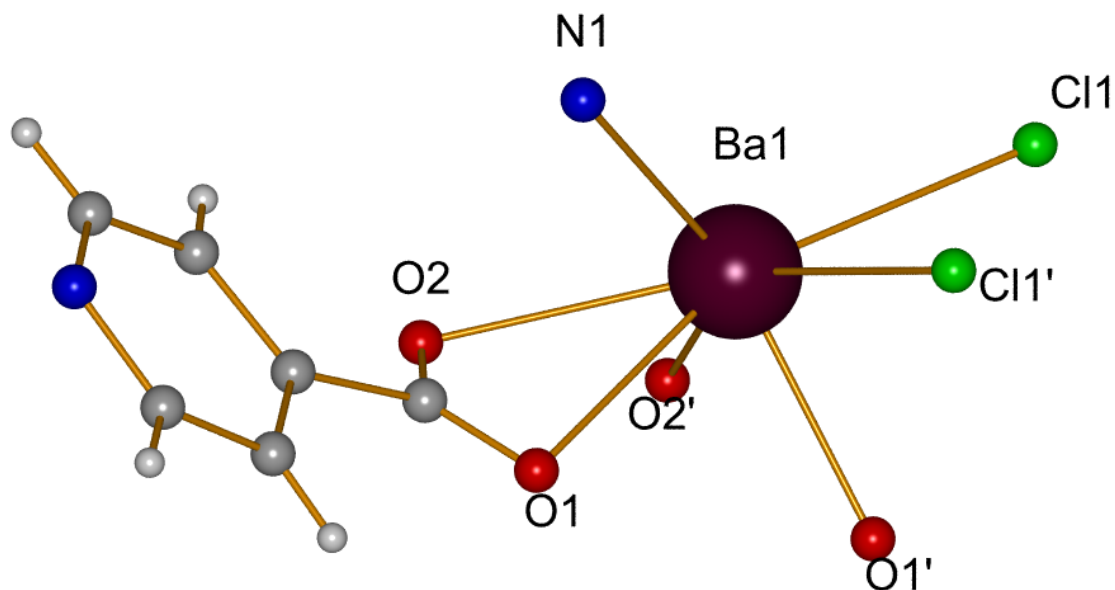


**Figure 5.11** The 7-coordinate barium center in **8**

**Table 5.5** Selected bond lengths (Å) and angles (°) for **8**

Ba(1)-O(1)'	2.668(11)	O(1)' <sup>2</sup> -Ba(1)-N(1)	131.60(4)
Ba(1)-O(1)	2.890(11)	O(1)-Ba(1)-N(1)	70.93(3)
Ba(1)-O(2)	2.867(11)	O(2)-Ba(1)-N(1)	72.70(3)
Ba(1)-O(2)'	2.704(11)	O(2)' <sup>2</sup> -Ba(1)-N(1)	137.20(4)
Ba(1)-N(1)	2.927(13)	O(1)' <sup>2</sup> -Ba(1)-Cl(1)	86.31(3)
Ba(1)-Cl(1)	3.197(5)	O(1)-Ba(1)-Cl(1)	124.89(2)
O(1)-Ba(1)-O(1)'	74.35(4)	O(2)-Ba(1)-Cl(1)	153.50(2)
O(1)-Ba(1)-O(2)	104.64(3)	O(2)' <sup>2</sup> -Ba(1)-Cl(1)	76.80(3)
O(1)' <sup>2</sup> -Ba(1)-O(2)'	45.46(3)	N(1)-Ba(1)-Cl(1)	117.95(3)
O(1)' <sup>2</sup> -Ba(1)-O(2)	78.42(4)		
O(2)-Ba(1)-O(2)'	69.85(4)		
O(2)' <sup>2</sup> -Ba(1)-O(1)	95.99(3)		

The main structural propagation in **8** is by chains formed by bridging chlorides, associating three barium centers in  $\mu_3\text{-}\eta^3$  coordination mode under formation of a 1D chain with a “zig-zag” motif, as shown in Figure 5.12. Furthermore, the ligand’s carboxylate moieties associate three metal centers through carboxylate bridges in a  $\mu_3\text{-}\eta^2\text{:}\eta^2$  chelating/bridging coordination mode, forming a second “zig-zag” 1D chain. The carboxylate-supported 1D chains associate with the chloride bridged chains under formation of 2D sheets, as shown in Figure 5.12.

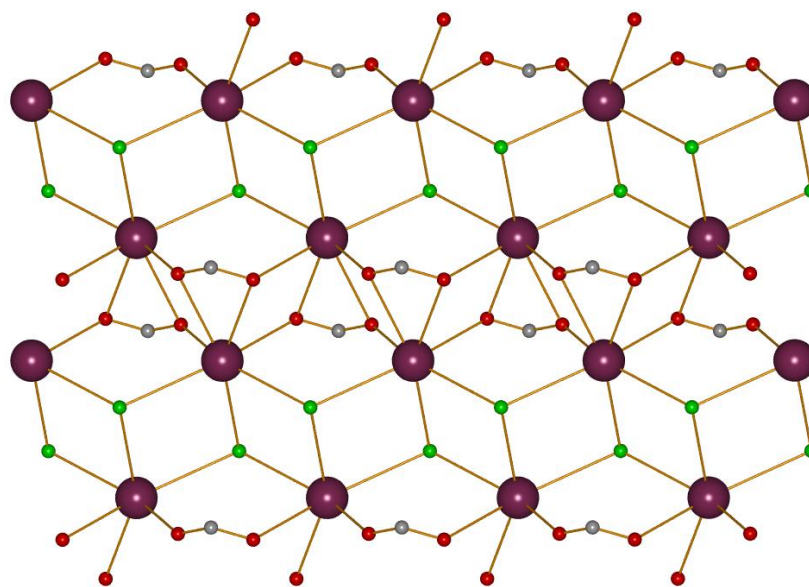


**Figure 5.12** 2D sheets in **8**, resulting from the association of  $\mu_3\text{:}\eta^3$  bridging chloride atoms and  $\mu_3\text{-}\eta^2\text{:}\eta^2$  chelating/bridging carboxylate moieties. Phenyl groups in the ligand have been removed for clarity.

The 2D sheets in **8** are spatially propagated by the isonicotinate ligands, which act as linkers between sheets. The pyridyl nitrogens in the ligand coordinate to metal centers in neighboring sheets, forming a 3D framework. In addition to this, the pyridyl rings stack *via* medium strength  $\pi$ --- $\pi$  stacking interactions, measuring 3.26 and 3.58 Å from centroid to centroid. These values are within those reported.<sup>[26]</sup>

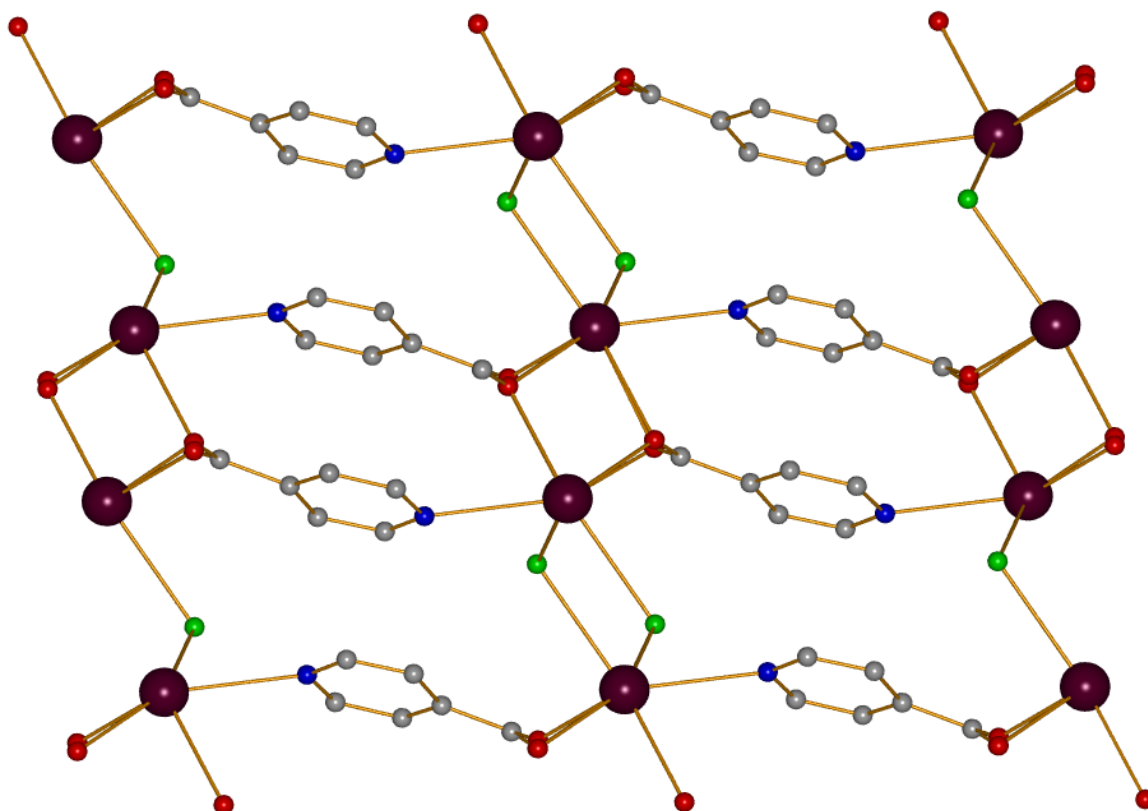


**Figure 5.13** Part of the 3-dimensional network in **8**, formed from the association of 2D sheets *via* the pyridyl rings. In addition  $\pi$ --- $\pi$  stacking interactions between the aromatic rings are present. Hydrogens removed for clarity.



The heavier metals display longer M-O bond distances as compared to the compounds reported in **Chapter 3** with the smaller Mg center. As expected, the average length of the M-O carboxylate bond increases with increasing metal radius and coordination number [M-O Ca (**5**, **6**): 2.298(5) and 2.308(2) Å, respectively; Sr (**7**) 2.590(5) Å; Ba (**8**) 2.782(4) Å]. These M-O carboxylate bonds are within commonly reported bond lengths for their respective coordination numbers [M-O **5-6** (CN 6),<sup>[27-29]</sup> **7** (CN 7),<sup>[30]</sup> **8** (CN 7)<sup>[31]</sup>].

While both compounds **5** and **6** show 6-coordinate centers, compound **5** displays [CaN<sub>2</sub>O<sub>4</sub>] core units and compound **6** shows [CaNO<sub>5</sub>] core units. The atoms coordinated to the metal center in compound **5** are also different from **6**. Compound **5** crystallizes donor free and is coordinated solely by atoms from the ligand, whilst compound **6** is coordinated by co-ligands (acetonitrile and water) in two positions. The co-ligand free nature of **5** results in its 3-dimensional nature, whilst in **6** the presence of a metal coordinated water propagates the pseudo 3-dimensional hydrogen bonded network.

In addition, our knowledge from analyzing CCDC data indicates that no fully 3-dimensional structures based on nicotinic acid and calcium have been reported before, as structures are limited to hydrogen-bonded complexes.<sup>[32, 33]</sup>

Compounds **7** and **8** are also 3-dimensional. Although the Sr atom in compound **7** is 7-coordinate, 7-coordinate strontium centers are rather uncommon,<sup>[30, 34]</sup> preferring coordination numbers of 8<sup>[35-37]</sup> or 9.<sup>[38-40]</sup>

To our knowledge, no 3-dimensional Sr isonicotinate structures have been reported before. The only example of a Sr isonicotinate structure is the hydrogen-bound, contact-separated species reported by Chen *et al.*,<sup>[32]</sup> which is isostructural to the barium isonicotinate (compound **4**)<sup>[41]</sup> detailed in **Chapter 4**.

Further, the channels in **7** lose their potential as hosts because of blockage by pyridyl rings from the ligands. Blockage of channels in MOFs is common, and may arise from guest solvent molecules, ions or ligands which crystallize pointing towards the channels.<sup>[42]</sup> Interestingly, as opposed to **8**, no incorporation of the chlorine atom from the SrCl<sub>2</sub> was observed.

Compound **8**, like **7**, is also 7-coordinate. It crystallizes as a dense 3-dimensional coordination polymer, in which the metal center forms a [BaO<sub>4</sub>NCl<sub>2</sub>] unit. A perfect example of increasing aggregation with increasing metal size, **8** is the only compound in the series to display  $\mu_3\text{-}\eta^2\text{:}\eta^2$  binding modes.

Incorporation of chlorine atoms in the structure results in chlorine bridges which are important for structural propagation. More examples of M-Cl-M bridging are reported for the lighter metals (116 examples in the CCDC database for Mg, 15 for Ca and 2 for Sr). However metal-chlorine bridges in **8** are longer than their lighter metal counterparts [Mg-Cl: 2.40-2.50 Å<sup>[43, 44]</sup>; Ca-Cl: 2.72-2.97 Å<sup>[45, 46]</sup>; Sr-Cl: ~3.06 Å<sup>[47, 48]</sup>], a result of the larger metal size. The metal-chlorine bridging distances in **8** are comparable in length to the only two structures reported in the CCDC database.<sup>[49, 50]</sup> They are also comparable in length to the metal-chlorine bridges in BaCl<sub>2</sub> salt.<sup>[51]</sup> It is noteworthy to mention that due to the larger size of the Ba atom, 7-coordinate barium complexes are rare, and coordination numbers 8-10 are preferred.<sup>[52-54]</sup>

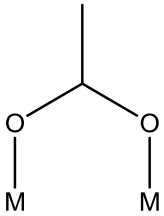
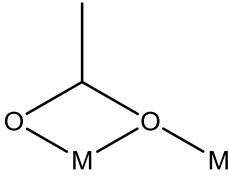
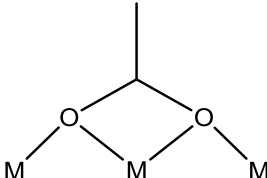
### 5.2.3 Analysis of the Carboxylate Binding Modes

Compounds **5-8** exhibit a variety of carboxylate-metal binding motifs (Table 5.6). In the case of the smaller calcium metal in **5** and **6**, where a coordination number of six is observed,  $\mu_2\text{-}\eta^1\text{:}\eta^1$  carboxylate coordination modes, corresponding to a carboxylate bridging two metal centers, is observed. For the larger strontium and barium centers in **7** and **8** (Sr CN: 7, Ba CN: 7), there are two types of binding motifs. In **7**, a  $\mu_2\text{-}\eta^2\text{:}\eta^1$  coordination mode corresponds to one carboxylate chelating to a strontium center and bridging another, and the bridging mode  $\mu_2\text{-}\eta^1\text{:}\eta^1$  which associates two metal centers. Compound **8** exhibits  $\mu_3\text{-}\eta^2\text{:}\eta^2$  binding modes, corresponding to a carboxylate moiety chelating a metal center and bridging to two others.

As expected and discussed above, in compounds **5 - 8**, the M-O distances increase as the metal size increases. This increase is consistent with the increasing ionic radii relative to Ca ( $\Delta\text{Sr}/\text{Ca}$ : 0.035 Å;  $\Delta\text{Ba}/\text{Ca}$ : 0.12 Å).<sup>[55]</sup>, which are also responsible for the increase in coordination number, as the larger metals require coordination to a larger number of ligands/donors to achieve steric saturation. Accordingly, compounds **5** and **6** are six-coordinate, whereas the strontium and barium species **7** and **8** are seven-coordinate.

A closer look reveals that the  $\mu_2\text{-}\eta^1\text{:}\eta^1$  bridging mode is a common feature in **5 - 7**, and the increase in M-O distance is evident as the metal size increases [ $\Delta\text{M-O}_{(\text{br, max})}$  **7 - 6** and **5** = 0.2 Å, M= Ca, Sr]. The  $\mu_2\text{-}\eta^1\text{:}\eta^1$  mode is not present in **8**, but our previous work<sup>[56]</sup> and others<sup>[57, 58]</sup> show the similar binding modes and values for barium with regard to calcium and strontium [ $\Delta\text{M-O}(\text{br, max}) = \text{Ba}^{[56]} - \text{Ca}^{\text{This work}}$ : 0.35 Å;  $\text{Ba}^{[56]} - \text{Sr}^{\text{This work}}$ : 0.16 Å]. The larger diameter of the heavier metals also facilitates for the chelating/bridging coordination modes<sup>[59]</sup> ( $\mu_2\text{-}\eta^2\text{:}\eta^1$ ,  $\mu_3\text{-}\eta^2\text{:}\eta^2$ ) and larger coordination numbers observed in **7 - 8**.

Table 5.6 Carboxylate binding motifs in 5-8

Mode			
	$\mu_2\text{-}\eta^1:\eta^1$	$\mu_2\text{-}\eta^2:\eta^1$	$\mu_3\text{-}\eta^2:\eta^2$
<b>5</b> Ca min	(br, O1) 2.274(2)	--	--
max	(br, O3) 2.329(2)	--	--
<b>6</b> Ca min	(br, O1) 2.284(9)	--	--
max	(br, O2) 2.332(9)	--	--
<b>7</b> Sr min	(br, O3) 2.487(11)	(ch, O1) 2.580(12)	--
max	(br, O2) 2.528(11)	(ch, O4) 2.764(11), (br, O4) 2.528(11)	--
<b>8</b> Ba min	--	--	(ch, O2) 2.867(11),
max	--	--	(br, O1') 2.668(11)
min			(ch, O1) 2.869(11),
max			(br, O2') 2.704(11)

br = bridging, ch = chelating

### 5.2.4 Effect of ligand structural isomerism

Since the isomeric nature of the pyridinecarboxylic acids involve variable positions of the N-donor atom in *para*, *meta*, *ortho* around the aromatic backbone, it is thought that this has an effect in the resulting framework characteristics.

The effect of ligand structural isomerism has previously been studied before for calcium species involving pyridinedicarboxylic acids (PDC) (mainly: 2,6-PDC; 3,5-PDC; 2,4-PDC; 2,5-PDC; 2,3-PDC and 3,4-PDC),<sup>[60]</sup> with motifs ranging from isolated octahedra to dense 3-dimensional frameworks. In **Chapter 3** and this **Chapter**, we report structures that were isolated from Hin and Hnic; several important structural features discussed above relate to the position of the N-donor atom.

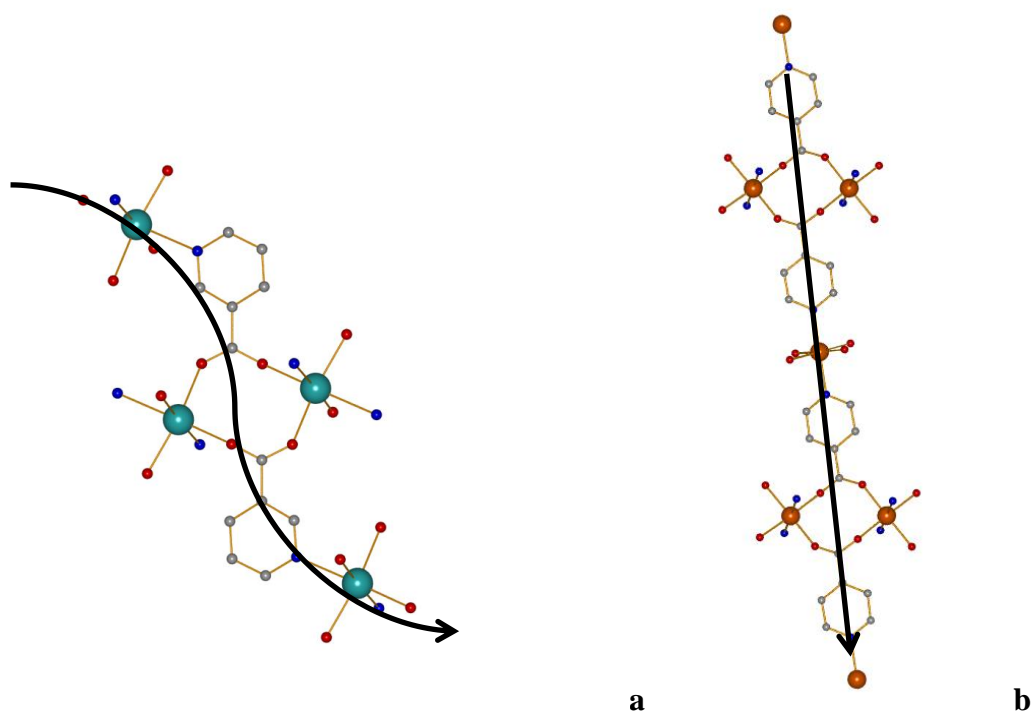
This is evident when comparing compound **5**, in this chapter, to compounds **1a-c** in **Chapter 3**. The core geometry around both metals (**5**: Ca; **1a-c**: Mg) is the same, with 6-coordinated metal centers forming  $[MN_2O_4]$  units. In both cases these units are associated through carboxylates in a  $\mu_2-\eta^1:\eta^1$  interaction (Figure 5.14a-b). Likewise, in both compounds, there is coordination to the metal from both the carboxylate moiety and the pyridyl nitrogen.

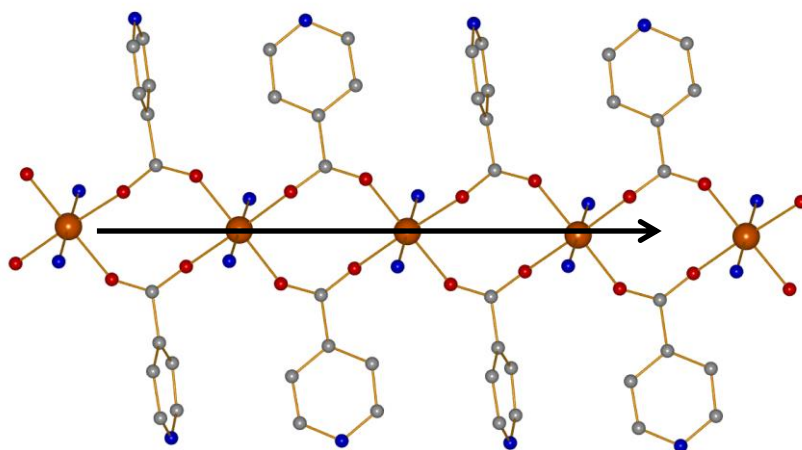
An analysis of the structural propagation reveals even more. For example, even if both compounds exhibit the same coordination numbers and coordination spheres, the *meta* position in the nicotinic acid ligand causes the formation of zig-zag chains in compound **5** (Figure 4.2b) whilst the chains formed in compounds **1a-c** display linear character for the *para* ligand.

Further inquiry shows that the nitrogens are in different positions with respect to the metal. The nitrogen atoms in compound **5** are *cis* (Figure 5.1, above), whilst the nitrogen atoms in compounds **1a-c** lie in *trans* positions (**Chapter 3**, Figure 3.3).

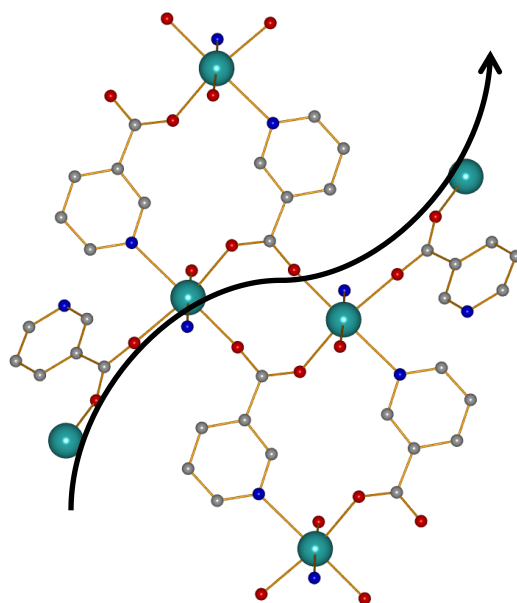
Unlike compounds **1a-c**, in which an array of  $\mu_2\text{-}\eta^1:\eta^1$  bridging interactions result in the formation of an infinite chain with linear character (Figure 5.14c), in compound **5**, the *cis* position of the N-donor atoms prevents the formation of these linear chains. Instead, the chain is twisted and the carboxylate is engaged in a  $\mu_2\text{-}\eta^1:\eta^1$  bridging mode with a neighboring calcium atom (Figure 5.14d).

The *cis* position of these nitrogen atoms, in both the ligand and the coordination sphere in compound **5**, may be the reason as to why compounds **1a-c** crystallize as open-frameworks, whereas compound **5** crystallizes as a dense coordination polymer.





c



d

**Figure 5.14** Comparison of structural propagation. The black arrows define direction of the chains. (a) zig-zag chains in **5** and (b) a set of chains displaying linear character in **1a-c** (c) Infinite chains found in **1a-c**, formed from carboxylates bridging Mg centers in  $\mu_2\text{-}\eta^1\text{:}\eta^1$  fashion (d) Twisting of chains in compound **5**, the *cis* positions of the N-donor atoms prevent formation of chains exhibiting linear character. For **5**, a dense 3-dimensional coordination complex is formed.

### 5.5 Thermal analysis of 5-8

A TGA study was performed on **5 - 8** to observe their thermal properties (Figure 5.15). Compound **5** shows relative stability until 330 °C, after which the compound begins to decompose. Compound **6** shows loss of both coordinated water and acetonitrile in the range of 30-142 °C (exp. 16%, calc. 17%), after which a stable plateau is observed until ~480 °C, at which the thermal decomposition of the organic ligands occurs. For compound **7**, initial loss of donors occurs until 330 °C, at which a gradual decrease in weight, with an abrupt drop at 500 °C, indicates the start of ligand decomposition. Compound **8** exhibits an initial loss of donors until 200 °C, at which a stable plateau forms until a sharp drop is observed at 300 °C, indicating the decomposition of the organic ligands.



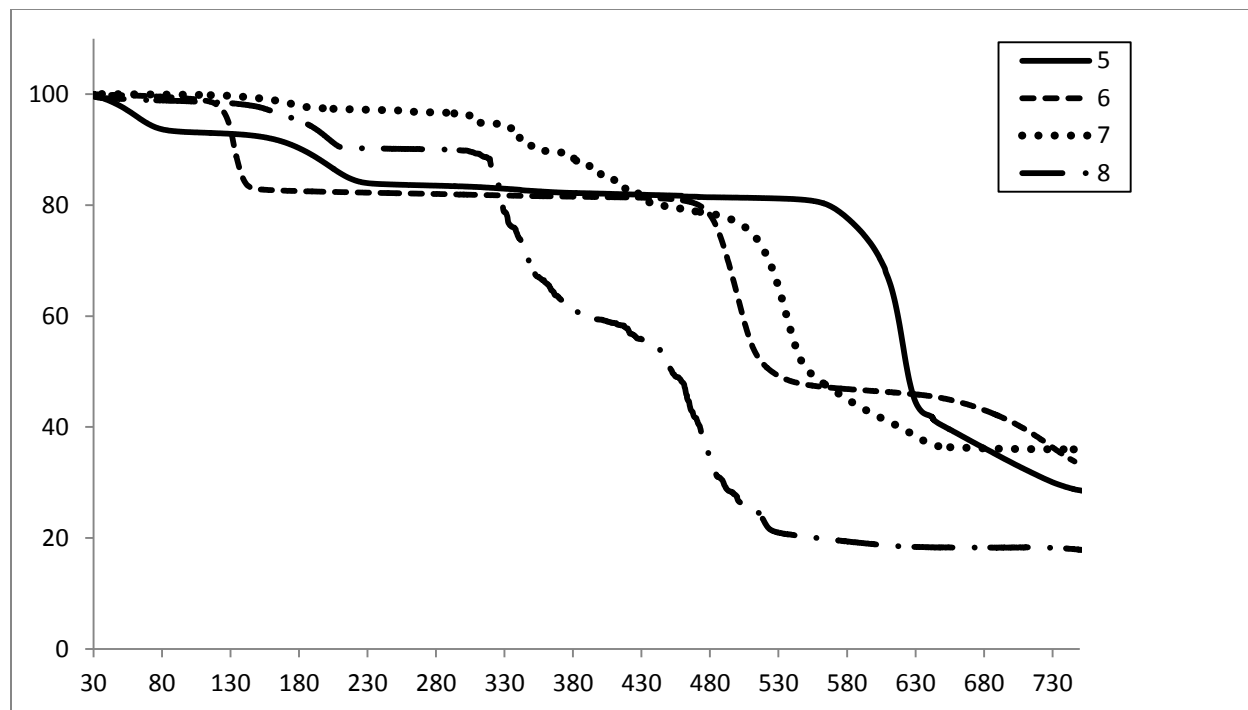


Figure 5.15 TGA analysis of 5-8

## 5.6 Conclusions

Our continuing work in preparing metal organic frameworks, based on the isonicotinate ligand family in conjunction with s-block metals, yielded four new coordination polymers based on the heavy alkaline earth metals (Ca, Sr and Ba) and (*p*, *m*) pyridinecarboxylic acid. The compounds **5**, **7** and **8** exhibit 3-dimensional architectures, whereas compound **6** consists of a hydrogen-bonded network.

Salient structural features in compounds **5-8** are the multiple carboxylate-metal binding modes that seem to change with the metal size. Bridging modes are evident for **5-7** ( $\mu_2\text{-}\eta^1\text{:}\eta^1$ ), whereas bridging/chelating modes ( $\mu_2\text{-}\eta^2\text{:}\eta^1$ ,  $\mu_3\text{-}\eta^2\text{:}\eta^2$ ) arise for the larger metals in **7** and **8**.

Ligand structural isomerism is also interesting in this work. A closer look at the structures reveals that propagation is highly ligand dependent, and that the open-frameworks are favored for the *p*-pyridinecarboxylic acid, as opposed to the *m*-pyridinecarboxylic acid (as also evidenced in **Chapter 3**).

Further, the thermal stability of **5-8** was also evaluated through thermogravimetric analysis. All compounds are highly stable, with decomposition temperatures occurring above 300 °C, after initial loss of co-ligands.

Peculiarly, compound **7** crystalizes as a closed-framework, in which the pyridyl rings from the ligand block access to the channels. The space filling model for **7** clearly shows that the channels are blocked by pyridyl rings, disabling them from functioning as hosts.

## 5.7 References

- [1] D. Banerjee, Z. Zhang, A.M. Plonka, J.B. Li, J.B. Parise, *Cryst. Growth Des.*, 12 (2012) 2162-2165.
- [2] J.-R. Li, Y. Ma, M.C. McCarthy, J. Sculley, J. Yu, H.-K. Jeong, P.B. Balbuena, H.-C. Zhou, *Coord. Chem. Rev.*, 255 (2011) 1791-1823.
- [3] T. Maity, D. Saha, S. Das, S. Koner, *Eur. J. Inorg. Chem.*, 2012 (2012) 4914-4920.
- [4] A.E. Platero-Prats, M. Iglesias, N. Snejko, A. Monge, E. Gutiérrez-Puebla, *Cryst. Growth Des.*, 11 (2011) 1750-1758.
- [5] A.R. Kennedy, J.B. Kirkhouse, K.M. McCarney, O. Puissegur, W.E. Smith, E. Staunton, S.J. Teat, J.C. Cherryman, R. James, *Chemistry*, 10 (2004) 4606-4615.
- [6] D. Zhang, R. Zhang, J. Li, W. Qiao, S. Wang, *Inorg. Chem. Commun.*, (2013) 307.
- [7] J. Soleimannejad, H. Aghabozorg, S. Hooshmand, H. Adams, *Acta. Cryst.*, (2007) m3089.
- [8] M.K. Kim, K.M. Ok, *CrystEngComm*, (2011) 4599.
- [9] P.-C. Liang, H.-K. Liu, C.-T. Yeh, C.-H. Lin, V. Zima, *Cryst. Growth Des.*, 11 (2011) 699-708.
- [10] C. Volkringer, T. Loiseau, G. Férey, J.E. Warren, D.S. Wragg, R.E. Morris, *Solid State Sciences*, 9 (2007) 455-458.
- [11] A.G. Goos, P.J. Rosado Flores, Y. Takahashi, K. Ruhlandt-Senge, *Alkaline Earth Metals: Organometallic Chemistry 2012*.
- [12] C.-T. Yeh, W.-C. Lin, S.-H. Lo, C.-C. Kao, C.-H. Lin, C.-C. Yang, *CrystEngComm*, (2012) 1219.
- [13] M.L. Foo, S. Horike, S. Kitagawa, *Inorg. Chem.*, (2011) 11853-11855.

- [14] Y. Yang, G. Jiang, Y.-Z. Li, J. Bai, Y. Pan, X.-Z. You, *Inorg. Chim. Acta*, 359 (2006) 3257-3263.
- [15] S. Chadwick, K. Ruhlandt-Senge, *Chem. Eur. J.*, 4 (1998) 1768.
- [16] S. Chadwick, U. English, B.C. Noll, K. Ruhlandt-Senge, *Inorg. Chem.*, 37 (1998) 4718.
- [17] G.M. Sheldrick, XShell 6.3.1, in, Siemens Analytical X-ray Instruments, Madison, Wisconsin: 1994.
- [18] G.M. Sheldrick, SADABS, Program for Empirical Absorption Correction of Area Detector Data, in, University of Gottingen, Gottingen, 1996.
- [19] C.-P. Li, M. Du, *Chemical communications* (Cambridge, England), 47 (2011) 5958-5972.
- [20] F.A. Almeida Paz, J. Klinowski, M.F.S. Vilela, J.P.C. Tomé, J.A.S. Cavaleiro, J. Rocha, *Chem. Soc. Rev.*, 41 (2012) 1088.
- [21] L.S. James, *Chem. Soc. Rev.*, 32 (2003) 276.
- [22] J. He, Y. Zhang, Q. Pan, J. Yu, H. Ding, R. Xu, *Microporous and Mesoporous Materials*, 90 (2006) 145.
- [23] A.M. Plonka, D. Banerjee, J.B. Parise, *Cryst. Growth Des.*, 12 (2012) 2460.
- [24] V. Stenger, *J. Chem. Eng. Data*, 41 (1996) 1111.
- [25] T. Liu, D. Luo, D. Xu, H. Zeng, Z. Lin, *Dalton Trans*, 42 (2013) 368-371.
- [26] W.L. Jorgensen, D.L. Severance, *J. Am. Chem. Soc.*, 112 (1990) 4768.
- [27] A. Panagiotopoulos, S.P. Perlepes, E.G. Bakalbassis, A. Terzis, C.P. Raptopoulou, *Polyhedron*, 29 (2010) 2465-2472.
- [28] S.K. Dimitriou, S.P. Perlepes, A. Terzis, C.P. Raptopoulou, *Polyhedron*, 29 (2010) 2213-2219.
- [29] E.A. Klop, A.J.M. Duisenberg, *Acta Cryst.*, C39 (1983) 1344.

- [30] A. Datta, N. Karan Kumar, S. Mitra, K.M. Malik Abdul, Z. Naturforsch. B., (2002) 1282.
- [31] G.B. Deacon, P.C. Junk, G.J. Moxey, M. Guino-o, K. Ruhlandt-Senge, Dalton Trans, (2009) 4878-4887.
- [32] Y.C. Chen, K.B. Wang, Y. Wang, Polyhedron, 29 (2010).
- [33] L.B. Cole, E.M. Holt, Inorganica Chimica Acta, 108 (1985).
- [34] F.J. Hollander, D.H. Templeton, Z. A., Acta Cryst., B29 (1973) 1303.
- [35] N.E. Braml, W. Schnick, Z. Anorg. Allg. Chem., (2013) 275.
- [36] A. Babai, A.-V. Mudring, Inorg. Chem., (2006) 3249.
- [37] A.R. Kennedy, J.B. Kirkhouse, L. Whyte, Inorg. Chem., (2006) 2965.
- [38] Y. Shen, J. Han, T. Ruffer, C. Du, Y. Pan, Inorg. Chim. Acta, (2004) 2205.
- [39] S. Jirong, H. Rongzu, K. Bing, L. Fuping, Thermochim. Acta, 331 (1999) 49.
- [40] S.J. Makowski, E. Calta, M. Hoermannsdorfer, W. Schnick, Z. Anorg. Allg. Chem., 638 (2012) 345.
- [41] P.J. Rosado, K. Ruhlandt-Senge, J. Coord. Chem., (2010).
- [42] J.H. Yoon, D. Kim, X. Song, S. Han, J. Shin, S.B. Hong, M.S. Lah, RSC Advances, 2 (2012) 11566.
- [43] J. Muldoon, C.B. Bucur, A.G. Oliver, T. Sugimoto, M. Matsui, H.S. Kim, G.D. Allred, J. Zajicek, Y. Kotani, Energy Environ. Sci., 5 (2012) 5941.
- [44] M. Horacek, I. Císarová, J. Cejka, K. Jindrich, L. Petrusová, K. Mach, J. Org. Chem., 577 (1999) 103.
- [45] M. Westerhausen, M.H. Digeser, C. Guckel, H. Noth, J. Knizek, W. Ponikwar, Organometallics, 18 (1999) 2491.

- [46] Y. Liu, Y. Zhao, X.-J. Yang, S.L. Li, J. Gao, P. Yang, Y. Xia, B. Wu, *Organometallics*, 30 (2011) 1599-1606.
- [47] S.P. Sarish, H.W. Roesky, M. John, A. Ringe, J. Magull, *Chem. Commun.*, (2009) 2390-2392.
- [48] W. Liao, R. Dronskowski, *Z. Anorg. Allg. Chem.*, 631 (2005) 1953-1956.
- [49] F. Gschwind, M. Jansen, *Acta Cryst.*, 68 (2012) m1319.
- [50] D. Fenske, G. Baum, *Z. Anorg. Allg. Chem.*, 619 (1993) 489.
- [51] E.B. Brackett, T.E. Brackett, R.L. Sass, *J. Phys. Chem.*, 67 (1963) 2132.
- [52] B. Masci, P. Thury, *CrystEngComm*, 9 (2007) 582.
- [53] S. Hazra, S. Sasmal, M. Nayak, H.A. Sparkes, J.A.K. Howard, S. Mohanta, *CrystEngComm*, 12 (2010) 470.
- [54] F. Gschwind, K.M. Fromm, *Z. Anorg. Allg. Chem.*, 637 (2011) 1871-1879.
- [55] R.D. Shannon, *Acta Cryst.*, A32 (1976) 751.
- [56] P.J. Rosado, K. Ruhlandt-Senge, *J. Coord. Chem.*, 64 (2011) 186-193.
- [57] C.A. Williams, A.J. Blake, C. Wilson, P. Hubberstey, M. Schroeder, *Crystal Growth Design*, 8 (2008) 911-922.
- [58] E.H.L. Falcao, R.K.F. Naraso, G. Wu, F. Wudl, A.K. Cheetham, *Inorg. Chem.*, 47 (2008) 8336.
- [59] D. Banerjee, J.B. Parise, *Cryst. Growth Des.*, 11 (2011) 4704-4720.
- [60] A.M. Plonka, D. Banerjee, J.B. Parise, *Cryst. Growth Des.*, 12 (2012) 2460-2467.

## CHAPTER 6

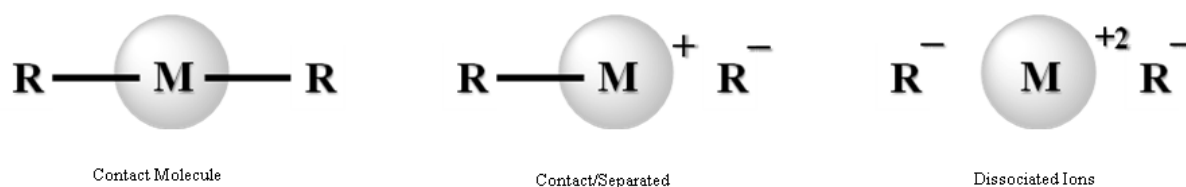
## The coordination chemistry of crown ether stabilized heavy alkaline earth metal tosylates

## 6.0 Introduction

The exploration of the coordination chemistry and ion association of heavy alkaline earth metal complexes remains an important field of study due to the close correlation of structure and function.<sup>[1-3]</sup> Heavy alkaline earth metals play critical roles in important materials, including ferroelectrics and high temperature superconductors, among others.<sup>[4]</sup> Extensive studies of potential precursor materials demonstrate the close correlation between structure and function, with special emphasis on aggregation and ion association.<sup>[5, 6]</sup> For the alkaline earth metals, this is an intriguing topic, because the divalent metals adopt three different ion association modes: a) contact molecules; b) dissociated ions, and c) an intermediate mode with one anion bound to the metal, whereas the other is unassociated, as illustrated in Figure 6.1. Separated ions are typically observed as donor assisted ion pairs (DAIP)<sup>[7, 8]</sup>; several compounds with one metal-bound ligand and the other unassociated have recently been reported.<sup>[9, 10]</sup> Factors responsible for the coordination chemistry and ion association include a) metal diameter; b) ligand or co-ligand steric demand; c) metal-ligand bond strength; d) ability of the ligand to distribute charge; e) hapticity of the co-ligand, and f) the presence of weak, non-covalent interactions.<sup>[3, 7, 8, 11, 12]</sup>

For the heavy congeners of group II a significant tendency towards aggregation is noticed; the presence of co-ligands, or a sterically demanding ligand, may suppress this tendency.<sup>[5, 11, 13-15]</sup> The role of secondary non-covalent interactions such as M—C- $\pi$ , M—H-C agostic and M—F interactions on the coordination chemistry of the heavy alkaline earth metals has been explored

in recent studies.<sup>[16]</sup> Frequently, M—C- $\pi$  and agostic interactions are observed simultaneously with metal-ligand and co-ligand coordination, making the prediction of structural features challenging yet exciting.



Our choice of the tosylate ligand stems from an earlier report by Lappert *et al.* dealing with the potential of tosylates as inexpensive starting materials to prepare heavy alkaline earth metal amides by salt metathesis. With this in mind, the anhydrous tosylates would provide an economical alternative to the expensive metal iodides.<sup>[17]</sup> While there is no structural information on the anhydrous tosylates, their very limited solubility suggests a highly aggregated structure, posing significant synthetic limitations. For example, in the transition metals (M = Mn, Fe, Co, Ni, Zn), hydrated tosylates occur in the form of extensive aggregated networks held together by hydrogen bonds and  $\pi$ -stacking interactions. Furthermore, in the presence of crown-ethers, the hydrated transition metal species (M = Mn, Co, Zn) display isomorphous DAIP's, propagated *via* extensive hydrogen-bonded networks involving metal bound water molecules and non-metal-bound tosylate ligands.<sup>[18]</sup>

For the transition metals (M = Mn, Fe, Co, Ni, Zn), hydrated tosylates occur in the form of extensive aggregated networks held together by hydrogen bonds and  $\pi$ -stacking interactions. In the presence of crown-ethers, the hydrated transition metal species (M = Mn, Co, Zn) display



isomorphous DAIP's, propagated *via* extensive hydrogen-bonded networks involving metal bound water molecules and non-metal-bound tosylate ligands.<sup>[18]</sup>

Secondly, no known heavier alkaline earth metal tosylate compounds are known, but water also played a major role in the coordination chemistry of magnesium and calcium tosylates. For magnesium, water coordination yields a DAIP with six water co-ligands saturating magnesium's coordination sphere according to the formula  $\{[\text{Mg}(\text{OH}_2)_6][\text{OTs}]_2\}_\infty$ . In contrast, the calcium congener, as rationalized by the larger metal diameter, displays a contact molecule of the form  $[\text{Ca}(\text{OTs})_2(\text{OH}_2)_4]_\infty$ .<sup>[18]</sup> Again, the water molecules in both compounds are engaged in hydrogen-bonding, yielding an extended structure consisting of a 3D hydrogen-bonded network. Thus, this work was designed to analyze the structural impact of crown ether on the coordination chemistry, as well as the tendency towards aggregation in the heavy alkaline earth metal tosylates.

This chapter examines the coordination chemistry of crown ether coordinated calcium, strontium and barium tosylates in the presence of water and 18-crown-6 to yield  $\{[\text{Ca}(\text{OH}_2)_2(18\text{-crown-6})(\text{OTs})_3]_3[\text{OTs}]_3 \cdot 3\text{H}_2\text{O}\}_\infty$ , **9**,  $\{[\text{Ca}(\text{OH}_2)_2(18\text{-crown-6})]_2[\text{OTs}]_4\}_\infty$ , **10**,  $[\text{Sr}(\text{OH}_2)(18\text{-crown-6})(\text{OTs})_2]_\infty$ , **11**, and  $[\text{Ba}(\text{OH}_2)_2(18\text{-crown-6})(\text{OTs})_2]_\infty$ , **12**. The elucidated ion association modes and aggregation patterns provide an overview of the coordination chemistry of this class of compounds.

## 6.1 Experimental

### 6.1.1 General and Physical Measurements

All chemicals were obtained commercially and used as received (purity of  $\text{MCO}_3$  (M = Ca, Sr, Ba) – 98%, *p*-toluenesulfonic acid – 98%). IR measurements were carried out as KBr films using a Nicolet IR200 FT-IR spectrophotometer between  $4000\text{ cm}^{-1}$  to  $400\text{ cm}^{-1}$ . TGA measurements were performed on a TGA Q500 series instrument (TA Instruments-Waters LLC) under an  $\text{N}_2$  balance/sample purge flow of 40 mL/min and 60 mL/min, respectively. The samples (wt. 6-20 mg) were loaded onto a platinum pan and heated, using a ramp method from room temperature to  $750\text{ }^\circ\text{C}$  (ramp rate:  $10^\circ\text{C}/\text{min}$ ). Melting point determinations (uncalibrated) were made using capillary tubes in a Mel-Temp II melting point apparatus.

All single crystal X-ray data were collected on a Bruker Kappa diffractometer equipped with an APEX 2 CCD detector and  $\text{MoK}\alpha$  radiation ( $0.7107\text{ \AA}$ ). Crystals were cooled using a Cryocool LN-3 low temperature device (Cryoindustries of America, Inc.) The crystals were submerged in highly viscous hydrocarbon oil (Infineum), mounted on a MITEGEN® mount and placed in the low temperature stream on the diffractometer, similar to the methods described previously.<sup>[19]</sup> Data collection parameters and refinement details have previously been described.<sup>[19]</sup> The crystal structures were elucidated using direct methods, followed by subsequent refinement by the full-matrix least-squares method on  $F^2$ .<sup>[20]</sup> All non-hydrogen atoms were refined anisotropically. Absorption corrections were performed using SADABS.<sup>[21]</sup> Hydrogen atoms, except those on water molecules, were placed on fixed positions. Water hydrogen atoms were located in the difference map and refined freely. For compound **9**, the non-centrosymmetrical space group Pc was verified (PLATON<sup>[22]</sup>) by confirming the absence of a  $2_1$  screw axis. Crystallographic data

can be obtained from the Cambridge Crystallographical Database under CCDC 940503, **9**; 940504, **10**; 940505, **11** and 940506, **12**. To verify bulk purity of **9** - **12**, powder XRD experiments were performed on a Bruker Kappa diffractometer equipped with an APEX 2 CCD detector, and Cu radiation (1.57 Å) at 85 K using a range of  $2\theta$ : 0-70° with a 0.02 sec/step (180 second collection) increase. The overlay of the calculated powder patterns obtained from the single crystal experiments with the experimental powder data from the bulk samples verified the purity of **9-12**. Compounds **9**, **11** and **12** display phase purity whereas for **10**, phase purity could not be achieved in multiple trials.

Anhydrous tosylates were used to prepare the target compounds because their well-defined nature permitted better control of reaction stoichiometry; as the corresponding hydrates do not crystallize readily as a well-defined product, but rather yield multiple hydrate phases. It is therefore preferable to remove the water of crystallization by gentle heating under vacuum to obtain the well-defined, anhydrous product, using a literature procedure.<sup>[17]</sup> Scheme 6.1 provides an overview of conditions needed to obtain the anhydrous starting materials.

### 6.1.2 General Syntheses

#### **$\{[\text{Ca}(\text{OH}_2)_2(\text{18-crown-6})(\text{OTs})_3]_3[\text{OTs}]_3 \cdot 3\text{H}_2\text{O}\}_\infty$ , 9:**

0.38 g (1 mmol)  $\text{Ca}(\text{OTs})_2$  was mixed with 0.26 g (1 mmol) 18-crown-6 in 5 mL of distilled  $\text{H}_2\text{O}$ . The reaction mixture was stirred for fifteen minutes, after which it was filtered using a Whatman No. 5 filter. The solution was left to evaporate for fourteen days, yielding colorless blocks suitable for single crystal X-ray crystallography. The product was sparingly soluble in pyridine and water. Mp: Turns brown at  $> 260^\circ\text{C}$ , dark brown at  $> 290^\circ\text{C}$  and black at  $305^\circ\text{C}$ . Yield (non-optimized): 78% (0.56 g). IR ( $\text{cm}^{-1}$ ): 3448 (br, w); 2926 (s); 1250 (m); 1195 (m); 1011 (w); 824 (m); 684 (s); 568 (s).

#### **$\{[\text{Ca}(\text{OH}_2)_2(\text{18-crown-6})]_2[\text{OTs}]_4\}_\infty$ , 10:**

0.38 g (1 mmol)  $\text{Ca}(\text{OTs})_2$  was mixed with 0.53 g (2 mmol) 18-crown-6 in 5 mL of distilled  $\text{H}_2\text{O}$ . The reaction mixture was stirred for fifteen minutes after which it was filtered using a Whatman No. 5 filter. The solution was left to evaporate for fifteen days during which crystal formation was observed. The product was sparingly soluble in pyridine and water. Mp: Turns brown at  $> 255^\circ\text{C}$ , dark brown at  $> 290^\circ\text{C}$ , and black at  $305^\circ\text{C}$ . Yield (non-optimized): 58% (0.40 g). IR ( $\text{cm}^{-1}$ ): 3460 (br, s); 2890 (s); 1637 (m); 1475 (m); 1203 (m); 1107 (m); 1011 (w).

#### **$[\text{Sr}(\text{OH}_2)(\text{18-crown-6})(\text{OTs})_2]_\infty$ , 11:**

0.43 g (1 mmol)  $\text{Sr}(\text{OTs})_2$  was mixed with 0.26 g (1 mmol) 18-crown-6 in 5 mL of distilled  $\text{H}_2\text{O}$ . The reaction mixture was stirred for fifteen minutes after which it was filtered using a Whatman No. 5 filter. Evaporation for five days yielded colorless crystals. The product was sparingly soluble in pyridine and water. Mp: Turns brown at  $> 255^\circ\text{C}$ , dark brown at  $> 310^\circ\text{C}$ , and black at

350°C. Yield (non-optimized): 86% (0.61 g). IR (cm<sup>-1</sup>): 3473 (br, s); 2920 (s); 1475 (s); 1016 (s); 684 (s); 565 (s).

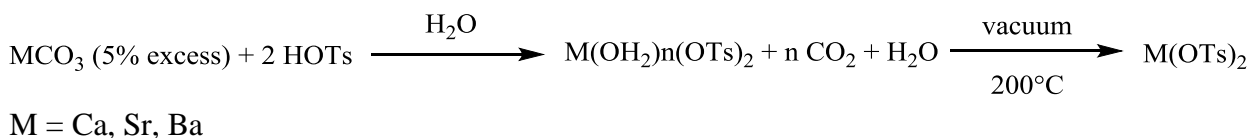
**[Ba(OH<sub>2</sub>)<sub>2</sub>(18-crown-6)(OTs)<sub>2</sub>]<sub>∞</sub>, 12:**

0.48 g (1 mmol) Ba(OTs)<sub>2</sub> was mixed with 0.26 g (1 mmol) 18-crown-6 in 5mL of distilled H<sub>2</sub>O. The reaction mixture was stirred for fifteen minutes followed by filtration using a Whatman No. 5 filter. Evaporation for eight days yielded colorless crystals. The product was sparingly soluble in pyridine and water. Mp: Brown at 250°C, dark brown at 280°C, and black at 295°C. Yield (non-optimized): 86% (0.67 g). IR (cm<sup>-1</sup>): 3423 (br, s); 2920 (m); 1467 (m); 1011 (s); 813 (w); 566 (s).

## 6.2 Results and Discussion

### 6.2.1 Synthesis Discussion

Hydrated alkaline earth metal tosylates are obtained in water *via* acid/base chemistry, involving the treatment of the commercially available carbonates with the acid in water (Scheme 6.1). The resulting hydrates occur as several phases and do not provide a well-defined, crystalline product. Due to the range of water content in the various phases, no uniform molecular weight can be assigned, preventing stoichiometric control if the species are used as reagents. It is therefore preferable to utilize the readily available anhydrous tosylates.



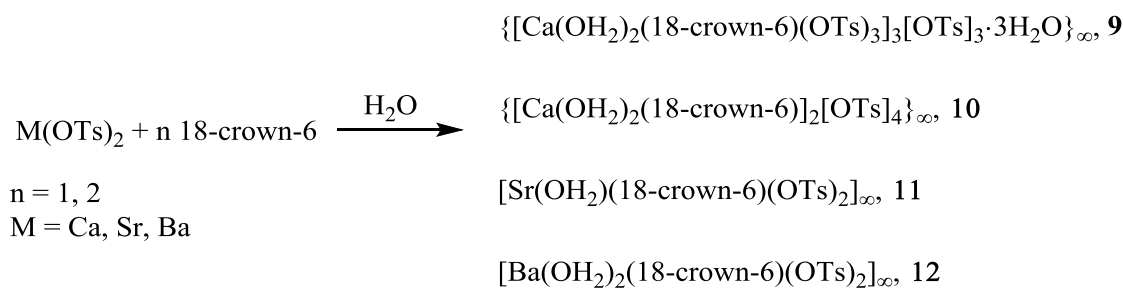
**Scheme 6.1** Preparation of alkaline earth metal tosylates

While water may be removed under mild conditions (see Figure 11), the anhydrous tosylates display very limited solubility. No structural data are available, but solubility data suggest highly aggregated structures. As co-ligand coordination has a profound effect on aggregation in this work we examined the impact of 18-crown-6 coordination on the heavy alkaline earth tosylates.<sup>[23]</sup>

Compounds **9**, **11**, and **12** were obtained using a 1:1 metal:crown ratio. Compounds **11** and **12** were also obtained if a 1:2 reagent ratio was utilized, whereas a 1:2 reagent ratio for calcium yields compound **10** (Table 6.1, Scheme 6.2). This suggests a delicate balance between structure determining factors such as ligand and co-ligand coordination in the formulation of the final products.

**Table 6.1** Metal:crown (M:C) ratio and its resulting compounds

Metal	M : C Ratio	Result
Ca	1:1	<b>9</b>
Ca	1:2	<b>10</b>
Sr	1:1	<b>11</b>
Sr	1:2	<b>11</b>
Ba	1:1	<b>12</b>
Ba	1:2	<b>12</b>



**Scheme 6.2** Synthesis of **9-12**

## 6.2.2 Structural characterization of 9-12

Compounds **9-12** were characterized by single crystal X-ray diffraction. Suitable, well-shaped crystals were obtained as described in the experimental section. All compounds display extended structures, (**9** as two-dimensional, hydrogen bonded sheets, **10 - 12** one-dimensional chains) obtained through hydrogen bonding interactions. Relevant crystallographic details are summarized in Table 6.2.

**Table 6.2** Crystallographic data and structural refinement for compounds **9-12**.

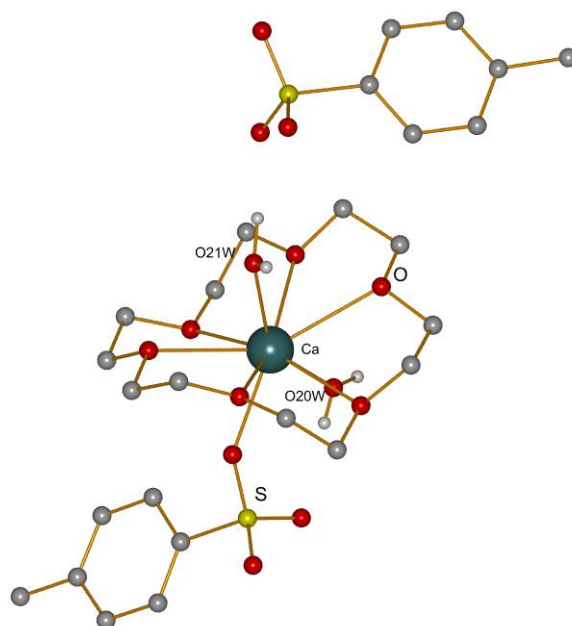
Compound	<b>9</b>	<b>10</b>	<b>11</b>	<b>12</b>
Empirical formula	$C_{78}H_{132}Ca_3S_6O_{45}$	$C_{26}H_{42}CaS_2O_8$	$C_{26}H_{40}SrS_2O_{13}$	$C_{26}H_{42}BaS_2O_{14}$
Formula weight	2102.50	688.80	712.34	780.07
Crystal system	Monoclinic	Orthorhombic	Triclinic	Monoclinic
Space group	Pc	$P2_12_12_1$	P-1	$P2_1/c$
T (K)	86(1)	83(2)	83(2)	83(2)
Unit cell dimensions ( $\text{\AA}$ , $^\circ$ )				
a	8.3932(9)	13.1482(8)	9.0390(18)	13.801(2)
b	44.372(4)	19.4443(13)	11.397(2)	15.090(2)
c	14.6394(13)	24.4742(17)	15.142(3)	14.965(2)
$\alpha, \gamma$	90	90	93.02(3); 92.49(3)	90
$\beta$	118.199(5)		91.87(3)	91.959(2)
Volume ( $\text{\AA}^3$ )	4805.0(8)	6257.0(7)	1555.3(5)	3114.8(7)
Z	2	8	2	4
Calculated density ( $\text{g/cm}^3$ )	1.451	1.462	1.521	1.663
Absorption coefficient ( $\text{mm}^{-1}$ )	0.396	0.401	1.930	1.476
$\theta$ range	3.59 to 25.68 $^\circ$	1.66 to 30.37 $^\circ$	1.35 to 25.00 $^\circ$	0.92 to 28.33 $^\circ$
Unique reflections	15251	18717	5443	7033
Total reflections	29092	55690	11614	26867
Goodness-of-fit on $F^2$	1.008	0.929	1.040	0.975
$R_1, wR_2$ (all data)	$R_1 = 0.1007,$ $wR_2 = 0.1116$	$R_1 = 0.0644, wR_2 = 0.0906$	$R_1 = 0.0285,$ $wR_2 = 0.0667$	$R_1 = 0.0392,$ $wR_2 = 0.0730$
$R_1, wR_2$ (Final)	$R_1 = 0.0606,$ $wR_2 = 0.0988$	$R_1 = 0.0399, wR_2 = 0.0802$	$R_1 = 0.0285,$ $wR_2 = 0.0647$	$R_1 = 0.0316,$ $wR_2 = 0.0708$
F(0 0 0)	2226	2920	740	1592

Compound **9** crystallizes in the non-centrosymmetric monoclinic space group Pc (see above for crystallographic details). Each asymmetric unit contains three independent, nine-coordinate calcium centers with one tosylate ligand and two waters coordinated to the metal (Figure 6.2). Charges are balanced by three non-metal-bound ligands. In addition, there are three lattice waters. The non-coordinate tosylate anion connects *via* hydrogen bonds to the metal-bound water yielding a hydrogen-bonded, 1-dimensional chain network throughout the crystal. Although **9** contains three independent molecules, their overall structural features are quite similar, with a relatively narrow range of Ca-O<sub>(crown)</sub> distances (2.510(4)-2.725(4) Å). There are slight differences in the degree of crown puckering a [ $\langle \text{O}_{(\text{crown})}\text{-M-O}_{(\text{crown})}\text{max} - \langle \text{O}_{(\text{crown})}\text{-M-O}_{(\text{crown})}\text{min} \rangle$ ] of Ca(3) 4.84°Δ > Ca(2) 2.09°Δ > Ca(1) 1.73°Δ] indicating the non-ideal fit for calcium in the crown cavity.<sup>[24-26]</sup> Expressing the multidentate nature of the crown, narrow O<sub>(crown)</sub>-Ca-O<sub>(crown)</sub> angles O<sub>(crown)</sub>-Ca-O<sub>(crown)</sub> ranging from 60.0(1) to 64.8 (1)° are observed. A more extensive compilation of bond lengths and angles is provided in Table 6.3.

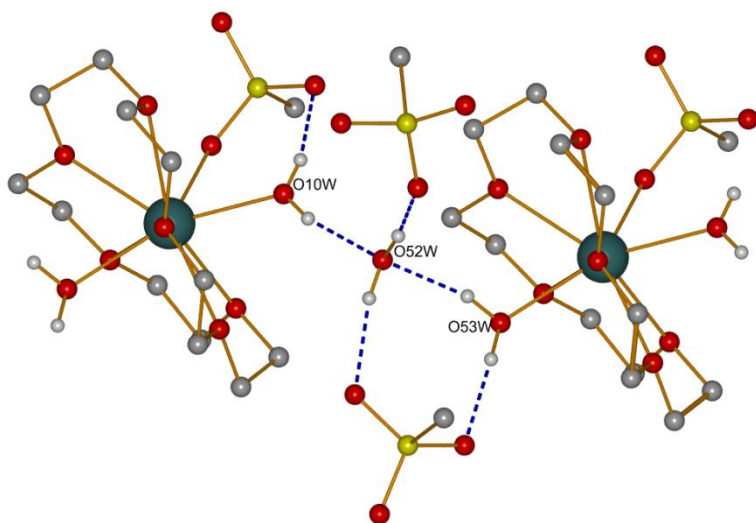
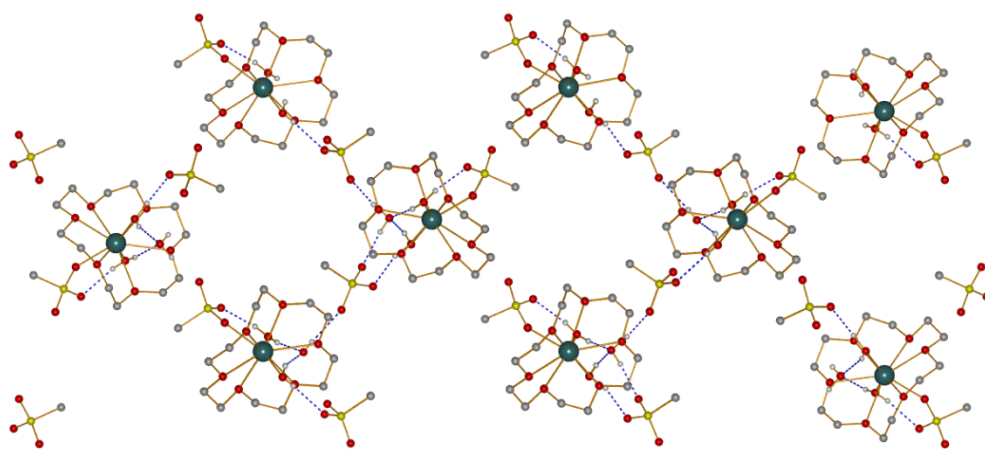
Compound **9** is nine-coordinate, with the crown being located in an approximate equatorial position. One trans position is occupied by one water; the other by one water and a tosylate anion. As a result, the crown is bent away from the doubly occupied trans position. The metal-bound waters play a significant role in the association of the compound *via* hydrogen bonding. The water located on the same face as the tosylate anion (O10w), hydrogen-bonds to the metal-bound anion, resulting in a 6-membered metallacycle (Figure 6.3a). The second hydrogen atom on this water molecule hydrogen-binds to a lattice water (O52w) that in turn is hydrogen-bound to the non-metal bound tosylate. The water of crystallization, (O52w), is also hydrogen bound to the metal-bound water. Donor---acceptor distances [2.755(6)-2.812(6) Å] and angles [161.7-171.8°] lie within expected values for moderate strength hydrogen bonding



interactions.<sup>[27]</sup> Hydrogen bonding also connects the 1D chains into 2D sheets, as shown in Figure 6.3b.



**Figure 6.2** Coordination environments at calcium in **9**. Only one of three independent molecules is shown. Hydrogen atoms except metal-bound water atoms have been omitted for clarity. Intermolecular interactions are also omitted.

**a****b**

**Figure 6.3 (a)** Segment of the hydrogen bonded network in **9**. Lattice water molecules serve as anchoring points connecting the calcium centers and tosylate anions to form 3D hydrogen bonded network. Tollyl groups on the tosylate anions have been removed for clarity, as have been hydrogen atoms on ligands and crown ether; **(b)** Part of the very dense hydrogen-bonded network of chains in the target compound.

**Table 6.3** Selected bond lengths (Å) and angles (°) for **9**

Ca(1)-O(1)cr	2.559(4)	O(1)cr-Ca(1)-O(2)cr	64.26(15)
Ca(1)-O(2)cr	2.534(4)	O(2)cr-Ca(1)-O(3)cr	62.20(15)
Ca(1)-O(3)cr	2.652(5)	O(3)cr-Ca(1)-O(4)cr	62.53(15)
Ca(1)-O(4)cr	2.626(5)	O(4)cr-Ca(1)-O(5)cr	63.28(14)
Ca(1)-O(5)cr	2.510(4)	O(5)cr-Ca(1)-O(6)cr	63.26(14)
Ca(1)-O(6)cr	2.606(4)	O(6)cr-Ca(1)-O(1)cr	63.02(13)
Ca(1)-O(7)tos	2.393(4)	O(11)cr-Ca(2)-O(12)cr	62.87(13)
Ca(1)-O(53)w	2.425(5)	O(12)cr-Ca(2)-O(13)cr	62.98(14)
Ca(1)-O(10)w	2.370(5)	O(13)cr-Ca(2)-O(14)cr	63.11(14)
Ca(2)-O(11)cr	2.567(5)	O(14)cr-Ca(2)-O(15)cr	61.85(15)
Ca(2)-O(12)cr	2.618(4)	O(15)cr-Ca(2)-O(16)cr	61.13(15)
Ca(2)-O(13)cr	2.542(4)	O(16)cr-Ca(2)-O(11)cr	63.94(14)
Ca(2)-O(14)cr	2.617(4)	O(22)cr-Ca(3)-O(23)cr	62.92(13)
Ca(2)-O(15)cr	2.699(5)	O(23)cr-Ca(3)-O(24)cr	62.70(13)
Ca(2)-O(16)cr	2.568(5)	O(24)cr-Ca(3)-O(25)cr	60.37(13)
Ca(2)-O(17)w	2.371(4)	O(25)cr-Ca(3)-O(26)cr	59.97(13)
Ca(2)-O(20)w	2.370(5)	O(26)cr-Ca(3)-O(27)cr	64.81(13)
Ca(2)-O(21)tos	2.398(6)	O(27)cr-Ca(3)-O(22)cr	62.21(12)
Ca(3)-O(22)cr	2.606(4)		
Ca(3)-O(23)cr	2.523(4)		
Ca(3)-O(24)cr	2.584(4)		
Ca(3)-O(25)cr	2.725(4)		
Ca(3)-O(26)cr	2.601(4)		
Ca(3)-O(27)cr	2.544(4)		
Ca(3)-O(31)w	2.351(5)		
Ca(3)-O(32)w	2.388(4)		
Ca(3)-O(28)tos	2.404(4)		

cr = crown, tos = tosylate, w = water

Compound **10** crystallizes as 1D strands in a donor-assisted ion pair (DAIP) in the orthorhombic space group  $P2_12_12_1$ . Each asymmetric unit contains two independent, but quite similar, eight-coordinate calcium centers, with charges balanced by two non-metal bound tosylates. As shown in Figure 6.4, the calcium centers are sequestered by 18-crown-6 molecules located in approximate equatorial positions, and two water molecules in axial positions. The Ca- $O_{(\text{crown})}$  distances for the two independent metal centers lie between 2.316(2) and 2.528(2) Å, whereas the Ca-OH<sub>2</sub> distances are 2.31(2) and 2.35(2) Å.  $O_{(\text{crown})}$ -Ca- $O_{(\text{crown})}$  angles are observed between 62.95(6) and 66.01(6)°. Bond lengths and angles are summarized in Table 6.4. Ca- $O_{(\text{crown})}$  bond lengths in **10** are significantly shorter than in **9** (Ca- $O_{(\text{crown})}$ : 2.510(4)-2.725(4)Å), an effect attributed to the increased cationic charge and the smaller coordination number (8 in **10** vs. 9 in **9**).

Similar to **9**, hydrogen bonding is responsible for the propagation of the structure as a chain, as shown in Figure 6.5. The metal-bound waters are hydrogen-bound to the tosylate anions, which serve as bridging points to yield 1D chains, quite similar to the extended structure of  $\{[\text{Mn}(\text{H}_2\text{O})_2(15\text{-crown-5})[\text{OTs}]]_\infty\}$ , in which 1D polymer strands are formed through a DAIP consisting of  $[\text{Mn}(\text{H}_2\text{O})_2(15\text{-crown-5})]^{2+}$  units, hydrogen bound to  $[\text{OTs}]^-$  ligands.<sup>[28]</sup>

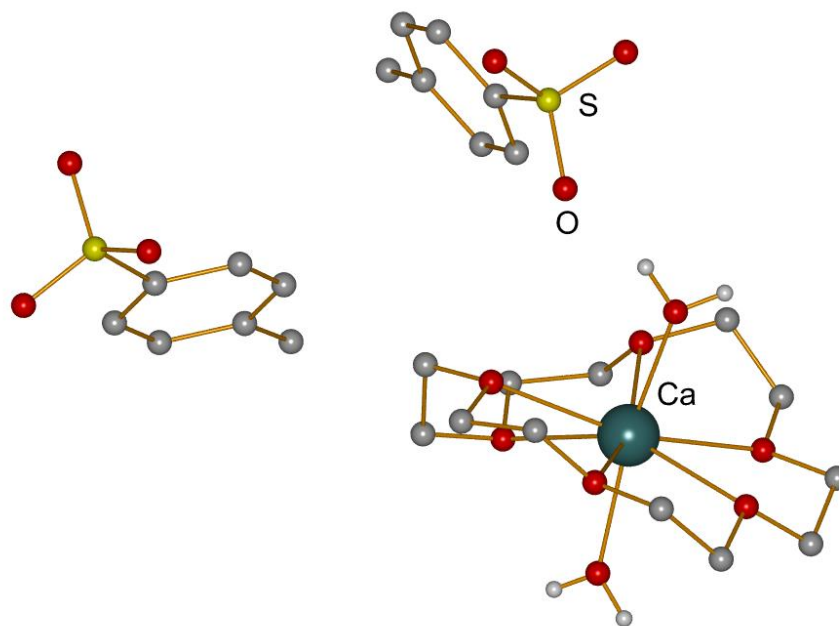


**Figure 6.4** Coordination environment at the calcium centers in compound **10**. As both calcium centers have rather similar coordination environments, only one example is shown. Hydrogen atoms, except those on the metal bound water donors have been omitted for clarity. No intermolecular contacts are shown.

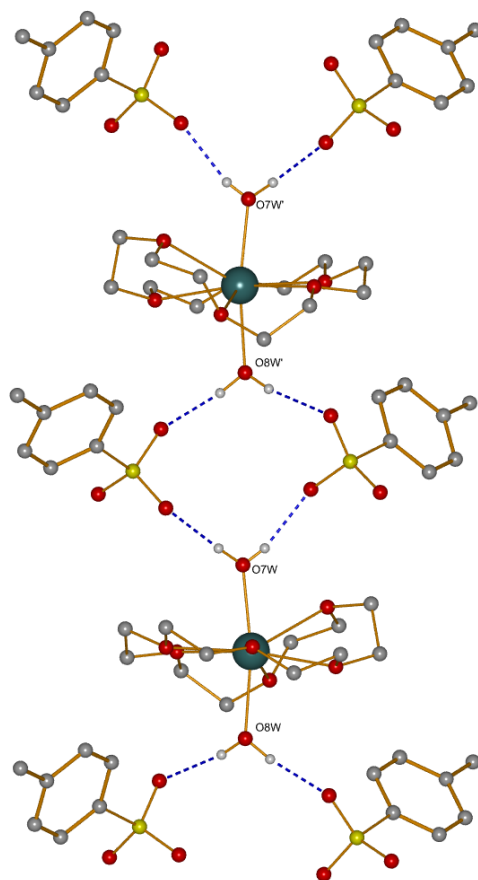


**Figure 6.5** Extended hydrogen bonded network of **10**. All non-water bound hydrogen atoms have removed for clarity.

**Table 6.4** Selected bond lengths (Å) and angles (°) for **10**

Ca(1)-O(1)cr	2.48(2)	O(1)cr-Ca(1)-O(2)cr	65.49(6)
Ca(1)-O(2)cr	2.52(2)	O(2)cr-Ca(1)-O(3)cr	62.95(6)
Ca(1)-O(3)cr	2.65(2)	O(3)cr-Ca(1)-O(4)cr	64.90(6)
Ca(1)-O(4)cr	2.51(2)	O(4)cr-Ca(1)-O(5)cr	65.84(6)
Ca(1)-O(5)cr	2.49(2)	O(5)cr-Ca(1)-O(6)cr	64.34(6)
Ca(1)-O(6)cr	2.53(2)	O(6)cr-Ca(1)-O(1)cr	64.07(6)
Ca(1)-O(7)w	2.31(2)		
Ca(1)-O(8)w	2.35(2)		

Compound **11** crystallizes as a contact molecule in the form of 1D chains in the triclinic space group P-1. Again, water coordination is responsible for the formation of an extended structure. The strontium center is nine-coordinate, comprised of the crown ether in an approximate equatorial position. The two axial positions are occupied by the tosylate anions, although one position carries an additional water molecule (Figure 6.6). As a result, the crown is bent away from the face occupied by the ligand and water. In addition, the metal is located slightly above the face of the crown (0.371 Å) bearing the ligand and water. Sr-O<sub>(tos)</sub> distances are 2.471(2) and 2.514(2) Å, slightly shorter than the Sr-O<sub>(crown)</sub> (2.471(2) to 2.782(2)) and the Sr-OH<sub>2</sub> (2.576(2) Å distance. The increase in values as compared to **9** and **10** correlates with the increase in metal radius (Sr/Ca 0.13Å).<sup>[29]</sup> In accord with literature data, O<sub>(crown)</sub>-Sr-O<sub>(crown)</sub> angles range from 59.08(5) to 61.45(5)° in a slightly puckered crown ether geometry (deviation from planarity 2.37°).<sup>[31]</sup> Table 6.5 summarizes selected bond lengths and angles for **11**.

Again, hydrogen bonding is responsible for the extension of the structure. By analogy to **10**, the metal-bound water and the tosylate form a 6-membered metallacycle. The second hydrogen atom on the metal bound water is responsible for the propagation of the structure as 1D columns, as shown in Figure 6.7. These bond distances and angles correlate with literature values for moderate strength hydrogen bond interactions.<sup>[27]</sup>

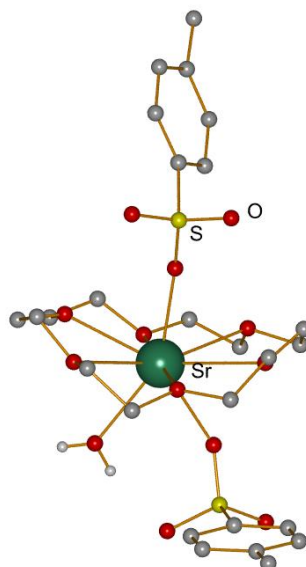


**Figure 6.6** Graphic representation of the nine-coordinate strontium center. Hydrogen atoms on crown ether and tosylate ligands have been removed for clarity.

**Table 6.5** Selected bond lengths (Å) and angles (°) for **11**

Sr(1)-O(1)cr	2.780(2)	O(1)cr-Sr(1)-O(2)cr	59.77(4)
Sr(1)-O(2)cr	2.624(2)	O(2)cr-Sr(1)-O(3)cr	59.08(5)
Sr(1)-O(3)cr	2.766(2)	O(3)cr-Sr(1)-O(4)cr	60.85(4)
Sr(1)-O(4)cr	2.782(2)	O(4)cr-Sr(1)-O(5)cr	59.46(4)
Sr(1)-O(5)cr	2.732(2)	O(5)cr-Sr(1)-O(6)cr	61.95(4)
Sr(1)-O(6)cr	2.695(2)	O(6)cr-Sr(1)-O(1)cr	60.42(4)
Sr(1)-O(7)tos	2.514(2)		
Sr(1)-O(8)tos	2.471(2)		
Sr(1)-O(9)w	2.576(2)		



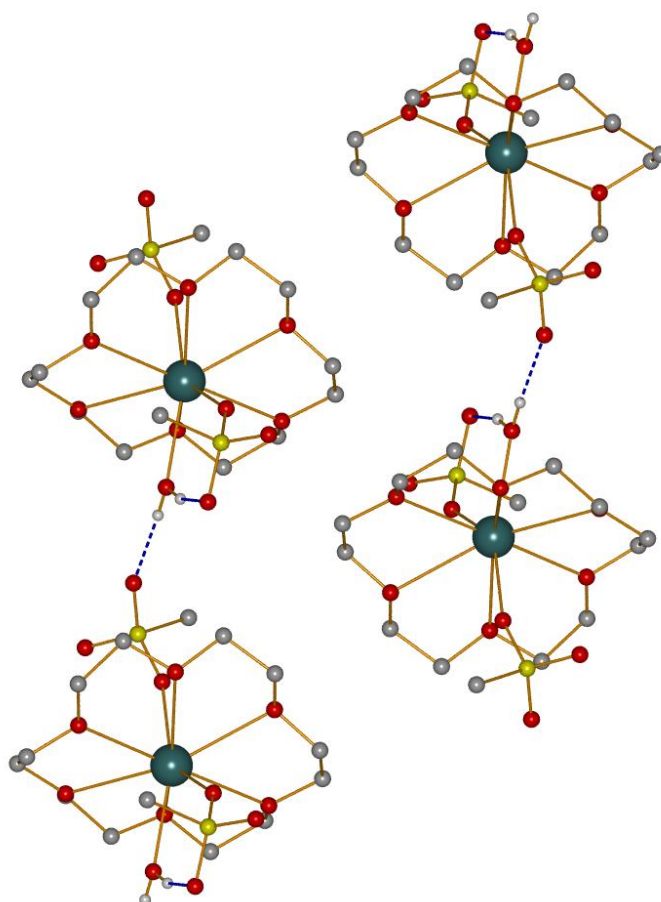


**Figure 6.7** Hydrogen bonded network in **11**. Tollyl groups on the tosylate ligands and all non-water bound hydrogen atoms have been removed for clarity. Shown are two strands.

Compound **12** displays a 10-coordinate metal center. Table 6.6 summarizes selected bond lengths and angles for **12**. The molecular units in **12** aggregate into 1D chains *via* hydrogen bonding. The metal environment is comprised of crown ether coordination in addition to two ligands and one water co-ligand. The crown ether is located in an approximate equatorial position. One trans position holds two tosylate anions and a water coligand; the other is occupied by one water. Metal-ligand distances are 2.749(2) and 2.850(2) Å; barium-water distances are of

similar lengths (2.786(3), 2.818(2) Å), whereas the barium- $O_{(\text{crown})}$  interactions are slightly longer (2.865(2)-2.920(2) Å). These values are in accord with the increased metal diameter (Ca/Ba:  $0.35\Delta\text{Å}$  ; Sr/Ba:  $0.16\Delta\text{Å}$ ).<sup>[29]</sup>

In accord with the different degree of crowding in the trans positions, the crown is bent away from the face holding the ligands and the water. Furthermore, the metal is located above the plane of the crown oxygen atoms by 0.825 Å towards the more crowded face (Figure 6.8). Because of the crown's displacement from the metal center, a slight compression is observed, as expressed by narrower  $O_{(\text{crown})}\text{-M-}O_{(\text{crown})}$  angles [ $57.22(6)$ - $58.60(6)^\circ$ ]. In accord with the increased metal radius, the crown conformation is flatter than in **9-11**, with a deviation from planarity of only  $1.38^\circ\Delta$ , resulting from the tighter barium:crown fit. The different degrees of puckering in calcium, strontium and barium 18-crown-6 compounds have been discussed previously.<sup>[12]</sup>

The two tosylate ligands are engaged with each other in a weak, slightly displaced  $\pi\text{---}\pi$  stacking interaction with a centroid-centroid distance of 3.66 Å, a value in agreement with literature data.<sup>[30-32]</sup>  $\pi\text{---}\pi$  stacking interactions were also observed in the previously studied alkaline earth/transition metal tosylates, in which herringbone (e.g.  $[\text{NH}_4(\text{OTs})]_\infty$ ) and face-to-face and edge-to-face interactions (e.g.  $[\text{Ca}(\text{OTs})_2(\text{H}_2\text{O})_4]_\infty$ ) were reported by Fewings *et al.*<sup>[18]</sup>. In these the stacking interactions are responsible for the extension of the network. In the case of **12**, the extension of the network is not achieved by  $\pi\text{---}\pi$  stacking, but rather by hydrogen bonding interactions (Figure 6.9).<sup>[28]</sup> As in **9 - 11**, propagation through hydrogen bonding between the metal-bound water and the tosylate anions results in the formation of a columnar structure.

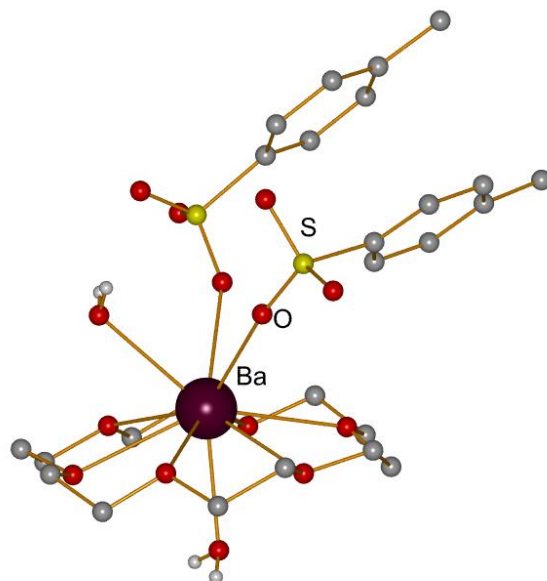


**Figure 6.8:** The coordination environment on the 10-coordinate barium in compound **12**.

Hydrogen atoms on the crown ether and ligands have been removed for clarity.

**Table 6.6** Selected bond lengths (Å) and angles (°) for **12**

Ba(1)-O(3)tos	2.850(2)	O(7)cr-Ba(1)-O(8)cr	57.29(6)
Ba(1)-O(6)tos	2.749(2)	O(8)cr-Ba(1)-O(9)cr	57.60(6)
Ba(1)-O(7)cr	2.887(2)	O(9)cr-Ba(1)-O(10)cr	58.60(6)
Ba(1)-O(8)cr	2.920(2)	O(10)cr-Ba(1)-O(11)cr	57.50(6)
Ba(1)-O(9)cr	2.854(2)	O(11)cr-Ba(1)-O(12)cr	57.44(6)
Ba(1)-O(10)cr	2.865(2)	O(12)cr-Ba(1)-O(7)cr	57.22(6)
Ba(1)-O(11)cr	2.912(2)		
Ba(1)-O(12)cr	2.911(2)		
Ba(1)-O(13)w	2.818(2)		
Ba(1)-O(14)w	2.786(3)		

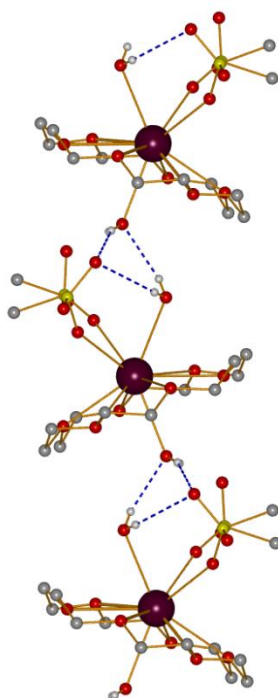


**Figure 6.9** The hydrogen bonded network in **12**. The phenyl groups on the tosylate ligands and hydrogen atoms on crown ether have been removed for clarity.

Compounds **9** - **12** provide a systematic study of the influence of metal diameter on the coordination chemistry of heavy alkaline earth metal crown ether species. The observed trends are dictated by the drive towards steric saturation, as achieved by a combination of ligand and co-ligand coordination. For the smaller calcium ion, DAIP's are observed; for the heavier metals contact molecules are preferred in order to achieve steric saturation for the large heavy alkaline earth metal centers. Demonstrating the challenge to predict structural features, the calcium compounds **9** and **10** adopt different degrees of ion association, depending on reagent stoichiometry. For strontium and barium, compounds **11** and **12** are observed regardless of metal:crown stoichiometry. Water coordination plays a major role, as it not only serves a significant role in achieving steric saturation, but also contributes towards aggregation in either 1-dimensional chain (**10-12**) or 2-dimensional sheet (**9**) arrangements. The hydrogen-bonding in **9-12** follows literature trends with D--H---A (donor-hydrogen---acceptor) distances and angles which correspond to moderate hydrogen bonds ( $\angle(DHA)$ :  $<130^\circ$  and  $d(D-H---A)$  between 2.5-3.2 Å).<sup>[27]</sup>

### 6.2.3 Hydrogen bonding in 9-12

Hydrogen bonding in **9** extends from the metal bound waters, and the waters of crystallization and the tosylate ligands. The interactions display typical geometries with almost linear O··H··O moieties (See Figure 6.3a). No waters of crystallization are observed in **10-12**. In **10** the major factor in structural propagation is the formation of 1-dimensional strands via hydrogen bonds to unbound tosylate ligands. **11-12** display intermolecular hydrogen bonds that provide assistance in the formation of the 1D chains, as described above.

### 6.3 Thermogravimetric analysis

Compounds **9-12** were analyzed by thermogravimetric analysis (TGA) to determine the extent and ease of water loss. Figure 6.10 provides an overview of the TGA analysis, while Table 6.7 provides a summary of pertinent data for **9 - 12**. TGA data for the hydrated species are provided in Figure 6.11 to allow a direct comparison of the impact of the crown ether on the ease of water loss.

**Table 6.7** TGA data for compounds **9-12** and crown-ether-free tosylates

Compound	$\Delta T$	%W <sub>exp</sub>	%W <sub>calc</sub>	nH <sub>2</sub> O
{[Ca(OH <sub>2</sub> ) <sub>2</sub> (18-crown-6)(OTs) <sub>3</sub> ] <sub>3</sub> [OTs] <sub>3</sub> ·3H <sub>2</sub> O} <sub>∞</sub> , <b>9</b>	30-89°C	4.86%	5.13%	9 H <sub>2</sub> O
{[Ca(OH <sub>2</sub> ) <sub>2</sub> (18-crown-6)] <sub>2</sub> [OTs] <sub>4</sub> } <sub>∞</sub> , <b>10</b>	30-156°C	10.1%	10.1%	2 H <sub>2</sub> O
[Sr(OH <sub>2</sub> )(18-crown-6)(OTs) <sub>2</sub> ] <sub>∞</sub> , <b>11</b>	30-130°C	2.38%	2.52%	1 H <sub>2</sub> O
[Ba(OH <sub>2</sub> ) <sub>2</sub> (18-crown-6)(OTs) <sub>2</sub> ] <sub>∞</sub> , <b>12</b>	30-106°C	5.28%	5.22%	2 H <sub>2</sub> O
[Ca(OH <sub>2</sub> ) <sub>4</sub> (OTs) <sub>2</sub> ] <sub>∞</sub> (Fig. 6.11)	30-88°C	16.2%	15.8%	4 H <sub>2</sub> O
[Sr(OH <sub>2</sub> )(OTs) <sub>2</sub> ] <sub>∞</sub> (Fig. 6.11)	30-89°C	4.31%	4.02%	1 H <sub>2</sub> O*
[Ba(OH <sub>2</sub> )(OTs) <sub>2</sub> ] <sub>∞</sub> (Fig. 6.11)	30-487°C	1.31%	3.62%	1 H <sub>2</sub> O*

$\Delta T$ : temperature range; %W<sub>exp</sub>: % experimental weight loss; %W<sub>calc</sub>: % theoretical weight calculated; nH<sub>2</sub>O: formula waters; \*based on approximate relative weights, no structural data available

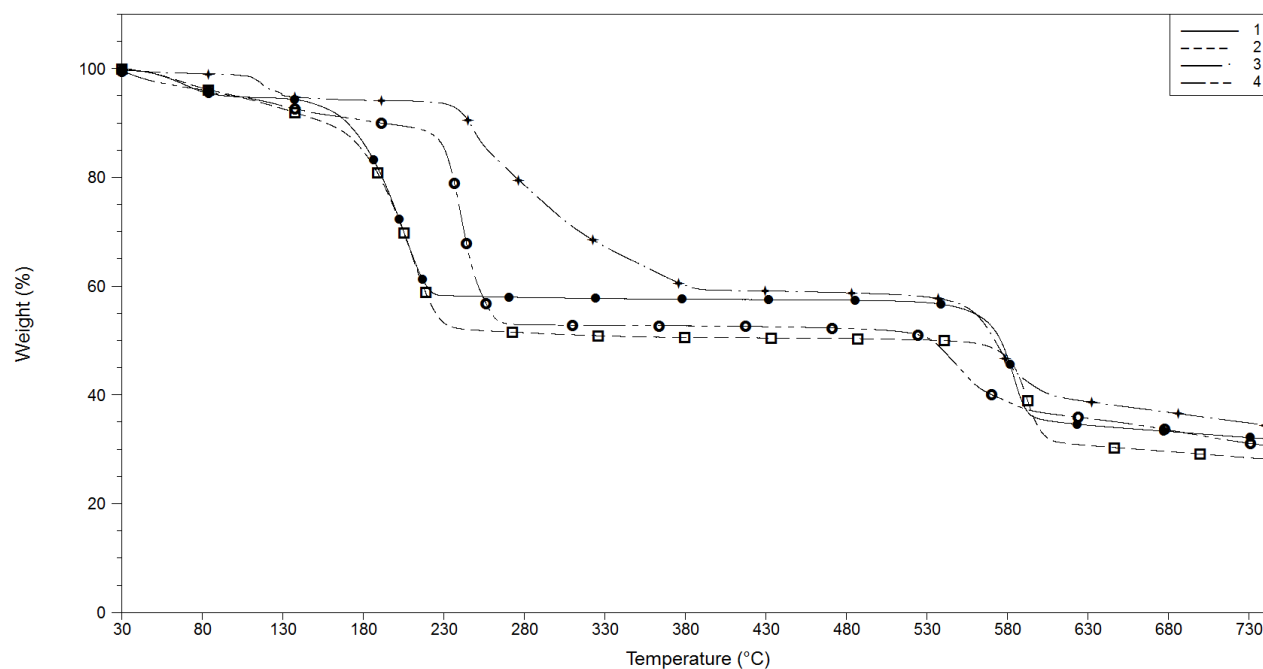


**Figure 6.10** TGA overlay of the crown ether based compounds **9-12** showing water loss

Water loss in **9 - 12** starts at room temperature and is completed under mild conditions, with **10** requiring the highest temperature (156°C) for dehydration. In contrast, dehydration in the partial contact molecule **9** is complete at 89°C, suggesting that the Ca-OH<sub>2</sub> interaction in the DAIP is stronger than those in **10-12**.

TGA analysis shows that crown ether coordination plays a major role in achieving steric saturation, as the crown ligated species **9-12** lose water at much lower temperature than the simple hydrates (Figure 6.11).

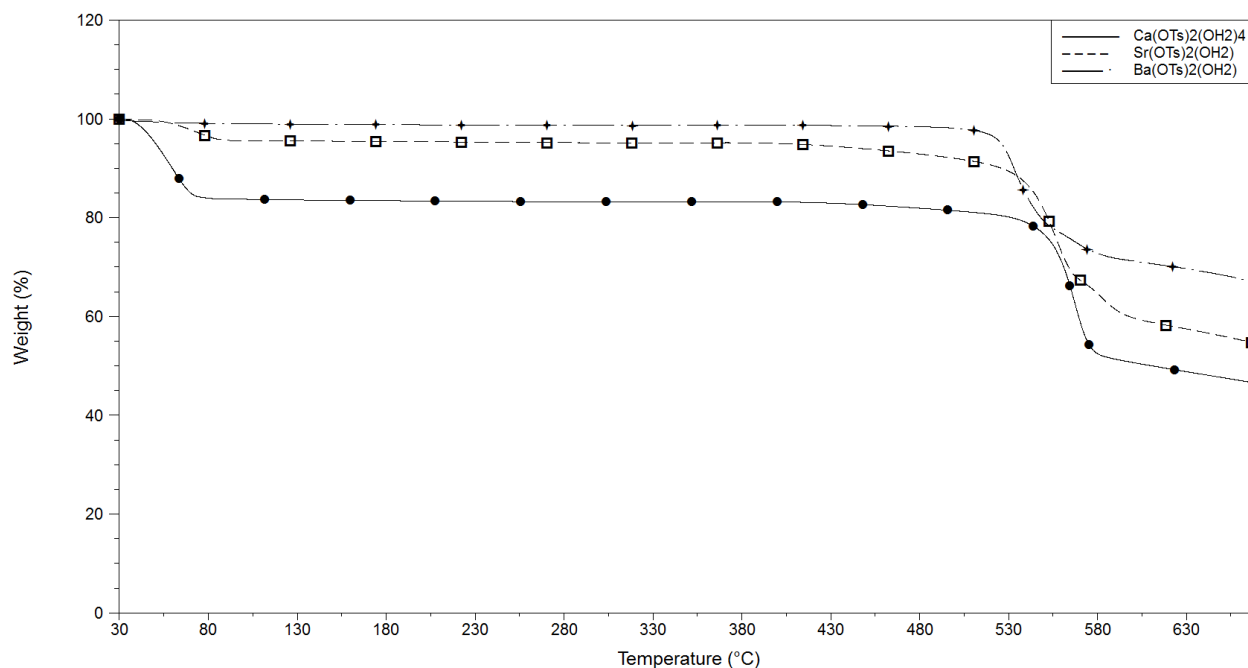


**Figure 6.11** TGA overlay of the tosylate hydrate compounds showing water loss

## 6.4 Conclusions

Four heavy alkaline earth crown ether tosylates were synthesized and characterized. Compounds **9-12** crystallize as hydrogen-bonded networks. Compounds **9 - 12** also demonstrate the delicate interplay between ligation and solvation involving the crown, the ligand and water. These compounds showcase nicely why the prediction of structural features is very challenging. The influence of ion association and crown coordination is also reflected in TGA studies; the dicationic species desolvate at higher temperature than the monocations, a direct correlation with Ca-OH<sub>2</sub> bond strength.



## 6.5 References

- [1] M.F. Zuniga, G.B. Deacon, K. Ruhlandt-Senge, *Inorg. Chem.*, 46 (2007) 10400.
- [2] M.F. Zuniga, G.B. Deacon, K. Ruhlandt-Senge, *Inorg. Chem.*, 47 (2008) 4669.
- [3] A. Verma, M.A. Guino-o, M. Kunnath-Gillet, W. Teng, K. Ruhlandt-Senge, *Z. Anorg. Allg. Chem.*, 635 (2009) 903.
- [4] T. Katase, H. Hiramatsu, T. Kamiya, H. Hosono, *Supercond. Sci. and Technol.*, 25 (2012) 084015.
- [5] W.D. Buchanan, M.A. Guino-o, K. Ruhlandt-Senge, *Inorg. Chem.*, 49 (2010) 7144.
- [6] W.D. Buchanan, D.G. Allis, K. Ruhlandt-Senge, *Chem. Commun.*, 46 (2010) 4449.
- [7] A. Torvisco, M.A. Guino-o, W. Teng, K. Ruhlandt-Senge, *Inorg. Chim. Acta.*, 389 (2012) 122.
- [8] A. Torvisco, A. O'Brien, K. Ruhlandt-Senge, *Coord. Chem. Rev.*, 255 (2011) 1268.
- [9] A. Torvisco, K. Ruhlandt-Senge, *Inorg. Chem.*, 50 (2011) 12223.
- [10] A. Torvisco, K. Ruhlandt-Senge, *Organometallics*, 30 (2011) 986.
- [11] G.B. Deacon, P.C. Junk, G.J. Moxey, M.A. Guino-o, K. Ruhlandt-Senge, *Dalton Trans.*, 25 (2009) 4878.
- [12] M.A. Guino-o, J.S. Alexander, M.L. McKee, H. Hope, U. Englich, K. Ruhlandt-Senge, *Chem. Eur. J.*, 15 (2009) 11842.
- [13] J. Hitzbleck, A. O'Brien, G.B. Deacon, K. Ruhlandt-Senge, *Inorganic Chemistry*, 45 (2006).
- [14] A. Torvisco, D. Katharina, F. Uhlig, K. Ruhlandt-Senge, *Inorg. Chem.*, 48 (2009) 11459.
- [15] W. Teng, M.A. Guino-o, J. Hitzbleck, U. Englich, K. Ruhlandt-Senge, *Inorg. Chem.*, 45 (2006) 9531.
- [16] W.D. Buchanan, E.D. Nagle, K. Ruhlandt-Senge, *Main Group Chemistry*, 8 (2009) 263.
- [17] A.D. Frankland, M.F. Lappert, *Dalton Trans.*, 22 (1996) 4151.

- [18] K.R. Fewings, P.C. Junk, D. Georganopoulou, P.D. Prince, J.W. Steed, *Polyhedron*, 20 (2001) 643.
- [19] S. Chadwick, K. Ruhlandt-Senge, *Chem. Eur. J.*, 4 (1998) 1768.
- [20] G.M. Sheldrick, XShell 6.3.1, Siemens Analytical X-ray Instruments, Madison, Wisconsin: 1994.
- [21] G.M. Sheldrick, SADABS, Program for Empirical Absorption Correction of Area Detector Data, in, University of Gottingen, Gottingen, 1996.
- [22] A.L. Spek, *Acta Cryst.*, D65 (2009) 148-155.
- [23] A. Brooks, Undergraduate Capstone Thesis, Syracuse University, 2012.
- [24] M.A. Guino-o, A. Torvisco, W. Teng, K. Ruhlandt-Senge, *Inorg. Chim. Acta.*, 389 (2012) 122.
- [25] S. Chadwick, U. Englich, B.C. Noll, K. Ruhlandt-Senge, *Inorg. Chem.*, 37 (1998) 4718.
- [26] U. Englich, K. Ruhlandt-Senge, *Z. Anorg. Allg. Chem.*, 627 (2001) 851.
- [27] T. Steiner, *Angew. Chem. Int. Ed.*, (2002) 48-76.
- [28] P.C. Junk, K.R. Fewings, D. Georganopolou, P.D. Prince, J.W. Steed, *Polyhedron*, (2001) 643.
- [29] R.D. Shannon, *Acta Cryst.*, A32 (1976) 751.
- [30] S.Y. Ming, F.Y. Dong, J.M. Dou, L. Da-Cheng, X.K. Gao, D.Q. Wang, *J. Chem. Cryst.*, 36 (2006) 315.
- [31] P.C. Junk, J.W. Steed, *J. Coord. Chem.*, 60 (2007) 1017.
- [32] W.L. Jorgensen, D.L. Severance, *J. Am. Chem. Soc.*, 112 (1990) 4768.

## CHAPTER 7

### Conclusions

The purpose of this work was to design alkaline earth metal coordination complexes that could potentially serve as gas storage and synthetic precursor materials. Alkaline earth coordination chemistry is heavily influenced by factors such as weak metal-ligand bonding, which pose a challenge in obtaining suitable stable compounds. This thesis focused on exploring multiple synthetic avenues towards the isolation of alkaline earth MOFs and crown stabilized alkaline earth tosylates.

Several synthetic routes were employed due to the challenges in the preparation of the target compounds. Mainly, hydro/solvothermal routes provided crystalline material, but other routes such as slow evaporation also provided X-ray quality crystals. Primarily, structural trends arising from varying the synthetic conditions were studied.

The reaction conditions that favored 3-dimensional frameworks were mixtures of polar organic solvents, particularly MeOH/donor mixtures, with ideal crystallization temperatures of 135 °C.

For Mg, three open-framework structures (**1a-c**), which host different solvents (DMF, ACN, THF) in the 1-dimensional rhombohedral channels, were isolated. Variable temperature XRD on these displayed stability at 300 °C, demonstrating retention of overall structural integrity. Initial gas adsorption studies determined that **1a** was non-porous to N<sub>2</sub>, on basis of the low surface area obtained.

A 2-dimensional framework consisting of hydrogen bound sheets was isolated from EtOH (**2**). The extended structure consists of 2-dimensional sheets associated through hydrogen bonding arising from a metal-coordinated terminal water molecule. In addition, a mixture of ACN/H<sub>2</sub>O resulted in the isolation of a zwitterion species, in which the N-donor atom is protonated and the metal center charge stabilized by an unbound nitrate.

The reaction conditions that yielded 3-dimensional frameworks for Mg were applied to the heavier metals, resulting in three 3-dimensional frameworks for Ca, Sr and Ba. For Ca, a 3-dimensional framework based on *m*-pyridinecarboxylic acid was isolated (**5**), in which instead of an open-framework the structure consists of a dense coordination polymer. In the case of (**6**), a hydrogen bonded network resulted from an ACN/MeOH mixture, in which water and acetonitrile coordinate to the metal center.

For the heavier Sr, a 3-dimensional structure (**7**) with *p*-pyridinecarboxylic acid was isolated, the extended structure shows oval-shaped channels which are blocked by pyridyl rings. The barium species consists of a 3-dimensional structure (**8**) in which, peculiarly, the incorporation of chlorine atoms from the BaCl<sub>2</sub> forms Ba-Cl-Ba bridges which contribute to structural propagation.

A closer look at the structures reveals that propagation is highly ligand dependent and that the open-frameworks are favored for the *p*-pyridinecarboxylic acid, as opposed to the *m*-pyridinecarboxylic acid.

Donor studies using the 18-crown-6 macrocycle resulted in the isolation of four novel crown-stabilized alkaline earth tosylate complexes based on Ca, Sr and Ba. Different ion association modes were evidenced as the metal:crown ratio was varied. For **9**, a contact-separated Ca species was isolated when using a 1:1 ratio, whereas **10** crystallizes as a separated species with a 1:2 ratio. **11** and **12** crystallize as contact Sr and Ba species, respectively. Compounds **9** – **12** demonstrate the delicate interplay between ligation and solvation involving the crown, the ligand and water. These compounds showcase nicely why the prediction of structural features is very challenging.

# PETER J. ROSADO

Phone: (315) 460-0330 | Email: pirosado@syr.edu

Address: 126 Jamesville Avenue · Syracuse, NY 13210

---

---

## SUMMARY OF QUALIFICATIONS

---

Detail-oriented, dedicated, and highly educated synthetic inorganic chemist with 6+ years of successful laboratory experience in the synthesis and characterization of organometallic complexes. Currently seeking a chemist position which will effectively utilize all acquired skills, abilities, and areas of expertise as follows:

- ◆ Gas adsorption in porous solids (ASAP 2020)
- ◆ Metal Organic Framework synthesis
- ◆ Thermal analysis (TGA, DTA, DSC)
- ◆ Single Crystal/Powder X-ray Diffraction (Bruker APEX 2 Duo SC, Bruker D8 Series II PXRD, Bruker Apex 2 Suite for crystal structure refinement)
- ◆ Instrument maintenance and calibration
- ◆ Project management
- ◆ Teaching/Instructing
- ◆ Bilingual (Spanish, English)
- ◆ Team Building/Collaboration
- ◆ Grant writing
- ◆ Materials Science
- ◆ Technical report writing
- ◆ Office Suite (Power Point, Excel, Word)
- ◆ Experienced in Computer Aided Design (AutoCAD)
- ◆ Laboratory management
- ◆ Interpretation of analytical data
- ◆ Solid state chemistry
- ◆ Analytical chemistry
- ◆ Biotechnology
- ◆ Anaerobic organic & inorganic Synthesis Techniques (Glove box, inert atmosphere, vacuum line)
- ◆ Expert in crystallizing organic and inorganic compounds
- ◆ Project managing
- ◆ Spectroscopy (UV-Vis, IR, NMR)
- ◆ Basic statistical skills
- ◆ Analysis of structure/function relationships in molecular complexes

## EDUCATION

---

**Syracuse University** | Ph. D. in Chemistry, 3.73 GPA Graduated May 2014

- ◆ Funding opportunities: DOE-SCGF Fellowship - Accepted - \$151K (09/2010 - Present), GEM Graduate Fellowship - Declined - \$14K, GAANN Fellowship - Accepted - \$15K - (01-08/2010)
- ◆ Master of Philosophy in Chemistry, 3.73 GPA (08/2009 – 05/2011)
- ◆ Notable Graduate Courses: Crystallography, Solid State Chemistry, Inorganic Chemistry

**Interamerican University of Puerto Rico** | B.S. in Chemistry, 3.95 GPA (05/2009)

- ◆ Summa Cum Laude, Ex-Alumni Medal, Chancellor's List, ExxonMobil LOFT Fellow

## EXPERIENCE

---

**LeMoyne College**

09/2014 - Present

**LPP/STEP Program Part Time Professional Chemistry Tutor** (09/2014 - Present)

- ◆ Serve as chemistry tutor, mentor and advisor to underrepresented and economically disadvantaged students of the Syracuse School District.

**Syracuse University**

06/2009 – 07/2014

**Research Assistant (06/2009 - Present)**

- ◆ Managed projects on synthesis and characterization of cost-effective reagents for salt metathesis reactions and novel main group 3D Metal Organic Frameworks (MOFs) for gas storage applications in fuel cells.
- ◆ Acquired skills in anaerobic solution and solid state inorganic synthesis (usage of glove box, inert atmospheres and vacuum lines).
- ◆ Strong skills in crystal structure data collection and refinement using the Bruker Suite APEX 2 software family: disorder refinement, twin refinement and phase determination.
- ◆ Designed and optimized synthetic routes towards isolating inorganic complexes through high pressure hydro/solvothermal crystallization techniques.
- ◆ Prepared 22+ novel inorganic compounds, fully characterized them using analytical techniques such as: X-ray diffraction, TGA, FTIR and NMR.
- ◆ Crystallized inorganic molecules, determined crystal defects and designed novel crystallization procedures.
- ◆ Carried out low and high temperature powder X-ray diffraction experiments for structural phase determination of inorganic/organic complexes.
- ◆ Prepared detailed written technical reports to the Chemistry Department and the Department of Energy (ORISE) regarding experimental procedures and results.
- ◆ Participated in conference talks, wrote scientific posters and published results in peer reviewed scientific journals.

**Teaching Assistant – (General Chemistry Recitation) CHEM 116 (01/2014 – 05/2014)**

- ◆ Supervised and taught 3 general chemistry recitation sections (30 students in total) of general chemistry lectures, proctored examinations and offered office hours.

**Teaching Assistant – (Honors Chemistry Laboratory) CHEM 129 (08/2013 – 12/2013)**

- ◆ Supervised and taught 3 sections (30 students in total) of general chemistry lectures, graded pre-laboratories and post-laboratories and assisted in student's experiments.

**Teaching Assistant – (General Chemistry Recitation) CHEM 106 (08/2009 – 12/2009)**

- ◆ Prepared and taught 3 sections (30+ students each) of general chemistry lectures, formulated quizzes, graded homework, and proctored examinations to ensure retention of classroom discussions.

**University of Pennsylvania**

06/2008 – 07/2008

**PREM Program Research Assistant**

- ◆ Conducted research on thermal and spectroscopic analysis of SnO<sub>2</sub> electrospun nanofibers for semi-conductors.
- ◆ Hands on experience with TGA, DTA, DSC techniques for determination of weight loss and thermal properties of SnO<sub>2</sub>/Polymer solutions.
- ◆ Hands on experience analyzing SnO<sub>2</sub>/Polymer solutions via UV/Vis spectroscopy.

**University of Kentucky**

06/2007 – 08/2007

**Research Assistant**

- ◆ Researched the development of glucose-responsive hydrogels based upon the incorporation of a genetically-engineered glucose binding protein dimer (GBPd).
- ◆ Acquired experience in protein purification/expression, autoclave, centrifugation, UV-Vis, and polymer synthesis techniques.
- ◆ Hands on experience with a variety of protein detection techniques including: western blot, northern blot and gel electrophoresis.

**LABORATORY MANAGEMENT**

---

- ◆ 3 years responsible for management of Bruker D8 Series II PXRD instrument in the Chemistry Department's X-ray laboratory: instrument maintenance, training of students and faculty in its usage.
- ◆ Collaborated and performed XRD experiments for faculty and students outside of the Chemistry Department, including phase structure determination of calcites, fluorites and temperature dependent PXRD experiments.
- ◆ Mentored and oversaw 2 undergraduate students in original, challenging chemistry projects.
- ◆ Managed \$15K in research allowance allocations from the DOE-SCGF award towards my Ph. D. project.

## **PUBLICATIONS**

---

Goos, A. G.; Rosado P. J.; Takahashi, Y.; Ruhlandt-Senge, K.; Alkaline Earth Metals: Organometallic Chemistry, *Encyclopedia of Organometallic Chemistry*. 2012. *In press Dec. 2012*.

Rosado, P. J.; Ruhlandt-Senge, K., Synthesis, Characterization and X-ray structure of the 3D MOF  $\{[\text{Ba}(\text{in})(\text{H}_2\text{O})_6][\text{in}]\}_\infty$ . *J. Coord. Chem.* 2011. *In press Jan. 2011*.

## **COMMUNITY CONTRIBUTIONS**

---

CienciaPR.org: Published an article on the book "Ciencia Boricua" which is currently in stores and integrated into Puerto Rico's public education system as a text book (2012).

## **PUBLIC SPEAKING & CONFERENCE EXPERIENCE**

---

- ◆ ERN 2013 – Oral talk on "Synthesis and Characterization of s-block Metal Organic Frameworks for Gas Storage Applications", obtained first prize for graduate student talk in chemistry
- ◆ NERM 2012 – Oral talk on "Synthesis and Characterization of s-block Metal Organic Frameworks for Gas Storage Applications" in the Organometallic Chemistry section
- ◆ Interamerican University of Puerto Rico, San German Campus (2012) – Invited guest speaker on "Synthesis and Characterization of s-block Metal Organic Frameworks for Gas Storage Applications" and a short seminar on Crystallography
- ◆ GRC Inorganic Chemistry Conference 2012 – Presented a poster on "Synthesis and Characterization of s-block Metal Organic Frameworks for Gas Storage Applications", conference fees were paid for by a Carl Storm Fellowship for underrepresented minorities
- ◆ GRC Inorganic Chemistry Seminar 2012 – Presented a poster on "Synthesis and Characterization of s-block Metal Organic Frameworks for Gas Storage Applications"
- ◆ IUPAC 2011 – Presented a poster on "Synthesis and Characterization of s-block Metal Organic Frameworks for Gas Storage Applications"
- ◆ DOE-SCGF Annual Meeting 2011 – Presented a poster on "Synthesis and Characterization of s-block Metal Organic Frameworks for Hydrogen Storage Applications" ~ Attended meeting in 2010.
- ◆ NERM 2010 – Presented a poster on "Synthesis and Characterization of Alkaline Earth Tosylates for Salt Metathesis Applications"
- ◆ Interamerican University of Puerto Rico, San German Campus (2009) - Oral presentation about the applications of cost-effective precursors to synthesizing alkaline earth amides and Metal Organic Frameworks